CHARLES UNIVERSITY

2nd Faculty of Medicine

Field of Study: Medical Biophysics

MUDr. Ing. Karolína Vocetková

Intelligent Nanofibres Functionalized with Growth Factors and Blood Derivatives for Dermatology Applications

Inteligentní nanovlákna funkcionalizovaná růstovými faktory a krevními deriváty pro dermatologické aplikace

PhD Thesis

Supervisor: Prof. RNDr. Evžen Amler, CSc.

Prague, 2018

Statement of originality:

I hereby declare that this thesis and the work reported herein was composed by and originated entirely from me. This thesis has not been submitted for any degree or other purposes. Information derived from the published and unpublished work of others has been acknowledged in the text and references are given in the list of sources.

I agree with prolonged accumulation of an electronic version of my work in the Theses.cz interuniversity database system project for the purposes of systematic checks on similarities among theses.

Prague, 17th of December 2018

Karolína Vocetková

Identifikační záznam:

Vocetková, Karolína. *Inteligentní nanovlákna funkcionalizovaná růstovými faktory a krevními deriváty pro dermatologické aplikace. [Intelligent Nanofibres Functionalized with Growth Factors and Blood Derivatives for Dermatology Applications].* Praha, 2018. Počet stran 162. Disertační práce (Ph.D.). Univerzita Karlova v Praze, 2. lékařská fakulta, Ústav biofyziky. Vedoucí práce Amler, Evžen.

Key words: Skin Tissue Engineering, Electrospinning, Centrifugal Spinning, Drug Delivery, Platelets.

Klíčová slova: Tkáňové inženýrství kůže, Elektrostatické zvlákňování, Centrifugační zvlákňování, Dodávání bioaktivních látek, Trombocyty.

LIST OF ABBREVIATIONS

3T3-A31	Murine fibroblast cell line
ADP	Adenosine diphosphate
ANOVA	Analysis of variance
ATP	Adenosine triphosphate
bFGF	Basic fibroblast growth factor
BMP-2	Bone morphogenetic protein-2
BMP-7	Bone morphogenetic protein-7
CCL-11	C-C motif ligand-11
CCL-4	C-C motif ligand-4
CCXL10	C-X-C motif ligand-10
CS	Centrifugal spinning
DiOC6(3)	3,3′-dihexyloxacarbocyanine iodide
DMEM	Dulbecco’s Modified Eagle’s Medium
ECM	Extracellular matrix
EDTA	Ethylenediaminetetraacetic acid
EGF	Epidermal growth factor
EGFR	Epidermal growth factor receptor
ELISA	Enzyme-linked immunosorbent assay
ES	Electrospinning
FBS	Foetal bovine serum
FDA	Food and Drug Administration
FGF	Fibroblast growth factor

FGF-1	Fibroblast growth factor-1, acidic FGF
FGF-10	Fibroblast growth factor-10
FGF-2	Fibroblast growth factor-2, basic FGF
FGF-7	Fibroblast growth factor-7
FTIR-ATR	Fourier transformation infrared spectroscopy with attenuated total reflectance
G-CSF	Granulocyte-colony stimulating factor
GF	Growth factor
GM-CSF	Granulocyte-macrophage colony-stimulating factor
HGF	Hepatocyte growth factor
hMSC	Human mesenchymal stem cells
IGF-1	Insulin-like growth factor-1
IL-1	Interleukin-1
IL-10	Interleukin-10
IL-12	Interleukin-12
IL-13	Interleukin-13
IL-15	Interleukin-15
IL-17	Interleukin-17
IL-1b	Interleukin-1b
IL-1ra	Interleukin-1ra
IL-1α	Interleukin-1α
IL-2	Interleukin-2
IL-4	Interleukin-4
IL-5	Interleukin-5

IL-6	Interleukin-6
IL-6	Interleukin-6
IL-7	Interleukin-7
IL-8	Interleukin-8
IL-9	Interleukin-9
INF-γ	Interferon-γ
IP-10	Interferon gamma-induced protein-10
KGF-1	Keratinocyte growth factor-1
KGF-1	Keratinocyte growth factor-2
LOQ	Limit of quantification
MCP-1	Monocyte chemoattractant protein-1
MCP-3	Monocyte chemoattractant protein-3
MIP-1	Macrophage inflammatory protein-1
MIP-1a	Macrophage-inflammatory protein-1a
MIP-1b	Macrophage-inflammatory protein-1b
MMP	Matrix metalloproteinase
MTS	3-(4,5-dimethylthiazol-2-yl)-5-(3-carboxymethoxyphenyl)-2-(4-sulfophenyl)-2H-tetrazolium
PBS	Phosphate buffer saline
PCL	Poly-ε-caprolactone
PDGF	Platelet-derived growth factor
PEG	Polyethylene glycol
PEO	Polyethylene oxide
PF-68	Pluronic F-68

PGA	Polyglycolic acid
PL	Platelet lysate
PLGA	Polylactic-co-glycolic acid
PLLA	Poly-L-lactic acid
PPP	Platelet-poor plasma
PRF	Platelet-rich fibrin
PRFM	Plasma-rich fibrin matrix
PRGF	Plasma-rich in growth factors
PRP	Platelet-rich plasma
PVA	Polyvinyl alcohol
RANTES	Regulated on Activation, Normal T Cell Expressed and Secreted
RH	Relative humidity
RMPI-1640	Medium developed in Roswell Park Memorial Institute
ROS	Reactive oxygen species
RPM	Revolutions per minute
SEM	Scanning electron microscopy
TGF-α	Transforming growth factor-α
TGF-β	Transforming growth factor-β
TGF-β1	Transforming growth factor-β1
TGF-β2	Transforming growth factor-β2
TGF-β3	Transforming growth factor-β3
TIMP	Tissue inhibitor of metalloproteinase
TNF-α	Tumour necrosis factor-α
TPA	12-O-Tetradecanoylphorbol-13-acetate

TSP-1	Thrombospondin-1
VEGF	Vascular endothelial growth factor
XB2	Murine keratinocyte cell line
XMAP	Luminex multi-analyte profiling

TABLE OF CONTENTS

1 INTRODUCTION

Tissue engineering and regenerative medicine represent a dynamically developing field of medicine. It aims to restore, maintain or improve the function of a tissue or an organ. Its principles emerge also in the tissue engineering of the skin. Skin represents a barrier protecting the human body against the outer environment. With the ageing of the population, unhealthy life style choices and the increasing incidence of the associated metabolic diseases, chronic wounds are becoming a worldwide issue and novel, effective wound dressings and/or skin substitutes are needed.

One of the most important factors in tissue engineering/regenerative medicine is the choice of scaffolding system. The scaffold should be nontoxic, biodegradable, should promote migration and adhesion of the cells of interest, and subsequently allow their expansion and extracellular matrix synthesis. Very promising scaffolding systems are nano- and microfibrous scaffolds fabricated using electrospinning and centrifugal spinning. These techniques allow further functionalization of the scaffolds with bioactive molecules. As a simple and cost-effective source of bioactive molecules, platelets may be used. The unique characteristics of platelets may be used in many forms with varying mechanical properties and content of the bioactive molecules, depending on the method of preparation of the platelet derivatives.

This work aims to investigate the effects of platelet-derived molecules in skin tissue engineering and to develop sophisticated and fine-tuned drug delivery systems, as well as systems with clear potential of clinical translation.

2 LITERATURE REVIEW

2.1 Skin

Skin is the largest organ of the human body, with the surface of 1.4–2.0 m^2 representing approximately 16% of body weight[1,2]. Its thickness varies greatly depending on the function and area of the body from about 0.5 mm to up to 4 mm^3. To the most important functions of the skin belongs its barrier function. It also plays role in electrolyte and fluid balance, provides protection against microbiological colonization, prevents photodamage by ultraviolet radiation, is involved in vitamin D synthesis and contains sensory receptors enabling sensation of touch, temperature, pressure or pain[1].

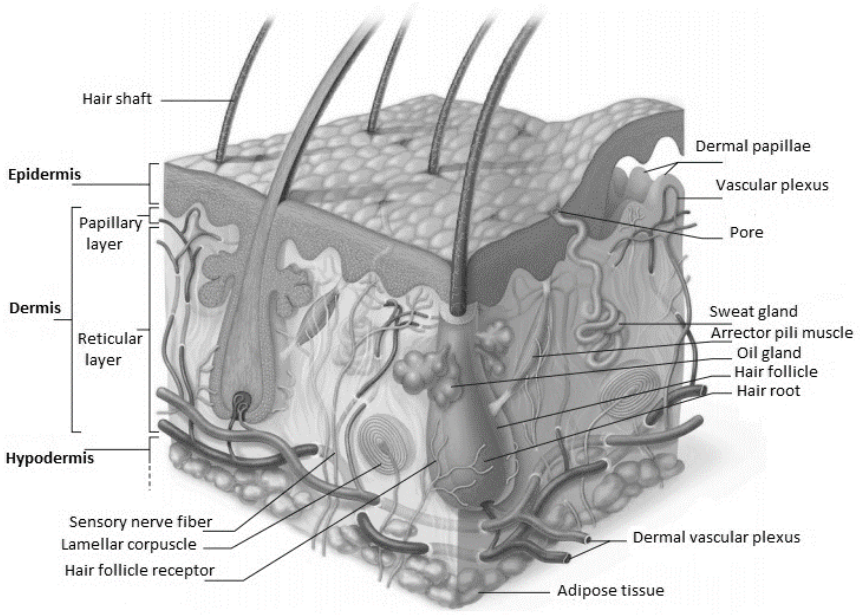

Figure 1 Structure of the skin. Adapted from[1].

The skin is composed of three layers: epidermis, dermis, and subcutaneous tissue (Figure 1).

2.1.1 Epidermis

Epidermis is formed by keratinized stratified squamous epithelium and contains keratinocytes and three types of dendritic cells: melanocytes, Merkel cells, and Langerhans cells. Furthermore, there are four epidermal layers: stratum corneum, granulosum, spinosum and basale (Figure 2)[1].

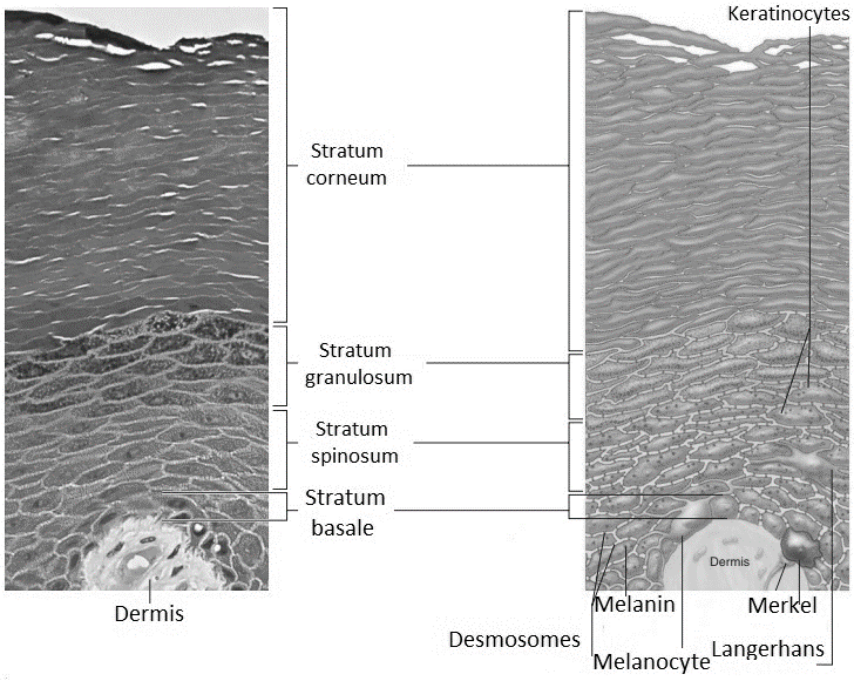

Figure 2 Epidermal cells and the layers of epidermis. Adapted from[1].

Keratinocytes are the predominant cells of epidermis. Their main aim is to form keratin, a tough fibrous protein responsible for the protective barrier function of the skin. Keratinocytes are formed in the deepest layer of epidermis and are pushed towards the surface by the newly formed cells[1]. By the time they reach the skin surface, they are dead, completely flat and filled with keratin. This process is called keratinization[4].

The deepest epidermal layer is called the **basal layer** (stratum basale) or the germinating layer. It is firmly attached to the underlying dermis and formed by a single row of columnar cells

of stem origin. The layer also contains scarcely distributed **Merkel cells** responsible for the tactile sensation[1]. **Melanocytes** are dendritic cells derived from the neural crest and account for approximately 10 to 25% of cells of the basal layer[4]. One melanocyte together with 35–45 keratinocytes form an epidermal melanin unit. To differentiate properly, melanocytes need contacts with the neighbouring keratinocytes and their growth factors, such as basic fibroblast growth factor (bFGF), hepatocyte growth factor (HGF), granulocyte-macrophage colony-stimulating factor (GM-CSF), or interleukin-1α (IL-1α)[5,6]. Melanocytes mainly synthesize melanin, a dark pigment responsible for UV protection of the cell nuclei. It is synthesized in their special rounded organelles called melanosomes and transferred to the neighbouring keratinocytes[1]. Increased exposure to the ultraviolet light stimulates melanogenesis and melanosome transfer[4].

The **spiny layer** (stratum spinosum) is composed of several (usually five to twelve) layers of cells that do not divide as rapidly as the cells in the basal layer[1,2]. The spiny layer contains **Langerhans cells**, dendritic cells produced in the bone marrow migrating to the skin, where they participate in the response of the immune system[2].

The **granular layer** (stratum granulosum) is formed by three to five rows of prolonged and flattened keratinocytes. The cells contain multiple granules filled with keratin and glycolipids responsible for slowing down the water loss through epidermis[1]. The blood supply of epidermis comes from the dermis. Therefore, the more superficial layers are too far from the dermal capillaries to receive nutrients and cells undergo apoptosis[1,2].

The **horny layer** (stratum corneum) is the most superficial layer of the skin, containing multiple rows of flat, keratin-filled keratinocytes (approximately 25 to 30 layers). Both the keratin

and the increased thickness of the plasmatic membrane protects the skin against injuries. Furthermore, the layer is impermeable for water[1].

2.1.2 Dermis

The dermis is responsible for providing nutrients and support to the epidermis[2]. It is composed of flexible connective tissue. It consists mainly of **fibroblasts**, macrophages, and mast cells. Blood cells (leukocytes, such as lymphocytes and plasmatic cells) enter dermis in response to various stimuli. Furthermore, it contains collagen, elastic, and reticular fibres synthesized by fibroblasts[4]. The dermis contains rich network of nerve fibres and blood vessels[1]. Their role is not only to provide nutrients and facilitate waste exchange, but thermoregulation as well[4].

There are two dermal layers, papillary and reticular layer. The **papillary layer** represents the superficial 20% of the dermis and is composed of a thin connective tissue. The deeper **reticular layer** accounts for the remaining 80% of the dermis. It consists of a dense connective tissue formed by a network composed of thick bundles of interconnected collagen and elastic fibres. The collagen fibres are responsible for strength and resilience of the skin, the elastic fibres enable the skin to stretch and contract[1]. Collagen accounts for approximately 70% of the dry weight of the dermis. Elastin forms finer fibres than collagen; elastin fibres are interwoven among the collagen fibres. With aging, collagen fibres lose their shape and elastin fibres lose their elasticity, leading to wrinkled appearance[3].

2.1.3 Subcutaneous tissue

The subcutaneous tissue consists mainly of adipose tissue. It anchors the skin to the underlying structures (i.e. muscles) so it can slide relatively freely. Given its poor conductive properties, it prevents heat loss[1].

2.2 Wound healing

With the increasing incidence of obesity, type 2 diabetes and ageing population, wound healing represents a global medical issue, with its early and late complications being a frequent cause of mortality and morbidity[7,8]. Often, they are disguised as a comorbid condition and thus represent a hidden epidemic. Given these facts, the anticipated risks of non-healing wounds continue to increase dramatically. It poses a major threat to the public health and economy. Currently, annual costs of chronic wound care are projected to exceed 25 billion USD in the United States and represent approximately 2% of the total EU financial resources[9,10]. A proper understanding of the process of wound healing is thus essential[11].

Wounding and wound healing take part in every tissue and organ, many of the processes are common for all tissues[8]. Wound can be generally characterized as a disruption of skin continuity. The most common cause of major skin loss is thermal injury, followed by trauma and ulcerations secondary to diabetes, pressure and venous stasis[12]. In order to completely close the wound and restore the integrity of the organism, it requires a coordinated interaction of cells, soluble mediators and extracellular matrix within the immune system, blood coagulation cascade and inflammatory pathways[13]. Thus, it represents a complex biological process in which many cell types (immune cells, endothelial cells, keratinocytes, and fibroblasts) undergo changes in their gene expression resulting in their proliferation, differentiation and

migration[13,14]. Disruption of the fine balance may result in failure of the wound to heal. Based on the healing timeframe, the wounds can be classified into acute and chronic wounds. For example, in the US, there were 35.2 million cases of significant skin loss in 1992 and out of these, 7 million of wounds become chronic[12]. In the Czech Republic, the prevalence of chronic wounds is approximately 1%, with a significant increase in the elderly population over 70 years of age (up to 4 to 5%)[15].

2.2.1 Acute wound healing

Acute wounds are wounds that close in a timely and orderly manner (usually up to 8 to 12 weeks), restoring both anatomical and functional integrity of the organism. For simplicity, acute wound healing is often artificially compartmentalized into four phases with considerable temporal overlap: the haemostasis, the inflammation, the proliferation and the remodelling[7,14] (Figure 3).

Shortly following the injury, **haemostasis** occurs. The main aim of haemostasis is to stop the immediate bleeding, and the key players are platelets and fibrin[16]. The exposed collagen leads to platelet activation and aggregation, coagulation cascade activation and, finally, results in fibrin matrix (clot) formation. Fibrin mediates both haemostasis and homeostasis. It provides provisional matrix for several cell types (e.g. fibroblasts or endothelial cells) and regulates their adhesion, proliferation and migration[17,18]. Furthermore, fibrin acts as a local reservoir of various growth factors and facilitates their spatiotemporal release in the area of wound[19]. Fibrin itself has pro-angiogenic properties. Not only it provides a supportive matrix, it also acts as a chemoattractant for endothelial cells in to the clot. The invading cell then replace fibrin with the newly formed extracellular matrix (ECM)[19].

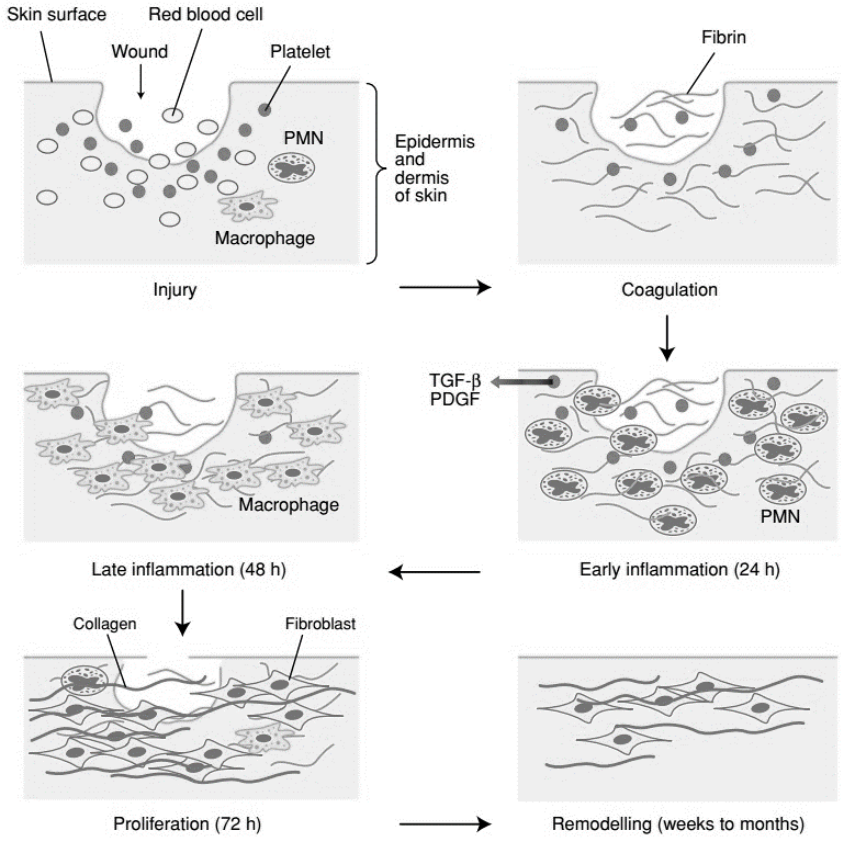

Figure 3 **Phases of wound healing**. Wound healing consists of four overlapping phases. PMN – polymorphonuclear neutrophil. Adapted from[16].

Blood clotting induces platelet degranulation and numerous cytokines and growth factors (e.g. platelet-derived growth factor (PDGF), insulin-like growth factor-1 (IGF-1), epidermal growth factor (EGF) and transforming growth factor-beta (TGF-β)) are released from the platelet alpha granules[20]. Thus, the released bioactive molecules initiate inflammatory cells chemotaxis and tissue repair[14].

The main aim of the **inflammatory phase** is to establish an immune barrier against microbial invasion. The inflammatory cells (polymorphonuclear neutrophils, macrophages) provide antimicrobial defence via phagocytosis and reactive oxygen species (ROS) and removal of the devitalized tissue due to the released proteases (elastase, collagenase and other proteases from the family of matrix metalloproteinases (MMPs))[14,21]. MMPs are involved

in the ECM degradation, cell migration and tissue remodelling; their elevated levels were associated with chronic wounds failing to close[22,23].

By secreting growth factors and cytokines, the inflammatory cells induce the formation of granulation tissue. Reestablishment of the normal blood flow leads to epidermal and dermal cell migration and proliferation, and as the number of inflammatory cells in the wound bed begins to decrease, usually few days following the initial wounding, the **proliferative processes** start to prevail[14]. The mechanism of resolution of the inflammatory phase is currently not fully understood. However, key players in the transition from inflammation to proliferation are believed to be macrophages. The phagocytic pro-inflammatory M1 subset of macrophages is transformed into the M2 macrophages, supporting the reparative processes and proliferation and inducing angiogenesis[24]. The synthesis of necessary growth factors is taken over by fibroblasts, keratinocytes and endothelial cells, maintaining proliferation and migration of the cells[14]. To support the reparation processes, an adequate blood supply and nutrient/gas exchange is required.

Thus, a robust **angiogenesis** and **vasculogenesis** must be initiated and sustained. The hypoxic environment of the wound fosters the production of proangiogenic molecules (vascular endothelial growth factor (VEGF), bFGF and PDGF)[14]. In response to the bioactive molecules, endothelial cells migrate towards the wound upon degradation of the basal membrane, proliferate and eventually form new blood vessels[25].

Normal blood supply fosters a suitable microenvironment for epidermal and dermal cell migration and proliferation, which leads to re-epithelialization and restoration of the integrity of the organism. Fibroblasts synthesize extracellular matrix, forming granulation tissue. The provisional, highly hydrated matrix consisting mainly of type III collagen, fibrin, fibronectin and

hyaluronic acid, is gradually changed into denser extracellular matrix synthesized by fibroblasts, containing mainly collagen I[25,26]. The collagen synthesis and degradation reach an equilibrium approximately three weeks after the injury and then, the rate of collagen synthesis gradually slows down[16]. The collagen crosslinking and reorganisation of the ECM occur within the **remodelling** phase for several weeks, leading to the formation of a relatively acellular scar with tensile properties reaching up to 80% of the tensile properties of the unwounded skin[7,26].

2.2.2 Chronic wound healing

Chronic wounds are defined as wounds failing to proceed with the timely and orderly manner of wound healing and persisting for more than three months following the initial injury[27,28]. Based on aetiology, they can be classified into vascular (due to venous hypertension and/or arterial insufficiency), diabetic and pressure ulcers[14]. They do not follow the precise cascade of processes, usually being halted in the inflammation phase, preventing the progression into the reparative synthetic phase[20]. Typically, they result as a complication of other underlying conditions, such as diabetes or other neuropathies, or local tissue hypoxia and heavy bacterial burden, or simply due to ageing[9,14,20]. The growing body of evidence is advancing our understanding of the background mechanisms of chronic wounds. So far, the identified factors impairing healing include: reduction in the bioavailability of the growth factors and receptors due to excessive proteolytic activity in the wound bed and lack of their inhibitors, abnormal production of matrix proteins, decreased proliferative potential of the residing cells, insufficient blood perfusion, persistent infection and formation of a drug-resistant biofilm[14]. Such diverse aetiology hinders the search for a single effective therapeutic agent[20].

2.2.3 Growth factors, cytokines and chemokines significant in wound healing

As was mentioned above, growth factors play an important role in the process of wound healing. To the best-characterized growth factors belong the growth factors of epidermal growth factor family, including among others epidermal growth factor and transforming growth factor-alpha, acting through an EGF receptor (a tyrosine kinase transmembrane protein)[29]. Activation of the EGFR stimulates keratinocyte proliferation and migration and thus represents a key factor in the process of reepithelization[30]. The **epidermal growth factor** is produced by multiple cells, including platelets, macrophages, and fibroblasts. In a paracrine fashion, it stimulates keratinocytes. It has been shown, that EGF is upregulated in acute wounds[29]. There are studies in chronic wounds showing EGFR localized in the cytoplasm of keratinocytes, instead of their membrane, suggesting down-regulation of the receptor, its mis-localization and subsequent inhibition of epithelialization[31]. Further studies describe degradation of EGF in the proteolytic environment of a chronic wound, in comparison to acute wounds[32]. **Transforming growth factor-alpha** (TGF-α) has similar effects to EGF, however, it has been found that its absence does not hinder wound healing[33]. Its role is in early stages of re-epithelialization. The effect of TGF-α is concentration- and duration-dependent. At low levels, it promotes healing by supporting production of growth factors by macrophages and stimulating inflammation. However, at high levels, particularly over prolonged periods of time, it prevents synthesis of ECM proteins and tissue inhibitors of metalloproteinases (TIMPs) and promotes synthesis of MMPs, and thus contributes to the inability of the wound to close[29].

Another important growth factor family is the **fibroblast growth factor** family (FGFs). The FGFs are synthesized by keratinocytes, fibroblasts, endothelial cells, smooth muscle cells, and mast cells[29]. They bind to a FGF receptor that needs proteoglycans (such as heparin) for

activation[34]. FGF-1 and FGF-2 (acidic or basic fibroblast factor, respectively) play a role in granulation tissue formation, reepithelialization, and tissue remodelling[35]. It regulates synthesis of components of the ECM, keratinocyte and fibroblasts migration and production of collagenases[29]. In contrast to acute wounds, the FGF-2 levels are decreased in chronic wounds[36]. Furthermore, **keratinocyte growth factor-1** and **-2** (KGF-1 and KGF-2, or FGF-7 and FGF-10, respectively) act in a paracrine fashion on keratinocytes and stimulate their proliferation and migration. In addition to that, they stimulate transcription of factors involved in ROS detoxification, preventing the ROS-induced apoptosis of keratinocytes[37]. FGF-7 is also a potent mitogen of vascular endothelial cells and plays an important role during later stages of neovascularization[38].

Transforming growth factor-beta1-3 (TGF β1-3) are proteins significant in wound healing. They are produced by fibroblasts, keratinocytes, platelets and macrophages[29]. Following an injury, expression of TGF-β1 increases. In the inflammation phase, it stimulates recruitment of immune cells and tissue debridement, however, in sterilized wounds it deactivates superoxide production in macrophages *in vitro* and thus plays role in protection of the surrounding healthy tissue and helps to prepare the wound for formation of granulation tissue[39–41]. It strongly stimulates collagen type I and III production. To inhibit the break-down of the newly-formed collagen, it decreases the production of metalloproteinases MMP-1, -3, and -9 and promotes synthesis of TIMP-1[29].

The members of **platelet derived growth factor** (PDGF) family are produced by platelets, macrophages, endothelial cells, fibroblast, and keratinocytes, and include 5 isoforms PDGF-AA, -AB, -BB, -CC, and –DD[29]. PDGF affects every stage of wound healing and belong to the first factors released in response to wounding. Shortly after injury, PDGF is released from

platelets and attracts immune cells and fibroblasts and stimulates their proliferation[42]. Furthermore, it promotes synthesis of other growth factors, such as TGF-β in macrophages and VEGF in endothelial cells[43,44]. During epithelialization, it stimulates production of IGF-1 (IGF-1 increases keratinocyte mobility) and thrombospondin-1 (TSP-1). TSP-1 postpones proteolytic degradation at the site of the wound and promotes proliferation[45,46]. Additionally, it induces the transformation of fibroblasts into myofibroblasts, and by affecting the levels of MMPs, it helps to break down the old collagen during remodelling[47].

Vascular endothelial growth factor (VEGF) is essential for proper angiogenesis. It is significantly upregulated in hypoxic environment, given its constitutional synthesis in the skin is almost negligible. During its early stages, it promotes endothelial cell migration and proliferation. The hypoxia in the wound stimulates VEGF release leading to angiogenesis, and, thus, the tissue perfusion is restored, and the oxygen tension increased. The expression of VEGF is further stimulated by other growth factors in a paracrine manner (e.g. TGF-β1, EGF, bFGF, and PDGF-BB)[35].

During the inflammatory phase of wound healing, **pro-inflammatory cytokines** such as interleukin-1 (IL-1), interleukin-6 (IL-6) or TNF-α play role. IL-1 is produced by immune cells (neutrophils, macrophages, and monocytes) and keratinocytes. It increases keratinocyte migration and proliferation and activates fibroblasts. Similarly, IL-6 is secreted by neutrophils and monocytes. It stimulates keratinocyte proliferation and in a autocrine manner, it further attracts neutrophils to the site of injury[29]. The inflammatory phase of wound healing is also governed by **chemokines** that attract various cell types to the site of injury. The presence of chemokine receptors on the cells residing in the wounded tissue suggests contribution of chemokines during angiogenesis, re-epithelialization, and remodelling as well[37].

2.2.4 Management of chronic wounds

Over the past decades, our understanding of the cellular and molecular mechanisms underlying wound healing has advanced greatly[12]. Based on the current knowledge of the problematics of wound healing, chronic wounds (regardless of their aetiology) are treated using a multistep approach. Firstly, the necrotic tissue must be removed using surgical tools or debriding agents (typically enzymatic, papain-based and collagenase-based preparations)[14]. The debridement of the necrotic tissue or any foreign material increases the chances of the wound to close and the presence of necrotic or foreign material further increases the risk of infection and prolongs the inflammatory phase[48]. Following wound debridement, it is necessary to minimize the present inflammation and infection using antibiotics, topical antiseptics, and anti-inflammatory agents. Furthermore, the injured tissue needs to be cover with a proper dressing. The dressings may be classified based on their function (i.e. debridement, antibacterial, occlusive or absorbent), type of the used material (biological, biosynthetic or synthetic), or the physical form of the dressing (ointment, film, foam, or gel)[48–50]. Moist dressings help to promote the inflammatory phase and accelerate the wound closure, on the other hand, traditional dry gauze dressings may degrade the process and disrupt the newly formed epithelium when removed. The golden standard of modern wound dressings is represented by a low-adherent dressing, such as hydrocolloids and hydrogels (material that absorbs the wound exudate while keeping the wound moist), alginate dressings or non-woven fibrous dressings with a high absorption capacity[51]. The traumatic removal of the dressing during dressing exchanged can be minimized using foam dressings made of collagen[52].

The therapy of large skin defects includes skin grafting as the wound dressings (whether traditional or modern) cannot make up for the lost tissue, especially in case of severe burns[48].

A skin autograft contains the patient's own full epidermis and a portion of dermis. This approach is called the split-thickness autologous skin grafting. However, there may be shortage of the donor skin for transplantation and, depending on the thickness of the transplanted dermis, the approach may lead to excessive scarring[53]. Full-thickness skin grafting (full epidermis and full dermis transplanted) is known to not be associated with so much scarring, but only defects <2% of the total body surface area can be treated using full-thickness grafting[54]. Skin allograft may address the donor site shortage, however, there is a risk of rejection of the transplanted tissue[12].

The increasing knowledge on molecular and biologic processes of wound healing led in the past decades to innovation of the wound care and development of techniques and dressings that facilitated more rapid closure of the wounds, more aesthetic scars and decreased incidence of keloid formation. Using the engineered dressings, proper moisture in the wound is established, and, finally, epithelialization and granulation tissue formation is promoted by specific therapies (e.g. delivery of growth factors)[14].

Generally, the levels of growth factors are decreased in chronic wounds, due to their susceptibility to the proteolytic environment[29]. Therefore, multiple clinical trials have been performed, evaluating the delivery of exogenous growth factors necessary for fostering the process of wound healing. However, given the promising *in vitro* results and the resulting expectations, the outcomes seemed to be rather inconclusive and not clearly convincing[35]. Topically administered EGF failed to significantly promote healing in the setting of a chronic venous ulcer[55]. Similarly, multiple clinical trials for chronic wound healing were failed by TGF-β[29], FGF or VEGF[35]. Up to date, the only growth factor approved by the Food and Drug Administration (FDA) in chronic wound healing is PDGF-BB. Efficacy of its topical

administration in pressure ulcers was investigated, showing significant acceleration of healing[56,57], and similarly promising results have been obtained in diabetic ulcers[58], leading to the FDA approval. Among the reasons why the topical administration of recombinant human growth factors did not yield better outcomes are the complex signalling of the individual growth factors and their concentration-dependent effects, maybe requiring combinations of the growth factors, and their insufficient retention at the site of the wound. Thus, novel strategies for delivering the bioactive molecules are desperately needed[35].

2.3 Skin tissue engineering

Tissue engineering, an interdisciplinary field, in general aims to restore the integrity and function of a damaged tissue or an organ in the condition of end-stage failure using cells and/or extracellular matrix. The exploration of the idea of seeding viable cells on an appropriately designed scaffold began in 1970s. The keratinocyte culture was established in 1975, resulting in transferring of sheets of keratinocytes to burn victims or using collagen-based matrix to promote the growth of fibroblasts[59,60]. These experiments were followed by development of novel scaffolds composed of synthetic, biodegradable polymer materials that would allow tailoring of chemical and physical properties to the designed purpose of the scaffolding systems[61].

Nowadays, there are two main strategies to fulfil this aim. Firstly, scaffolds can be used simply as a supporting material for cells that are expanded *in vitro*. The cells then synthesize extracellular matrix, a foundation of the newly formed tissue for transplantation. Following the transplantation, proportionally to the new ECM synthesis, the scaffold is gradually degraded. This represents the main idea of tissue engineering in the narrow sense of the word. The

second approach, in the narrow sense of the word called the regenerative medicine, uses the scaffold as a drug or bioactive molecule delivery system, inducing cell recruitment, their migration, adhesion, proliferation and/or differentiation into the preferred type upon the transplantation of the scaffold into the body (Figure 4)[12].

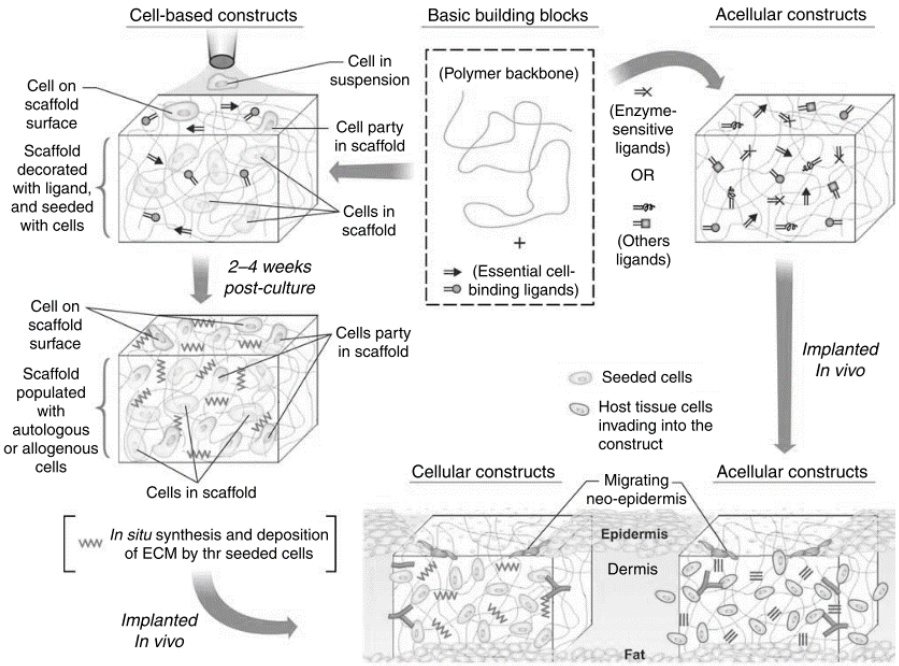

Figure 4 Summary of principles of skin tissue engineering and regenerative medicine. Adapted from[12].

However, the above-mentioned strategies do not exclude themselves and it is possible to easily combine them together[62]. Whether the scaffolding systems contain cells or not, they are usually fabricated using polymers (synthetic or natural), and functionalized with bioactive molecules to stimulate the cells to migrate, proliferate, and differentiate[63]. An ideal skin substitute be sterile, biodegradable, non-toxic, non-inflammatory and non-immunogenic, it should act as a barrier against microbial contamination and adhere to the wound rapidly. Furthermore, it should be easy to handle and cost-effective. The available skin substitutes may be categorized based on the anatomical structure as epidermal, dermal, or epidermal-dermal

or based on their composition as acellular and cellular, based on the biomaterial used as biologic (autologous, allogeneic or xenogeneic) or synthetic[53].

2.3.1 Acellular skin substitutes

The acellular skin substitutes represent the most basic type of the substitutes, acting primarily as a barrier to fluid loss and microbial contamination[64]. They serve as a temporary cover and are removed when the wound is healed or when an autograft is available. Usually, they are used in mid-dermal partial thickness wounds[53]. These products contain Biobrane®, Alloderm®, and Integra®. The Biobrane® is a two-component epidermo-dermal substitute, composed of a very thin nylon membrane serving as a dermal analogue and a very thin silicon membrane servings as an epidermal analogue. Both components are covered with porcine type I collagen peptides. The Integra® is a bilayer consisting of a silicon epidermal analogue and dermal analogue composed of porous bovine collagen and shark chondroitin-6-sulphate glycosaminoglycan. Upon wound revascularization, the silicone layer is removed and replaced by a thin split-thickness skin graft[53,65]. The Alloderm® is a human decellularized lyophilized dermis with no epidermal layer, providing matrix for the infiltrating fibroblasts. The disadvantages of the above-mentioned skin substitutes include accumulation of the exudate[64,65].

2.3.2 Cellular skin substitutes

Cellular skin substitutes consist of a matrix or a mesh in combination with expanded fibroblasts and/or keratinocytes, depending whether the skin substitute is epidermal, dermal, or composite. The cellular skin substitutes may be allogeneic or autologous.

The autologous epidermal substitutes include Epicel®, Bioseed® and Laserskin®. The Epicel® is an FDA-approved permanent skin substitute composed of sheets of patient's keratinocytes expanded from skin punch biopsies delivered on a petrolatum gauze support[53]. The keratinocytes may be further delivered using other scaffolding systems, such as hyaluronan membrane (Laserskin®) or fibrin sealant (Bioseed®)[48]. An example of an autologous dermal substitutes is Hyalograft3D. The autologous cultured fibroblasts are seeded on a 3D hyaluronic acid-derived meshes[66]. The TissueTech autograft system is a combination of an epidermal substitute (Laserskin®) and a dermal substitute (Hyalograft3D). The epidermal substitute is applied 7 days after the dermal substitutes. The efficacy of the system was evaluated in patients with non-healing ulcers of various aetiology with promising outcomes[67].

The allogeneic dermal substitutes include Dermagraft® and Transcyte®. The Dermgraft® is composed of a biodegradable polyglycolic acid (PGA) mesh seeded with neonatal foreskin fibroblasts. The PGA mesh is resorbed within three to four weeks[65]. The Transcyte® is a bilayer product, composed of a silicone membrane and a nylon/collagen mesh seeded with neonatal foreskin fibroblasts. The silicone membrane protects the wound and allows its visual inspection[66]. Both products are cryopreserved. The freezing process destroys the cells, reducing the risk of an immune reaction while maintaining the synthesized ECM and growth factors. These constructs provide a dermal matrix that facilitates re-epithelialization of the wound by the patient's keratinocytes. An example of an allogeneic composite substitute is Apligraf®. It was approved by the FDA in 1998 and it was the first composite skin graft used in the indication of venous and neuropathic leg ulcers[64]. It contains both neonatal foreskin allogeneic fibroblasts and keratinocytes delivered in a bovine collagen gel. Firstly, the fibroblasts are seeded in the collagen gel and within 14 days, the fibroblasts synthesize a new,

dense collagen matrix. After the two weeks, the construct is seeded with keratinocytes and the cells proliferate for 4 days. Following cell expansion, the substitute is lifted to the liquid/air interface and the keratinocytes differentiate and form a stratum corneum. Then, the skin substitute is ready to use[65]. The Apligraf® construct was successfully used in non-healing venous ulcers, diabetic ulcers and pressure ulcers[68].

However, the acellular constructs represent a more promising solution to the issues associated with wound healing. They are less complex to fabricate, more cost-effective, user-friendly and minimize the risk of transmission of infectious agents. The material of the construct should be conductive and should recruit cells of the host tissue. The dressings are usually made of synthetic or natural biopolymers; however, the only marketed products are made of natural biopolymers (i.e. collagen, fibrin, and/or hyaluronan). Engineered drug delivery vehicles are needed to improve the outcomes and electrospun fibrous mats may represent a viable solution[69].

2.4 Nanofibrous scaffolds

Nanofibres are fibres with diameter in the nanometre range. Their unique properties predetermine them for tissue engineering applications. The properties include[70]:

- high volume-to-surface ratio, allowing easy and tailorable functionalization with bioactive molecules;
- controlled porous structure with high pore interconnection, allowing nutrient and waste exchange;
- microarchitecture in the nanoscale range, resembling the topography of native ECM, and thus promoting cell adhesion, proliferation, and differentiation.

These features significantly distinguish nanofibers from the conventional woven textiles, as their diameters are in the micrometre scale and their surface-to-volume ratio is lower[71]. However, nanofibres may not only mimic the structure of ECM but its function as well. Generally, cells respond to three types of stimuli contained in the ECM; to its topography and microarchitecture, physical properties (elastic modulus and other mechanical properties, such as resilience or strength), and finally to biochemical stimuli (such as the charge, hydrophobicity/hydrophilicity, sequence of amino acids or functional groups)[72]. Therefore, functionalization of nanofibres with bioactive molecules, such as growth factors, adhesive molecules, differentiation factors or drugs, may help to induce the desired effect.

Various nontoxic, biodegradable and biocompatible synthetic and natural polymers may be spun into nano- and/or microfibres. Biologic polymers (proteins such as collagen, gelatine, or fibrinogen, or polysaccharides such as cellulose, chitin or chitosan) provide their own intrinsic bioactive properties, allowing them to enhance the cellular response of the prepared system[73]. However, the adjustment of their mechanical or degradation properties is not optimal. In contrast, it is usually possible to tailor the mechanical properties of the synthetic polymers to the specific application (such as porosity, degradation time or mechanical properties) and they allow uniform, large-scale production and prolonged shelf-time in comparison to the natural polymers[73,74]. Several synthetic polymers were used to develop synthetic polymer scaffolds for skin tissue engineering, including poly-ε-caprolactone (PCL), poly-L-lactic acid (PLLA) or polyglycolic acid (PGA). PCL is an FDA-approved biocompatible, biodegradable synthetic polymer; its degradation products do not induce local pH decrease. The degradation rate is determined by the molecular weight of the polymer and the physical properties of the scaffolds[75].

It was shown the cell recognition of the synthetic scaffolds may be somewhat limited. Therefore, to combine the advantages of both the synthetic and natural polymers, novel blend materials have been developed[76]. These materials included for example chitosan/PCL[77], collagen/PCL[78,79] and collagen/polylactic-co-glycolic acid (PLGA)[80] blends for skin tissue engineering, furthermore, gelatine has been shown to improve wound healing outcomes when combined with PCL[81].

The most common techniques of nanofibre fabrication include the electrospinning, centrifugal spinning, phase separation, and self-assembly. The latter two techniques are laboratory techniques and the likelihood of their prospective commercialization is rather low. Furthermore, only a limited number of polymers may be used for fibre fabrication using these techniques which will be described only briefly. The phase separation and a subsequent production of nanofibres from a homogenous polymer solution is induced by its rapid cooling. During the cooling, gelation of the solution occurs, with an internal network of nanofibers. Finally, the solvent is removed. The self-assembly technique uses small molecules such as peptides or nucleic acids bound with noncovalent interactions to form nanofibres[82].

2.4.1 Electrospinning

Electrospinning is the most commonly used technique to produce nanofibres, resulting in continuous, long fibres with a diameter ranging from 3 nm to 10 μm[82]. The method may be used to spin almost any polymer (conductive and nonconductive) and enables encapsulation of various bioactive compounds[83,84] as well. During electrospinning, fibres are formed using an electrostatic force generated by a high voltage. The high voltage applied to the polymer solution induces migration of free electrons, and thus, a charge is formed at the surface of the polymer

and, consequently, an electric field is established between the surface of the polymer and a collector (charged or grounded). When increasing the voltage applied, and thus the intensity of the formed electric field, the surface tension of the polymer solution is overcome, and polymer jets are formed. On the way to the collector, the fibres elongate and become thinner. Finally, dried nanofibres are deposited on the collector in a random manner[85].

The common laboratory setup (also known as the capillary electrospinning) consists of a source of high voltage, syringe with a needle and a collector. However, the yield of such setup is low (only one polymer jet is formed) and the obtained layer is not homogenous. Therefore, for commercial purposes, a method using self-formation of the polymer jets on a free liquid surface was developed by Elmarco (the Nanospider™ technology). The principles underlying the electrospinning from a free liquid surface were described by[86].

The process of electrospinning may be affected by various variables: characteristics of the polymer solution, parameters of the electrospinning itself and parameters of the environment.

The characteristics of the polymer solution include mainly the viscosity of the solution, surface tension and conductivity of the solution. The polymer viscosity is closely linked to the polymer concentration and its molecular weight. Increasing both the parameters leads to increase in polymer chain entanglement and thus its viscosity. If the viscosity of the solution is low, micro- and nanoparticles are formed during the process called electrospraying. With increasing viscosity, firstly, beaded fibres are formed (fibres containing spherical defects), followed by smooth fibres with further increase in the solution viscosity. The diameter of the fibres further increases with the increasing viscosity. However, too high viscosity of the solution prevents the electrospinning process from occurring. The beaded defects may also occur if the surface tension of the polymer solution is too high. To lower the surface tension, solutions such

as ethanol or surfactants are added to the solvent. Furthermore, increase in the conductivity of the solution leads to decrease in the diameter of the formed fibres. The conductivity may be increased by addition of mineral salts or bioactive molecules[87].

The parameters of the process include the applied voltage, polymer flow rate, the needle orifice, collector-electrode distance and the morphology of the collector itself. The electrospinning process may also be influenced by the relative humidity or temperature[88].

2.4.2 Centrifugal spinning

Centrifugal spinning is an alternative technology of ultrafine fibre fabrication that does not require the high voltage. Instead of the electrostatic forces, the technology uses centrifugal forces to produce fibres from melts or solutions[89]. The polymer solution/melt is placed in a rotating spinning head, giving rise to formation of centrifugal forces. Similarly, as in case of electrospinning, when the centrifugal forces overcome the surface tension of the polymer (i.e. the rotary speed reaches a critical value), a polymer jet is ejected from a nozzle of the spinning head. The fibres undergo stretching and elongation and are eventually deposited on a collector[90]. The mean diameter of the centrifugal spun fibres is higher (in the range of hundreds of nanometres to tens of micrometres)[91] in comparison to the diameters obtained via electrospinning, with higher variance due to the less controlled fabrication procedure[92]. The centrifugal spun fibres form rather 3D-like fluffy layers with higher porosity, improving the cell penetration that is somewhat hampered in case of the 2D-like electrospun layers[91]. The Figure 5 illustrates the basic principles and differences in electrostatic (Figure 5A) and centrifugal (Figure 5B) spinning.

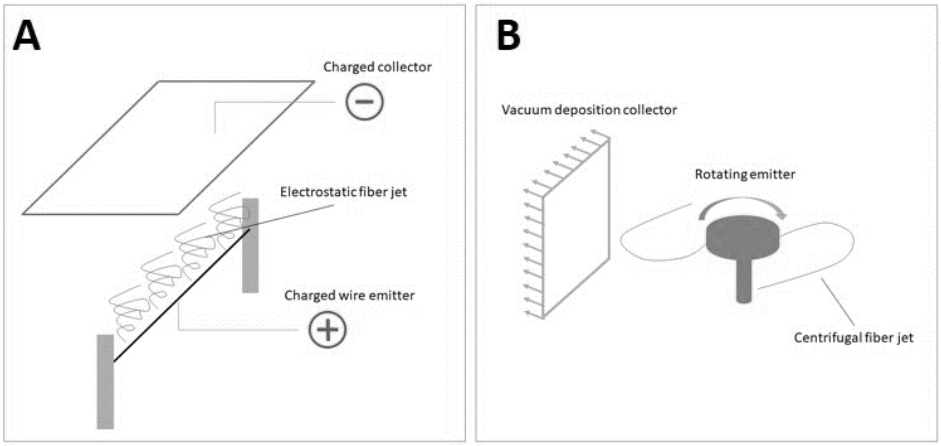

Figure 5 **Schematic illustration of the fibre forming techniques**. A – Scheme of electrostatic spinning illustrates the deposition of polymer fibres formed on a wire electrode and deposited onto a charged collector due to high voltage applied to the wire electrode. B – Scheme of centrifugal spinning illustrates polymer fibres deposited under vacuum from a rotating emitter (Lukasova et al., submitted manuscript).

2.4.3 Functionalization of the fibrous scaffolds with bioactive molecules

To induce the desired cellular response, nanofibres may be functionalized with various bioactive molecules. The half-time of the bioactive molecules is rather low, therefore, various drug delivery systems have been developed to protect the susceptible molecules from the environment and to maintain their sustained release. The process of functionalization may occur during their preparation, leading to blend, coaxial, or emulsion fibres, or by simple adsorption of the bioactive molecules to the surface of the already fabricated nanofibres (Figure 6)[83].

The **surface adsorption of the bioactive molecules** represents a viable post-spinning modification of the nanofibres (Figure 6A). It enables to deliver different bioactive molecules from the same scaffold and, furthermore, the drug is not exposed to any risks arising from the fabrication process (i.e. the high voltage in electrospinning or solvents). The disadvantage of such system is the relatively rapid burst released of the adsorbed molecules[93]. For example, antibiotics were adsorbed to poly-ε-caprolactone electrospun nanofibers. A significant decrease

in post-operative abdominal adhesions was observed in rat model in the antibiotics-loaded nanofibres when compared to the plain nanofibres[94]. Furthermore, the release may be prolonged by a covalent coupling of the drug to the polymer matrix of the scaffold. EGF was chemically immobilized to the surface of PCL/polyethylene glycol (PEG) nanofibres and its effect on wound healing was evaluated in primary keratinocyte culture and *in vivo* in dorsal wound in diabetic mice. The immobilized EGF showed superior healing properties in comparison to the plain PCL and EGF solutions adsorbed to the PCL nanofibres without any chemical modification[95].

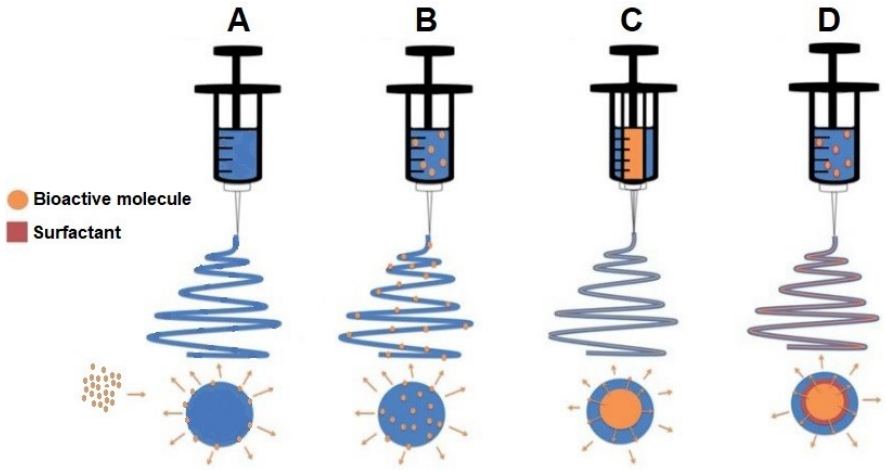

Figure 6 **Nanofibre functionalization with bioactive molecules**. The scheme shows post-spinning adsorption of the bioactive molecules to the surface of the nanofibres (A) and functionalization of the nanofibrous mats during their fabrication: blend electrospinning (B), coaxial electrospinning (C), and emulsion electrospinning (D). Adapted from[69].

Other options include addition of the bioactive molecule to the polymer solution prior to the fabrication of the nanofibres. The release characteristics of the bioactive molecule may be adjusted through the spinning properties. The simplest technique is the **blend spinning** (Figure 6B). The bioactive molecules are simply added to the polymer solution and are later incorporated in the polymer matrix[96]. However, during the spinning process, the bioactive molecules are in contact with the harsh organic solvents and together with the high voltage in case of electrospinning, it may result in changes of the protein conformation or its biological

activity[97]. Furthermore, it was shown that blend electrospinning of a horseradish peroxidase enclosed in liposomes led to their disintegration and release of the enzyme outside of the nanofibres. On the contrary, coaxial electrospinning of the horseradish peroxidase-containing liposomes resulted in increase of the encapsulation efficiency and maintained the bioactivity of the enzyme[84].

Therefore, **coaxial spinning** may be used to protect the susceptible molecules (Figure 6C). Two separate channels for two separate solutions (polymer with an organic solvent and an aqueous phase containing the bioactive molecules) are used, giving rise to nanofibres of a core/shell nature[97]. The process of spinning is so fast the solutions do not mix. Furthermore, by adjusting the core and/or shell polymer characteristics, the release kinetics of the encapsulated molecules may be adjusted[98].

The needle-in-needle setup of the coaxial electrospinning requires special adjustments to the electrode to be made. Therefore, core/shell nanofibres can be fabricated by the **emulsion spinning** technique without the need to adjust the spinning device (Figure 6D). The emulsion is formed by two immiscible fluids (usually a polar and a nonpolar in nature); a surfactant may be added to stabilize the solution. Usually, the aqueous solution containing the bioactive molecules is dispersed in the organic polymer solution. Depending on the amount of the aqueous droplets, they may be interconnected into a continuous core in the core/shell nanofibers[91].

2.5 Platelet-derived bioactive molecules

The process of tissue healing is regulated by a number of cytokines, growth factors and other bioactive molecules, as was described above. The important growth factors include e.g.

VEGF that triggers angiogenesis or PDGF-BB that induces mesenchymal stem cell recruitment to the site of injury. Although the knowledge on the mechanisms and role of the growth factors has advanced greatly, the clinical transfer of synthetic growth factors has been somewhat limited. Some clinical efficacy was shown in clinical trials of PDGF-BB, bone morphogenetic protein-2 (BMP-2), and bone morphogenetic protein-7 (BMP-7)[99], however, there are concerns regarding its safety[100,101] and cost-effectiveness[102]. Furthermore, trying to mimic the complex wound healing cascade using single growth factors would be oversimplified and inefficient[103]. Therefore, platelet-derived bioactive molecules could represent a suitable solution. The rationale for the use of platelet derivatives to promote tissue healing is in their high content of native growth factors and cytokines in physiological ratios[104]. Their translation is further driven by their availability, relative cost-effectiveness[105], autologous nature and applications ranging from dermatology, to orthopaedics and ophthalmology[103].

2.5.1 Platelets

Platelets are multifunctional anucleated cells. Their key role is in haemostasis; however, they also participate in the wound healing cascade. Platelets are shed from the cytoplasm of megakaryocytes in the bone marrow, then they enter the blood circulation. They are of discoid shape and approximately 2.0–4.0 μm in size[106]. In blood, their normal concentration is 150,000–450,000 cells/μL. On average, platelets remain in the circulation for 8 to 10 days; after then, they are sequestered by the spleen and liver[107]. Thanks to their shape and size, they constantly monitor the integrity of the vascular wall. If the endothelial integrity is disrupted and subendothelial components (such as collagen, fibronectin or von Willebrand factor) are exposed, adhesion and activation of platelets occurs, followed by their secretion[106].

Briefly, platelets are anchored to the exposed collagen and von Willebrand factor via the glycoprotein GP IIb/IIIa and GPIa/IIa, respectively, followed by further potentiation of the reaction by the platelet-platelet interaction. Platelets are activated and undergo morphological changes, resulting in a spiny sphere with multiple pseudopod extensions[106]. Finally, platelets release the bioactive molecules contained in their granules. The bioactive molecules contain pro-inflammatory cytokines and chemokines attracting immune cells and stimulatory/inhibitory mediators of cell migration and/or proliferation; the wound healing cascade is initiated[108].

Within platelets, the bioactive molecules are stored in three types of granules: alpha-granules, dense granules, and lysosomes. The alpha-granules (200 to 500 nm) are the most abundant type of granules; there are approximately 50 to 80 granules per platelet, comprising 10% of the platelet volume. There are much fewer dense granules (150 nm), approximately 3 to 6 per one platelet. Finally, the lysosomes are approximately 150 to 300 nm in size[109]. The content of the granules is summarized in Table 1.

Table 1 **Examples of bioactive molecules contained in platelets**. Adapted from[108,110]. RANTES = Chemokine Regulated on Activation, Normal T Cell Expressed and Secreted; MCP-1,-3 = Monocyte chemoattractant protein-1,-3; MIP-1 = Macrophage inflammatory protein-1; VEGF-1,-C = Vascular endothelial growth factor-1,-C; IGF-1, -2 = Insulin-like growth factor -1,-2; FGF = Fibroblast growth factor; PDGF-AA,-AB,-BB = Platelet-derived growth factor-AA,-AB,-BB; EGF = Epidermal growth factor; TGF-β = Transforming growth factor-β; ADP = Adenosine diphosphate; ATP = Adenosine triphosphate.

Granules	Bioactive molecule	Function
Alpha-granules		
Haemostasis	Factors V, XI, and XIII	Thrombin activation, fibrin clot formation
	Plasminogen	Plasmin production
	α_2-antiplasmin	Inactivation of plasmin
Chemokines	RANTES, MCP-1, MCP-3, MIP-1α	Chemotaxis, inflammation modulation
Adhesion Molecules	P-Selectin	Binding and recruitment of leucocytes
	Vitronectin	Cell adhesion, chemotaxis
	Fibrinogen	Fibrin clot formation
Growth factors	VEGF-A, VEGF-C	Angiogenesis
	IGF-1, -2	Cell proliferation, maturation
	FGF	Angiogenesis, fibroblast proliferation
	PDGF-AA, -AB, and –BB	Chemoattraction, cell proliferation
	Thrombospondin	Inhibition of angiogenesis
	EGF	Cell proliferation
	TGF-β	Stimulation of matrix synthesis
Dense granules	ADP, ATP, Serotonin, Ca^{++}, Epinephrine, Histamine	Platelet activation, haemostasis
Lysosomes	Elastase, collagenase, cathepsin	Degradation of ECM, remodelling

2.5.2 Platelet derivatives

Platelet concentrates represent essential therapeutic agents in transfusion medicine. The platelet concentrates are routinely used as a haemostatic tool in case of thrombocytopenia or platelet dysfunction. Generally, the shelf-life of the collected platelet in transfusion products is 5 days[107]. After 5 days, the risk of transmission of a disease is too high and the platelets lose

their haemostatic activity and are considered outdated. There is an overall shortage of the platelet products and yet, even in developed countries, approximately 10 to 20% of the produced platelet concentrates are discarded[111]. Despite the rather rapid loss of their haemostatic function, platelets have been shown to maintain their proliferative potential for up to 21 days[112]. The regenerative potential of platelet derivatives was described more than 40 years ago, when the positive influence of addition of platelets to platelet-poor plasma on stimulation of monkey arterial smooth muscle cells proliferation was described[113]. Since then, various platelet derivatives have been prepared and tested.

Blood consists of various cellular, sub-cellular, and molecular components crucial for the wound healing process and tissue regeneration. In general, it is composed of plasma (containing adhesive proteins such as albumin, fibrinogen or clotting factors, together with electrolytes and growth factors) and red blood cells, white blood cells, and platelets. Blood separation results in the production of various blood derivatives, see Figure 7[114].

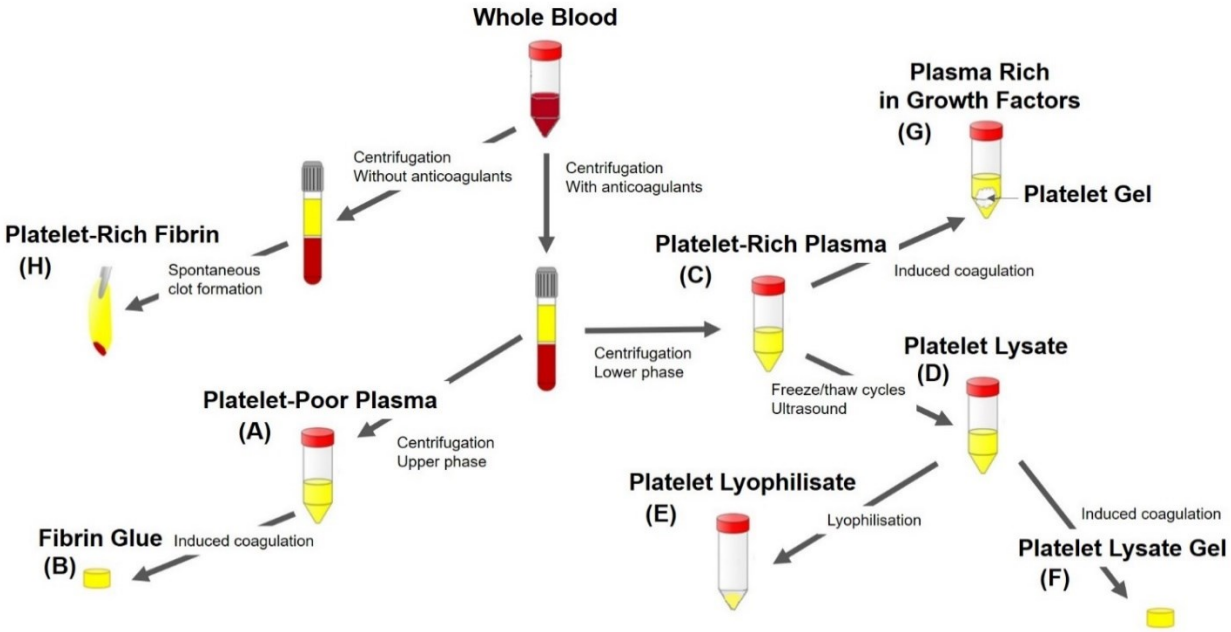

Figure 7 Summarized production of various blood derivatives. Adapted from[114].

The obtained products differ in their content, i.e. in the concentrations of fibrin, leucocytes, and growth factors[114]. Generally, blood derivatives may be classified according to their leucocyte content, fibrinogen/fibrin content and platelet content. The varying composition of the product affects its behaviour. For example, it has been shown that both the leucocyte-rich platelet-rich plasma (PRP) and leucocyte-poor PRP stimulate proliferation of tendon stem/progenitor cells and induce their differentiation into tenocytes, however, the leucocyte-rich PRP induced mainly catabolic, inflammatory changes in the tenocytes, in contrast to the mainly anabolic changes induced by the leucocyte-poor PRP[115]. Similarly, the platelet derivatives rich in fibrinogen/fibrin provide not only stimuli thanks to the bioactive molecules contained in the platelets, but a provisional matrix for the cells as well[114,116]. The lack of standardization of the preparation methods in terms of number of the donors, anticoagulant agent, applied centrifugation speed and its duration, and a potential activation method. All the mentioned parameters affect the resulting blood derivative and the presence, concentration, protection, release, stability and diffusion of the contained bioactive molecules[114].

Generally, during the first step, the whole blood is processed using a “soft spin” (brief centrifugation at low acceleration) to obtain three layers: red blood cells, buffy coat layer (containing platelets and leucocytes) and the platelet-poor plasma (PPP). Then, the platelet-poor plasma together with, depending on the desired final product, the superficial layer of the buffy coat (pure PRP) or the entire buffy coat (leucocyte-rich PRP) are transferred to a new tube. Following a “hard spin” (high acceleration), most of the PPP layer is discarded and the final product is the PRP[117] (Figure 7).

The **platelet-poor derivatives** include the platelet-poor plasma, a liquid of a very low cellular content (Figure 7A). Although the PPP is almost depleted of platelet-derived GFs, it

contains some GFs, such as HGF or IGF-1[118]. By clotting the PPP, the predecessor of today's **fibrin glue** may be formed (Figure 7B). However, the adhesive qualities of the autologous fibrin glues were poor as the concentration of fibrinogen in the PPP was rather low[119]. With the improvement of isolation and concentration techniques of the clotting factors, the fibrin glue systems started to advance. There are several commercial products available in Europe, such as Tisseel® (Vienna, Austria), composed of a fibrinogen solution and a thrombin solution rich in calcium. The commercial fibrin sealants have improved mechanical properties compared to the autologous fibrin glues[120], thanks to the higher fibrinogen content.

Besides their application as haemostatic agents and tissue sealants, fibrin glues have been used as a drug delivery system, owing to its approval by the medical agencies. The properties of the fibrin sealants (fibre diameter, pore size) depend on the crosslinking time that can be varied by the concentration of the two components and by ionic strength of the thrombin solution [121]. Therefore, the release kinetics of the encapsulated bioactive molecules may be modified. Furthermore, fibrin serves as a reservoir for various growth factors[122]. Delivery of bFGF[123] and VEGF[124,125], TGF-β1[126], or PDGF-AB[127] was investigated, together with delivery of lidocaine for post-operative pain reduction[128] or vancomycin to treat difficult infections[129]. Besides drugs, fibrin can be successfully used to deliver cells such as skeletal myofibroblasts[130], human dermal fibroblasts[131–133], or keratinocytes[134,135].

The **platelet-rich plasma** (Figure 7C) is defined as a volume of autologous plasma containing platelets at a concentration above their normal blood range (i.e. 150,000 platelets/μL to 450,000 platelets/μL)[114]. The platelet concentration has a major effect on the GF content and thus the therapeutic outcomes. Therefore, for clinical applications, the working definition of PRP is considered to be 1,000,000 platelets/μL (i.e. 3- to 7-fold increase in the normal blood platelet

concentration)[136]; all suspensions of platelets above the blood baseline are generally termed platelet concentrates.

The PRP may be used directly, or it is possible to activate it by addition of e.g. thrombin or calcium salts. The activation results in formation of a fibrin clot containing the activated platelets (**platelet gel**) and the supernatant contains the released GFs (**plasma rich in growth factors**, PRGF) (see Figure 7G). The content of the GFs released to the supernatant is dependent of the method of activation and may vary[114,118,137,138]. Furthermore, the method of activation and coagulation degree also affect the resulting morphology and mechanical properties of the fibrin clot[139], ranging from supplements of cell culture media[140], to bioactive PRGF-coated dental implants[141] or fibrillar scaffold-like structures for maxillofacial surgery[142]. A similar product, platelet-rich fibrin matrix (PRFM), was prepared by clotting the PRP during a high-speed centrifugation. The resulting PRFM was used to treat non-healing lower-extremities ulcers in a pilot study with promising results in terms of wound closure, as PRFM represents a safe, autologous and easy-to-use adjuvant modality[143]. Furthermore, a study performed in diabetic patients with a chronic non-healing diabetic ulcer compared the efficacy of PRP and PPP. The results showed that the healing of diabetic ulcers was significantly faster in case of PRP vs PPP[144].

Another blood derivative is the **platelet lysate** (PL) (Figure 7D). The platelet lysate is obtained via disruption of the platelet membranes using freeze/thaw cycles or ultrasound, resulting in a liquid rich in bioactive molecules[114]. The PL contains most of the GFs found in the other platelet-rich derivatives, however, the levels of some GFs (e.g. PDGF) are significantly lower[145]. Despite that, the PL offers several advantages: it is easier to standardize its preparation, as it only requires freeze/thaw cycles and no further activators; during the

processing, platelet debris or any clots are removed and thus the solution is highly unlikely to clot spontaneously; it can be frozen and stored for further use[146].

In regenerative medicine, the PL has multiple applications. It may be used in the form of a **platelet lysate gel**, following addition of a clotting agent (see Figure 7F). Platelet lysate gels have been used to treat chronic leg ulcer with encouraging results[147], as a drug/cell delivery system to promote mesenchymal stem cells (MSCs) chondrogenesis[148] or to foster endothelial progenitor cells proliferation and neovascularization[149]. Furthermore, platelet lysate gel was shown to possess antimicrobial activity[150]. The **platelet lysate** may also be loaded into various drug delivery systems to prolong the therapeutic efficacy of the GFs *in vivo*, as their half-time is generally very short (several minutes)[151,152]. Using drug delivery systems, high doses and/or frequent administration of the GFs may be prevented, lowering the toxicity and cost of a such therapy[153].

The platelet lysate also represents the prevailing alternative to the foetal bovine serum (FBS) for *in vitro* expansion of mesenchymal stem cells[154] and multiple other cells[108] in clinical applications. There are several risks associated with the FBS-supplemented cell culture, such as the risk of xeno-immunization, transmission of pathogens, or ethical issues in terms of the FBS collection[155]. The use of platelet lysate enables its large-scale manufacturing due to its possible allogeneic use. As was described above, the method of preparation influences the protein/GFs profile of the resulting products. Additionally, the characteristics of the donor (age, sex, platelet count, and diseases[156]) affect the GF content and the ability of the platelet derivative to induce the desired response[108,155,157]. Thanks to pooling of the platelet lysate, the interindividual variability of the platelet derivatives can be minimized. The storage conditions of the platelet lysate may be further improved by their lyophilisation, resulting in platelet

lyophilisate (Figure 7E); such supplement could provide an “of-the-shelf” product. The lyophilized platelet lysate showed to retain its biological properties when compared to the fresh platelet lysate[158]. Another advantage of the lyophilized platelet lysate is its possible reconstitution in various solvents during fabrication of drug delivery systems, and its possible further concentration.

The final platelet derivative is the **platelet rich fibrin** (PRF) (Figure 7H). The second generation platelet-rich derivative does not require the second centrifugation step and no further clotting agents are added to the mix, as the PRF is produced by spontaneous clot formation[120]. Besides platelets, it also contains red blood cells and white blood cells, however, the determining element responsible for the clinical outcome is the fibrin matrix. The resulting fibrin membranes may be used for superficial cutaneous or mucous healing, however, due to its autologous origin, the amount of the PRF is limited[159]. The PRF shows promising results in healing of osseous defects, as fibrin serves a net for cells and promotes angiogenesis[160]. In chronic wound healing, the effect of PRF on epithelialization was investigated in a randomized clinical trial; no significant differences re-epithelialization rate in PRF vs no intervention were observed[161]. Furthermore, the study of growth factor levels in cell culture with the use of PRP and PRF was conducted and showed, that the PRP contained significantly more GFs vs PRF[162]. On the other hand, the release profiles of the GFs may be significantly different. In PRP, a clear decrease in release of TGF and PDGF was observed after day 1 versus their prolonged release for up to one and two weeks, respectively[163].

2.5.3 Platelet derivatives and drug delivery systems

The half-life of the growth factors (synthetic or natural) is generally very short (order of minutes). *In* vivo, their degradation or deactivation may be caused by their denaturation, oxidation or proteolysis, restricting their bioavailability[114,164]. Similarly to the naturally occurring fibrin matrix, biomaterial matrix would protect the soluble growth factors and prevent their fast clearance and/or diffusion from the site of administration and their degradation in the proteolytic environment[13]. Therefore, platelet derivatives have been combined in numerous applications in regenerative medicine / tissue engineering to control the spatial-temporal release profile of the entrapped growth factors.

Several drug delivery systems were developed and tested in skin tissue engineering, ranging from polymeric micro- and nanospheres to nanofibres, hydrogels and other forms of gels, and their combinations[165]. For example, platelet lysate was successfully adsorbed to the surface of chitosan/chondroitin sulphate nanoparticles. The results showed release of the GFs contained in the platelet lysate for up to one week[153]. Furthermore, it was shown these PL-enriched nanoparticles self-assemble into 3D hydrogel structures at high concentrations. In the system, a strong initial burst release of PDGF-BB and TGF-β1 (92% and 80% respectively) was observed on day 1[166]. Another study examined the loading of platelet-rich plasma (prepared by various centrifugation techniques) into a chitosan freeze-dried scaffolds, resulting either into a PRP-loaded gel or “sponge”. The release of the observed growth factors (PDGF-BB, IGF-1, and TGF-β1) was prolonged to up to 20 days if the PRP was added to the chitosan prior to the freeze-drying and not applied to its surface during post-processing[167].

Polymer nanofibres containing PRP were fabricated. Firstly, blend electrospun chitosan/polyethylene oxide (PEO) nanofibres containing platelet lysate were prepared and used to promote dermal cells proliferation. Although the majority (70%) of the enclosed platelet lysate was released within 3 hours (and the total content of the PL within 24 hours), the fabricated nanofibres fostered keratinocyte proliferation[168]. Coaxial electrospinning of PCL/PRGF solutions and co-electrospinning of a PCL solution and a PRGF solution (one common collector) were compared. The results showed sustained release of the incorporated proteins for up to 35 days, however, the coaxial electrospinning resulted in almost 6-fold increase in encapsulation efficiency when compared to the co-spinning technique[169]. Emulsion electrospinning of dextran-stabilized PRGF into PCL/gelatine nanofibres improved the release characteristics of the nanofibres. Still, a burst release was observed (50% of the enclosed content released approximately by day 5), however, the fibres maintained a sustained release of the observed growth factors (TGF-β1, FGF, and PDGF) for at least 30 days[170]. Furthermore, platelet alpha-granules were encapsulated into PCL/polyvinyl alcohol (PVA)γ core/shell nanofibres. The system was compared with platelets adhered to the surface of the PCL nanofibres; the concentration of TGF-β1 was used as a measure of the GFs released. On day 1, the concentration of the released TGF-β1 was almost 6 times higher vs the incorporated coaxial samples, with the half-time of TGF-β1 release was 7 days. In contrast, the coaxial samples showed delayed release of the encapsulated content (50% of the enclosed TGF-β1 was released by day 14)[171]. These results illustrate that the combination of platelet derivatives with a proper biomaterial may represent a suitable strategy to maximize the therapeutic potential of the plethora of bioactive molecules contained in platelets.

3 AIMS OF THE THESIS

1. To investigate the effect of various bioactive molecules contained in the platelet lysate in skin cell (fibroblasts and keratinocytes) culture in a biomimetic environment with the use of nanofibrous scaffolds. To determine the optimum conditions for skin cell culture and optimize the culture protocols for FBS replacement.
2. To develop a nanofibrous scaffold functionalized with platelets as a source of growth factors with possible application in wound healing and feasible translation to clinical practice. To demonstrate the potential of such system *in vitro*.
3. To develop a platelet lyophilizate-loaded nanofibrous scaffold for long-term delivery of bioactive molecules derived from platelets. To compare two fibre-fabricating technologies, electrospinning and centrifugal spinning. To demonstrate the potential of such systems for tissue engineering applications in an *in vitro* study.

4 EXPERIMENTAL PART

The experimental part of the manuscript is divided into three sections consisting of four experiments.

In the first section of the experiments (Experiment 6.1), platelet lysate as a promising FBS replacement was investigated. Skin cell (fibroblasts and keratinocytes) culture using the platelet lysate was established using the biomimetic environment of electrospun PCL nanofibres. The obtained data confirm the suitability of the platelet lysate as an FBS replacement, highlight its potential for skin cell expansion, and thus, the proposed system composed of PCL nanofibres and PL may represent an efficient tool in skin tissue engineering.

The second section of the experiments (Experiment 6.2) evaluated a simple system consisting of PCL nanofibres and platelets in their native form. Firstly, the PCL nanofibres prepared by electrospinning were functionalized by simple adhesion of platelets to the surface of the nanofibres. The potential of the system was evaluated using the skin cells (fibroblasts, keratinocytes, and melanocytes) and various concentrations of platelets. The main advantage of the platelet-functionalized nanofibres is the more sustained released of the bioactive molecules contained in the platelets, as the half-time of the growth factors itself is very short. Furthermore, the relatively easy preparation enables on-site preparation of the scaffold with the use of patient's autologous platelets and thus potential clinical translation of the system to wound healing applications.

The positive effect of the bioactive compounds contained in the platelets on melanocytes was further investigated in the third experiment of the manuscript (Experiment 6.3). Two fibre-forming technologies (electrostatic and centrifugal spinning) were employed and compared and

the prepared fibrous scaffolds were functionalized with human native platelets. The functionalization of the surface of the centrifugal spun samples resulted in a 2-fold increase in the number of platelets adhered to the surface, and thus in the number of bioactive molecules within the platelets. Furthermore, detectable amounts of thrombospondin-1 and TGF-β1 were detected in the centrifugal spun system with the highest platelet concentration even after 14 days, suggesting a significant improvement of the drug delivery concept.

In the last section (Experiment 6.4), an emulsion-based drug delivery system for regenerative medicine applications was developed. The core/shell electrospun and centrifugal spun nanofibres were enriched by platelet lyophilizate. The lyophilization of the platelet lysate firstly overcomes the issues associated with the short life-span of native platelets and, furthermore, it facilitates the loading of the proteins into the fibrous systems, as it allows the solubilization of the proteins in suitable solvents. The study compared different composition of the fibres and the effect of the differing concentration of platelet lyophilizate released from the fibres on the seeded keratinocytes and fibroblasts. The results of the study indicated that the emulsion core/shell nanofibres are a suitable system for tissue engineering, delivering bioactive proteins in prolonged time scales.

5 MATERIALS AND METHODS

5.1 Scaffold fabrication techniques

The electrospun PCL scaffolds (used in the Experiments 6.1, 6.2 and 6.3) were fabricated using the Nanospider™ NS 500 device (Elmarco, Czech Republic). To perform the electrospinning process, a 24% (w/v) solution of PCL (MW 45,000; Sigma Aldrich, MO, USA) dissolved in a mixture of chloroform and ethanol (volume ratio 9:1) was used. The polymer solution was connected to the high-voltage source (Spellman HV, NY, USA). The voltage used for electrospinning was 70 kV, the distance was set at 35 cm and the polymer flow rate was 50 mL/h. The solution was electrospun using a needleless wire electrode and the nanofibres were deposited on a non-woven supporting Spunbond textile (Pegas Nonwovens, Czech Republic). The conditions during the process were maintained at 23±2 °C and 60±15% relative humidity.

The centrifugal spun PCL scaffolds (used in the Experiment 6.3) were fabricated using a centrifugal spinning device (Cyclone L-1000D Forcespinning® device; FibeRio, TX, USA). To perform the centrifugal spinning process, a 40% (w/v) solution of PCL (MW 45,000; Sigma Aldrich, MO, USA) dissolved in a mixture of chloroform and ethanol (volume ratio 9:1) was used. An orifice G30 at a rotation speed of 6,000 g was used to prepare the layers. The formed fibres were deposited on a non-woven textile (Pegas Nonwovens, Czech Republic) using vacuum-assisted deposition.

The electrospun core/shell samples (used in the Experiment 6.4) were prepared using needleless emulsion electrospinning technique (water-in-oil emulsification, W/O). The shell of the fibres was made of PCL (MW 45,000, Sigma Aldrich, MO, USA) and the core of the fibres

consisted of poloxamer 188 Pluronic F68 (PF-68, Sigma Aldrich, MO, USA) combined with platelet lyophilizate. A 24% (w/v) PCL was prepared dissolving PCL in a mixture of chloroform and ethanol (volume ratio 9:1). Emulsification was performed with water phase containing the platelet lyophilizate dissolved in 50% ethanol and pure ethanol to achieve a core solution of 1% (w/v), 5% (w/v) or 10% (w/v) PF-68. The final core mixture contained 70% ethanol. Control PCL samples were prepared by electrospinning of 24% PCL, as described above. All samples were electrospun using a wire electrode using a Nanospider™ NS 500 device as described above. The precise composition of the samples is shown in Table 2.

The centrifugal spun core/shell samples (used in the Experiment 6.4) were prepared using emulsion centrifugal spinning technology based on W/O emulsification. The shell of the fibres consisted of 40% PCL solution and the core of the fibres consisted of poloxamer 188 Pluronic F68 (PF-68, Sigma Aldrich, MO, USA) combined with platelet lyophilizate. The precise composition of the samples is given in the Table 2. The 30% (w/v) PF-68 dissolved in 90% ethanol was mixed with the platelet lyophilizate dissolved in 50% ethanol and pure ethanol, to achieve a solution of 1% (w/v), 5% (w/v) or 10% (w/v) PF-68. The mixing process was performed by drop-wise mixing of the lyophilizate to the agitated PF-68 solutions, followed by sonication. The final core mixture contained 70% ethanol. The mixture of PF-68 and the platelet lyophilizate was subsequently emulsified with 50% PCL dissolved in chloroform to obtain 40% PCL solution in a mixture of chloroform and ethanol at a volume ratio of 4:1. The ethanol phase was added drop-wise under stirring. The prepared emulsion was immediately processed by the centrifugal spinning process. The control sample was prepared by the spinning of 40% (w/v) PCL in a mixture of chloroform and ethanol at a volume ratio of 4:1. The centrifugal spinning was performed using the centrifugal spinning technology of the Cyclone L-1000D device

(FibeRio, TX, USA). All samples were processed by G30 needles at 11,000 RPM and a collector distance of 10 cm. The fibres were collected using a vacuum assisted deposition system to prepare more condensed samples.

Table 2 **Precise composition of the fabricated electrospun and centrifugal spun samples**.

Sample	Core polymer	Shell polymer	Platelet lyophilizate
ES1	1% PF-68	24% PCL	15 mg/mL
ES5	5% PF-68	24% PCL	15 mg/mL
ES10	10% PF-68	24% PCL	15 mg/mL
ES Control	---	24% PCL	---
CS1	1% PF-68	40% PCL	15 mg/mL
CS5	5% PF-68	40% PCL	15 mg/mL
CS10	10% PF-68	40% PCL	15 mg/mL
CS Control	---	40% PCL	---

5.2 Scaffold characterization using scanning electron microscopy

The structure of the scaffolds fabricated in the Experiments 6.1, 6.2, 6.3 and 6.4 was visualized using scanning electron microscopy (SEM). The dry samples were sputter coated with gold using an Q150RS device (Quorum, UK). Vega3 SBU (Tescan, Czech Republic) microscope was used for image acquisition. The fibre diameter and pore size of the prepared samples was determined using ImageJ software from at least 200 independent measurements.

5.3 Scaffold characterization via Fourier-transformation infrared spectroscopy

The presence of the embedded platelet lyophilizate in the Experiment 6.4 was confirmed using Fourier-transformation infrared spectroscopy with attenuated total reflectance (FTIR-ATR). The testing was performed on IRaffinity 1 system (Shimadzu, Japan). All samples were

moulded into tablets by 2t press. The measurement was performed in the range of 500–4,200 cm^{-1} with Happ-Gazel apodization.

5.4 Functionalization of the fibrous scaffolds with native platelets

The surface of the prepared electrospun and centrifugal spun PCL samples was functionalized with different concentrations of platelets. The fabricated PCL samples (diameter 6 mm) were punched out of the fibrous matts. The samples were sterilized using 70% ethanol and rinsed with PBS (three times). Fresh human leukocyte-poor platelet concentrate derived from buffy-coat (in additive solution) was obtained from Blood Transfusion Service (Šumperk, Czech Republic). The bag was prepared from blood of four donors. The platelet concentration in the bag in the case of Experiment 6.2 was $1{,}030 \times 10^9$ platelets/L, the platelet concentration in the bag in the case of Experiment 6.3 was 967×10^9 platelets/L. The platelet concentrations in the Experiment 6.2 are given in Table 6, the platelet concentrations in the Experiment 6.3 are given in the

. The solutions containing the appropriate concentration of platelets were prepared by diluting the platelet concentrate in SSP+ additive solution (Macopharma, France). In case of a solution with platelet concentration higher than the platelet concentration in the bag (Experiment 6.3), the platelet concentrate was firstly centrifuged (3,100 g for 10 minutes) and then resuspended in the appropriate volume of SSP+ to obtain the desired platelet concentration. Finally, 50 µl of the prepared solutions were added to the sterile nanofibrous samples in a 96-well plate. The samples were incubated for 2 hours at a temperature of 22 °C. Afterwards, the samples were washed with PBS and placed into new wells.

5.5 Platelet lysate preparation

Platelet lysate was prepared for use in the Experiment 6.1. Fresh human leukocyte-poor platelet concentrate derived from buffy-coat (in additive solution) was obtained from blood transfusion service (Šumperk, Czech Republic). The platelet concentration in the bag was $800x10^9$ platelets/L. The bag was prepared from the blood of 16 donors to minimize interindividual differences. Platelet lysate (PL) was prepared using the freeze-thaw method. Briefly, the entire bag was frozen (-80 °C) and thawed (37 °C) three times in total to disrupt the platelets. Then, the solution was centrifuged (4,100 g for 15 minutes) to dispose of the cellular debris. The PL was stored at -80 °C until use.

5.6 Platelet lyophilizate preparation

Platelet lyophilizate was prepared for the Experiment 6.4. Fresh human leukocyte-poor platelet concentrate derived from buffy coat in additive solution was obtained from a blood transfusion service (Šumperk, Czech Republic). The platelet concentration in the bag was $917x10^9$ platelets/L. The bag was prepared from blood of four donors. The platelets were centrifuged (3,100 g, 10 minutes) and resuspended in distilled water. Subsequently, the solution was aliquoted, frozen (-80 °C) and thawed (37 °C) three times in total to disrupt the platelet cellular membranes. The platelet lysate was centrifuged (4,100 g for 15 minutes) to get rid of the cellular debris. Subsequently, the platelet lysate was lyophilized under 480 mTorr (VirTis BenchTop Pro Freeze Dryer, SP Scientific, PA, USA) for 24 hours. The lyophilized platelet lysate (platelet lyophilizate) was stored at -80 °C until use.

5.7 Bioplex analysis of bioactive molecules contained in platelets

To characterize the cytokine content in the platelet lysate (Experiment 6.1), platelets (Experiment 6.3), and platelet lyophilisate (Experiment 6.4), the Bio-Plex 200 Multiplex System (Bio-Rad Laboratories, CA, USA) was employed. The commercially available cytokine panel (Bio-Plex ProTM Human Cytokine 27-plex Assay, Bio-Rad Laboratories, CA, USA) was used, in accordance with the manufacturer's instructions. The assay allows multiple cytokines to be quantified simultaneously in one well. The following cytokines were quantified: interleukin-1b (IL-1b), interleukin 1ra (IL-1ra), interleukin-2 (IL-2), interleukin-4 (IL-4), interleukin-5 (IL-5), interleukin-6 (IL-6), interleukin-7 (IL-7), interleukin-8 (IL-8), interleukin-9 (IL-9), interleukin-10 (IL-10), interleukin-12 (IL-12), interleukin-13 (IL-13), interleukin-15 (IL-15), interleukin-17 (IL-17), granulocyte-colony stimulating factor (G-CSF), granulocyte-macrophage colony stimulating factor (GM-CSF), interferon-gamma (INF-γ), tumour necrosis factor-α (TNF-α), monocyte chemoattractant protein-1 (MCP-1), CXCL10 chemokine (C-X-C motif ligand-10), macrophage inflammatory protein-1a (MIP-1a), MIP-1b (C-C motif ligand-4, CCL-4), RANTES, eotaxin (CCL-11), platelet-derived growth factor (PDGF), basic-fibroblast growth factor (bFGF), and vascular endothelial growth factor (VEGF).

5.8 Determination of total protein content

The protein content in the platelet lysate (Experiment 6.1) and platelet lyophilizate (Experiment 6.4) was determined using Quant-iT™ Protein Assay Kit, (Invitrogen Life Technologies, CA, USA) in accordance with the manufacturer's instructions.

To determine the release profiles from the platelet lyophilizate-containing samples in the Experiment 6.4, total protein released from the samples was determined. The samples were

weighed (80 mg) and to each sample, 500 µL of PBS was added. The samples were kept at 37 °C. On day 1, 3, 7 and 14 of the experiment, the PBS was collected, frozen (-80 °C) and replaced by new PBS. The concentration of total protein released from the samples was determined using Quant-iT™ Protein Assay Kit, (Invitrogen Life Technologies, CA, USA) in accordance with the manufacturer's instructions

5.9 Growth factor release from the platelet-functionalized samples

To determine the release profiles of growth factors from the platelet-functionalized samples in the Experiment 6.2, EGF was chosen as a model molecule. On day 1, 3, 7 and 14 of the experiment, cell culture media were collected and frozen (-80 °C). The concentration of EGF released from platelets and/or synthetized by the seeded cells was quantified by the enzyme-linked immunosorbent assay (ELISA) in accordance with the manufacturer's instructions (DuoSet®; R&D Systems, MN, USA).

To determine the release profiles of growth factors from the platelet-functionalized samples in the Experiment 6.3, TSP-1 was chosen as a model molecule. The samples were weighed (80 mg) and to each sample, 500 µL of PBS was added. The samples were kept at 37 °C. On day 1, 3, 7 and 14 of the experiment, the PBS was collected, frozen (-80 °C) and replaced by new PBS. The concentration of TSP-1 released from platelets adhered to the electrospun and centrifugal spun samples was quantified by the enzyme-linked immunosorbent assay (ELISA) in accordance with the manufacturer's instructions (DuoSet®; R&D Systems, MN, USA).

5.10 Cell culture & cell seeding

Murine XB2 cell line (keratinocytes) and murine melan-a cell line (melanocytes) were purchased from the Welcome Trust Functional Genomics Cell Bank at St. George's, University of London, 3T3-A31 cell line (fibroblasts) from Sigma-Aldrich (MO, USA). The cells were cultured in a humidified incubator (37°C, 10% CO2 and 80–90% relative humidity). Keratinocytes and fibroblasts were cultured in Dulbecco's Modified Eagle's Medium (DMEM) supplemented with 10% FBS (Sigma Aldrich, MO, USA) and penicillin/streptomycin (100 IU/ml, 100 µg/ml respectively) mixture. Melanocytes were cultured in RPMI-1640 medium supplemented with 10% FBS (Sigma Aldrich, MO, USA), penicillin/streptomycin (100 IU/ml, 100 µg/ml respectively), 2 mM L-glutamine and 200 nM TPA (12-O-Tetradecanoylphorbol-13-acetate) mixture. Sub-confluent cells were washed with PBS-EDTA solution and treated with 0.05% trypsin. The scaffolds were seeded with cells at densities given in Table 3. The cell culture medium was supplemented with 10% FBS or 5% FBS during the experiment (precise cell medium composition is given in Table 3).

Table 3 **Summary of cell culture conditions**. Cell culture conditions, sterilization techniques and cell seeding densities of the individual experiments.

Experiment	Scaffold sterilization	FBS content in medium	Cells	Seeding density (cells/cm^2)	Medium change
6.1	70% ethanol	10%	Fibroblasts Keratinocytes	14,200 14,200	Every 3 to 4 days Total volume
6.2	70% ethanol	10%	Keratinocytes Fibroblasts Melanocytes	7,800 7,800 12,500	Every 7 days Half of the volume
6.3	70% ethanol	10%	Melanocytes	17,850	Every 7 days Half of the volume
6.4	Ethylene oxide	5%	Fibroblasts Keratinocytes	17,850 17,850	Every 7 days Half of the volume

5.11 Cell metabolic activity testing

On experimental days, the metabolic activity of cells was determined using the MTS assay (CellTiter96® AQueous One Solution Cell Proliferation Assay; Promega, WI, USA). To each scaffold, 20 µl of MTS solution and 100 µl of fresh medium were added. After incubation (37°C, 10% CO2, 80-90% relative humidity; 2-hour for keratinocytes and fibroblasts, 3-hour for melanocytes) the absorbance of the media was detected at 490 nm with a microplate reader (Infinite® M200 PRO; Tecan, Switzerland). The background absorbance (690 nm) was subtracted from the measured data, as well as the absorbance of plain media. Platelets contain mitochondrial enzymes and thus metabolize the MTS substrate. To exclude misrepresentation of the cell metabolic activity due to the presence of platelets on the surface of nanofibres, an MTS assay of samples with platelets was performed (for Experiment 6.2 and 6.3). The detected absorbance was subtracted from the measured data. The summary of performed tests and experimental days within the individual experiments is given in Table 4.

5.12 Cell proliferation testing

Cell proliferation was determined on the experimental days using a fluorescence-based kit (Quant-iT™ PicoGreen® dsDNA Assay Kit, Invitrogen Life Technologies, CA, USA). The samples used for the MTS assay were transferred to cell lysis buffer (10 mM Tris, 1 mM EDTA, 0.2% v/v Triton X-100). To facilitate the cell lysis and DNA release, the samples underwent three freeze/thaw cycles. In between the cycles, the samples were vortexed. Fluorescence intensity was detected using the microplate reader (Infinite® M200 PRO; Tecan, Switzerland; λex = 485 nm, λem = 528 nm) and the DNA content was determined according to the λDNA

calibration curve of the kit. The summary of performed tests and experimental days within the individual experiments is given in Table 4.

5.13 Melanin content determination

Melanin content on the scaffolds was determined using the alkali extraction method in the Experiment 6.2 on day 1, 3, 7 and 14. The nanofibrous samples with seeded cells were transferred to 300 µl of 1 M NaOH and incubated for 2 hours at 80 °C. Afterwards, the samples were vortexed to facilitate solubilization of melanin and centrifuged (10,000 g, 1 minute, MiniSpin®, Eppendorf) to sediment the PCL debris. Absorbance of the supernatant was detected at 405 nm using a microplate reader. The melanin content on the scaffolds was determined according to a calibration curve (synthetic melanin, Sigma-Aldrich, MO, USA).

5.14 Cell visualization using confocal microscopy

Confocal microscopy was used to visualize the cells. The cells seeded on scaffolds were fixed with methanol (-20°C), rinsed with PBS and stained. DiOC6(3) was used to visualize the cellular membranes (1 µg/ml in PBS, 30 minute) and propidium iodide (5 µl/ml, 10 minute) to visualize the cell nuclei. Between the incubations the samples were rinsed with PBS. A Zeiss LSM 510 DUO confocal microscope was used for imaging (λex maximum = 488 nm, λem maximum = 501 nm for DiOC6(3); λex maximum = 536 nm, λem maximum = 617 nm for propidium iodide). In case of melanocytes, confocal images were merged with images scanned in visible light to visualize the melanin present on the scaffolds.

5.15 Cell visualization using scanning electron microscopy

To visualize the cells adhered on the scaffolds, SEM was used. Platelets adhered to the surface were visualized after 2-hour incubation in Experiments 6.2 and 6.3. The keratinocytes and fibroblasts cultured on the platelet-lyophilizate scaffolds were visualized using SEM on day 7 in Experiment 6.4. The samples were fixed with 2.5% glutaraldehyde (Sigma-Aldrich, MO, USA) at 4 °C. After 2 hours, the samples were dehydrated with ethanol changes (35%, 48%, 70%, 96% and 100% ethanol). Hexamethyldisilazane (Sigma-Aldrich, MO, USA) was used to remove any residual water from the samples. The samples were sputter-coated with gold (app. 30 nm) and visualized using Vega 3 SBU microscope (Tescan, Czech Republic).

5.16 Statistical analysis

The acquired data were statistically evaluated using SigmaStat 3.5 software. To test the normality of the data Kolmogorov-Smirnov test was used; to test the equality of variances Levene's test was used. In case the data passed the normality test and the test of equality of variances, statistical significance between a pair of groups was determined using ANOVA testing. Tukey's comparative test was used for post-hoc analysis. Statistical significance between a pair of groups without normal distribution was determined by conducting Kruskal-Wallis test and using Dunn's multiple comparisons test for post hoc analysis. The data are presented as a mean value plus/minus standard deviation. A value of $p<0.05$ was considered statistically significant.

5.17 Summary of performed tests

For the sake of clarity, the performed tests in the individual experiments are summarized below in Table 4.

Table 4 **Summary of the tests performed within the individual experiments**. D1 stands for day 1 etc.

Experiment	Metabolic activity	Proliferation	Confocal microscopy	SEM	Release characteristics
6.1	D1, D3, D7, D10	D1, D3, D7, D10	D1, D7, D10	---	---
6.2	D1, D3, D7, D14	D1, D3, D7, D14	D1, D7, D14	Scaffolds with platelets after 2-hour incubation	D1, D3, D7, D14
6.3	D1, D3, D7, D14	D1, D3, D7, D14	D7, D14	Scaffolds with platelets after 2-hour incubation	D1, D3, D7, D14
6.4	D1, D3, D7, D14, D17	D1, D7, D14, D17	D7, D17	D7	D1, D3, D8, D14, D24, D31

6 RESULTS AND DISCUSSION

6.1 Platelet lysate as a serum replacement

Given the issues associated with the use of xenogeneic FBS for human cell expansion in clinical practice, a possible FBS alternative was investigated. Platelet lysate was used to verify the effect of the growth factors contained in the platelets on skin cells. Platelet lysate was used as an FBS replacement (cell culture medium supplemented with platelet lysate only) and in combination with FBS (cell culture medium supplemented with combination of platelet lysate and FBS). Different platelet lysate and FBS concentrations were used and their effect was evaluated. The skin cells (murine keratinocytes XB2, fibroblasts 3T3-A31, and melanocytes melan-a) were cultured on PCL nanofibres prepared by needleless electrospinning, to mimic the natural microenvironment of the cells. For simplicity, Table 5 illustrates the names of the samples used within the manuscript.

Table 5 **Summary of sample coding used in the manuscript.**

Sample	**FBS content (%, v/v)**	**Platelet lysate content (%, v/v)**
0F2.5L	0%	2.5%
0F5L	0%	5%
0F7L	0%	7%
0F10L	0%	10%
10F0L	10%	0%
5F2.5L	5%	2.5%
5F5L	5%	5%
5F7L	5%	7%
5F10L	5%	10%
5F0L	5%	0%

6.1.1 Characterization of the scaffold

The structure of the fabricated PCL nanofibrous scaffolds were visualized using scanning electron microscopy. The stereological measurements in the ImageJ software showed a combination of nano- and microfibres with minimum of non-fibrous defects. The mean diameter of the thin nanofibrous fraction was 229 ± 79 nm, and the thicker fibres had a mean diameter of 579 ± 133 nm. In addition, a fraction of less abundant microfiber fraction was detected with a mean diameter of 2,442 ± 925 nm. The porosity of the nanofibrous scaffold was determined to be 38 ± 3%.

6.1.2 Characterization of the platelet lysate

The content of the platelet lysate was characterized. The total protein, albumin and fibrinogen levels were determined, together with specific mediators using the XMAP technology and ELISA (Figure 8).

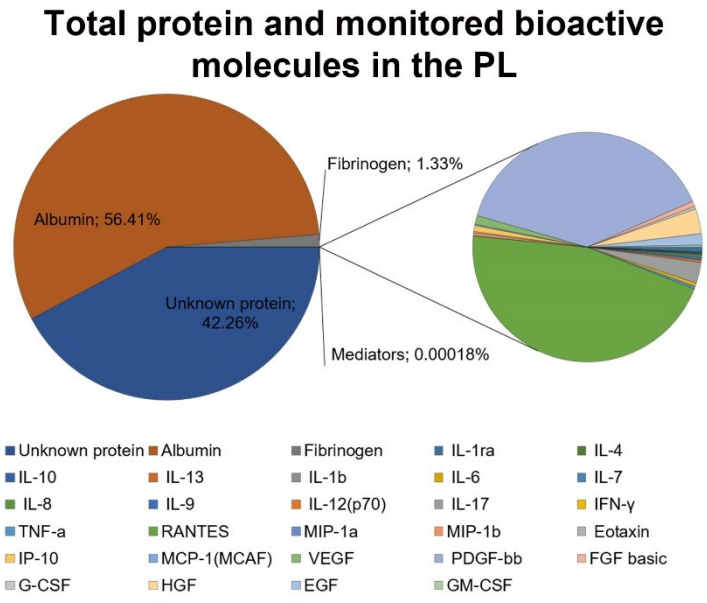

Figure 8 **Proteins and specific mediators contained in the platelet lysate**. Graphical illustration of the relative composition of the assayed proteins and mediators in the platelet lysate[172].

The Figure 8 illustrates that the concentrations of the monitored bioactive molecules were negligible in comparison to the total protein content of the platelet lysate. Nevertheless, most of the monitored analytes occurred at concentrations sufficient to fulfil their physiological functions.

The platelet lysate contained various anti-inflammatory and pro-inflammatory cytokines, chemokines, and growth factors. The most abundant anti-inflammatory cytokine was IL-1ra (235.87 ± 4.77 pg/mL), a cytokine known to modulate a variety of immune and inflammatory responses. Other anti-inflammatory interleukins, such as IL-4, IL-10 and IL-13, were found at significantly lower concentrations. Similar concentrations of pro-inflammatory interleukins, such as IL-8, IL-9, IL-12, and IFN-γ and TNF-α, were detected (100–200 pg/mL). High concentration of interleukin 17 was observed (1,022.52 ± 56.43 pg/mL). However, very low concentrations of other pro-inflammatory cytokines (IL-1b, IL-6, IL-2, IL-5, IL-15), anti-inflammatory cytokines (IL-4 and IL-13) and MIP-1a were observed. RANTES was the most abundant cytokine found in the platelet lysate. Its concentration was 10,000-times higher when compared to the concentration of other cytokines and chemokines. Additionally, there were growth factors detected in the PL. The most abundant growth factor detected was PDGF-BB. Furthermore, EGF and HGF were present at concentrations higher than 500 pg/mL. The analysis showed that the concentrations of GM-SCF and G-CSF were low compared to the concentration of other growth factors. The Figure 9 summarizes the concentrations of the assayed pro-inflammatory and anti-inflammatory mediators together with the concentrations of chemokines and other growth factors.

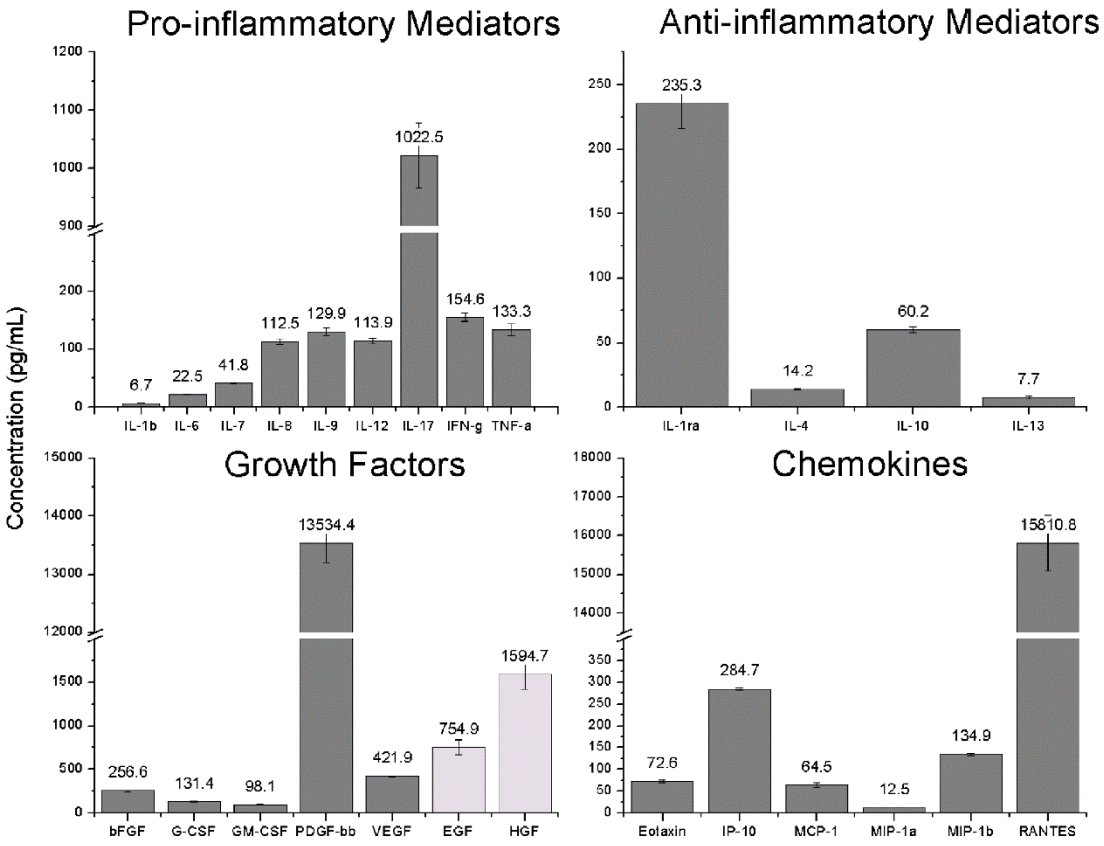

Figure 9 **Concentration of the assayed mediators in the platelet lysate**. The mediators detected using the XMAP technology are depicted in dark grey colour, the mediators detected using ELISA in light grey colour[172].

Up to now, platelet lysate is one of the most promising FBS replacements, being used in various cell types culture ranging from hMSC to myofibroblasts and fibroblasts[173–176]. However, it suffers from considerable donor-to-donor variability. The variability was tested in hMSC culture, showing significant differences in hMSC proliferation when supplemented with PL from various patients[177]. To reduce the variability, the platelet lysate used in our studies was prepared from 16 donors. Bioactive molecules contained in the PL concentrations were determined using a multiplex XMAP technology. Another study used the multiplex assay to evaluate the content of the bioactive molecules in PRP[178]. Their analysis detected very similar levels of most of the anti- and pro-inflammatory cytokines, chemokines and growth factors, with the differences attributing to the donor-to-donor variability. The study investigated samples from

10 female donors and 6 male donors. The only significant difference was detected in the levels of PDGF-BB, with PDGF-BB levels being significantly higher in male donors when compared to the female donors. This may be explained by the fact that the platelet function may be influenced by gender, race or diet[179].

The proper ratio of pro- and anti-inflammatory cytokines, chemokines and growth factors is crucial for the precise regulation of physiological healing. The most abundant anti-inflammatory cytokine was IL-1 receptor antagonist (IL-1ra). The lack of IL-1ra leads to prolonged inflammation and causes a delay in the wound healing process[180]. Very similar proportion of anti-inflammatory cytokines, with IL-1ra present at the highest concentration, was observed in the PRP[178].

Pro-inflammatory cytokines such as IL-1b and IL-6 were observed at low concentrations in the PL. The most abundant pro-inflammatory cytokine detected in the PL was IL-17. IL-17 mediates pro-inflammatory responses and contributes to neutrophil and monocyte recruitment. Recent studies assume that IL-17, derived from innate and adaptive sources, may act against various pathogens at different phases and locations of infection, pointing out the complexity of immune response[181]. Furthermore, IL-17 and TNF modulate expression of melanocyte mitogens (CXCL1, IL-8, IL-6, CXCL2, CXCL3 or BDNF), which may affect proliferation and growth of melanocytes[182].

The most abundant chemokine was RANTES. It plays role in attraction of many different cell types and accelerates the regenerative processes[183]. RANTES plays an active role in recruiting T-cells, eosinophils, basophils, and in the activation of natural killer cells at the site of inflammation. A similarly high concentration of RANTES was measured not just in our PL,

but also in the PRP. In the PRP, the RANTES concentration was even 2-times higher than in the PL[178,184].

Furthermore, the PL contained various growth factors that are essential for stimulation of skin cell proliferation and ECM production. For example, PDGF-BB, which plays an important role in wound healing, re-epithelization and tissue remodelling**,** was found at the highest concentration[185]. Interestingly, the concentration detected in the platelet lysate was almost 10-times higher when compared to the PDGF-BB levels detected in the PRP[178]. The levels of PDGF-BB were established also in PRGF, where similar results in PDGF-BB concentrations were observed[118]. Furthermore, EGF was detected at a concentration higher than 500 pg/mL, which was in concordance with levels detected in the PRGF when expressed as the amount of EGF per 10^6 platelets[118]. EGF significantly stimulates keratinocyte proliferation and enhances their migration in acute wounds[29]. During angiogenesis, endothelial cells can undergo proliferation, which is stimulated by the vascular endothelial growth factor (VEGF), IL-8, and eotaxin[186,187]. The observed differences among the various preparations further reinforce the need for standardization of the preparation procedure in order to make any comparisons feasible[118,178].

6.1.3 In vitro activity of fibroblasts supplemented with platelet lysate

The effect of the platelet lysate was on the cultured fibroblasts was determined by measurement of the metabolic activity of the cells (Figure 10A).

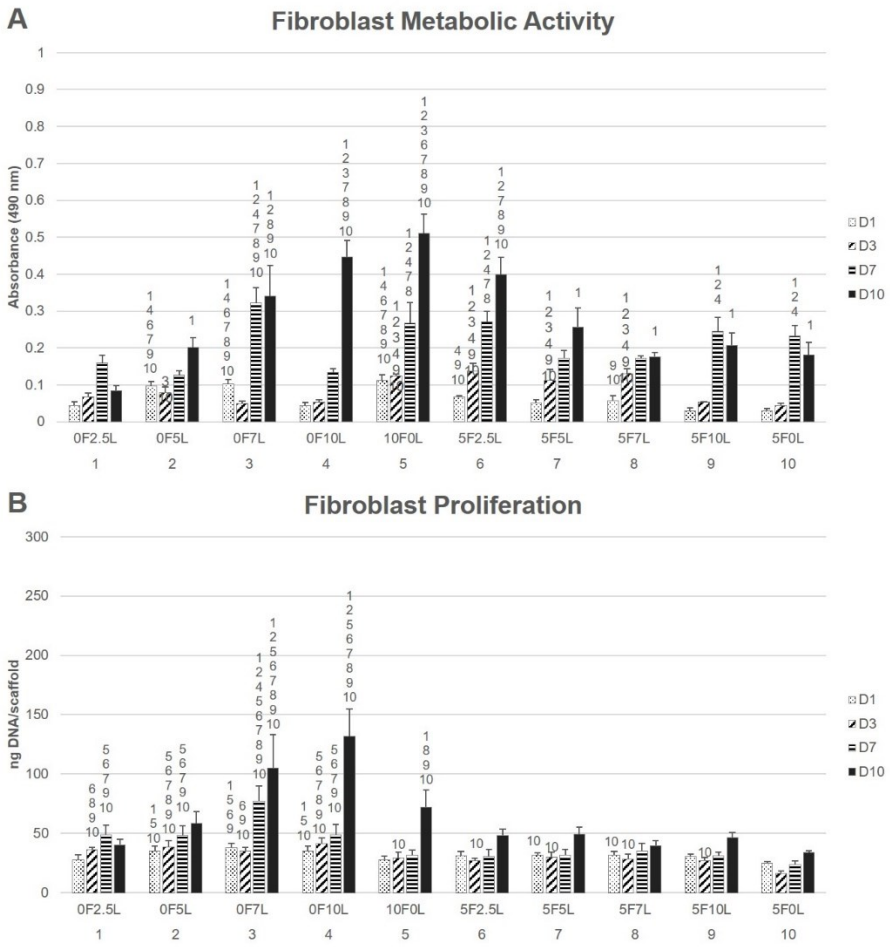

Figure 10 **Metabolic activity and proliferation of fibroblasts**. A – Metabolic activity of fibroblasts was measured by MTS assay (statistical analysis $p < 0.05$), B – Proliferation of fibroblasts determined by PicoGreen® assay (statistical analysis $p < 0.05$). The sample name (XFYL) codes the supplement concentration in the medium; X stands for concentration of FBS (v/v), Y for concentration of PL (v/v). The numbers above the bars indicate statistical significance[172].

The metabolic activity was gradually increasing in the groups 0F10L, 10F0L, 5F2.5L, 5F5L and 5F7L. The viability of the cells cultured in groups supplemented with 0F2.5L, 5F10L and 5F0L increased until day 7, and then rather stagnated or declined. The results indicated that 7% platelet lysate or higher was sufficient to replace the FBS. There was no statistically significant difference between the groups containing either 10% FBS (10F0L) or 10% platelet lysate (0F10L). In the groups containing the combination of FBS and PL, a lower concentration of PL (up to 7%) resulted in improved cell viability until day 3, whereas in the group with the highest concentration of PL (5F10L), the cell metabolic activity rapidly increased on day 7.

Furthermore, it was shown that low concentration (2.5%) of PL in combination with 5% FBS (5F2.5L) yielded better effect in regard to the metabolic activity of fibroblasts compared to the samples with a higher concentration of lysate when combined with FBS. We assume that the higher concentrations of growth factors and bioactive molecules contained in FBS and the PL resulted in rather inhibitory effect in the fibroblast culture.

Additionally, proliferation of fibroblasts seeded on the electrospun nanofibrous PCL scaffolds was determined (Figure 10B). The most pronounced proliferation of the 3T3 fibroblast was detected in groups containing high concentration of either FBS or the platelet lysate, i.e. in the groups 0F7L, 0F10L and 10F0L. The groups with a combination of FBS and PL, or 5% FBS and low concentrations of PL (0F2.5L and 0F5L) alone, showed low proliferation activity throughout the entire experiment. The results were in concordance with the results of the MTS assay, and showed that 7% and higher concentration of PL could stimulate fibroblast proliferation better than the 5% FBS.

Confocal microscopy was used to visualize the cells adhered to the nanofibrous scaffolds. The cells were well spread on the scaffold, exhibiting morphology typical for fibroblasts (Figure 11). According to the images, the bioactive molecules supported gradual proliferation from day 1 until day 10. In the case of the FBS-free groups, the cells supplemented with a low concentration of lysate (0F2.5L, 0F5L), exhibited clustering of the cells, indicating unfavourable culture conditions.

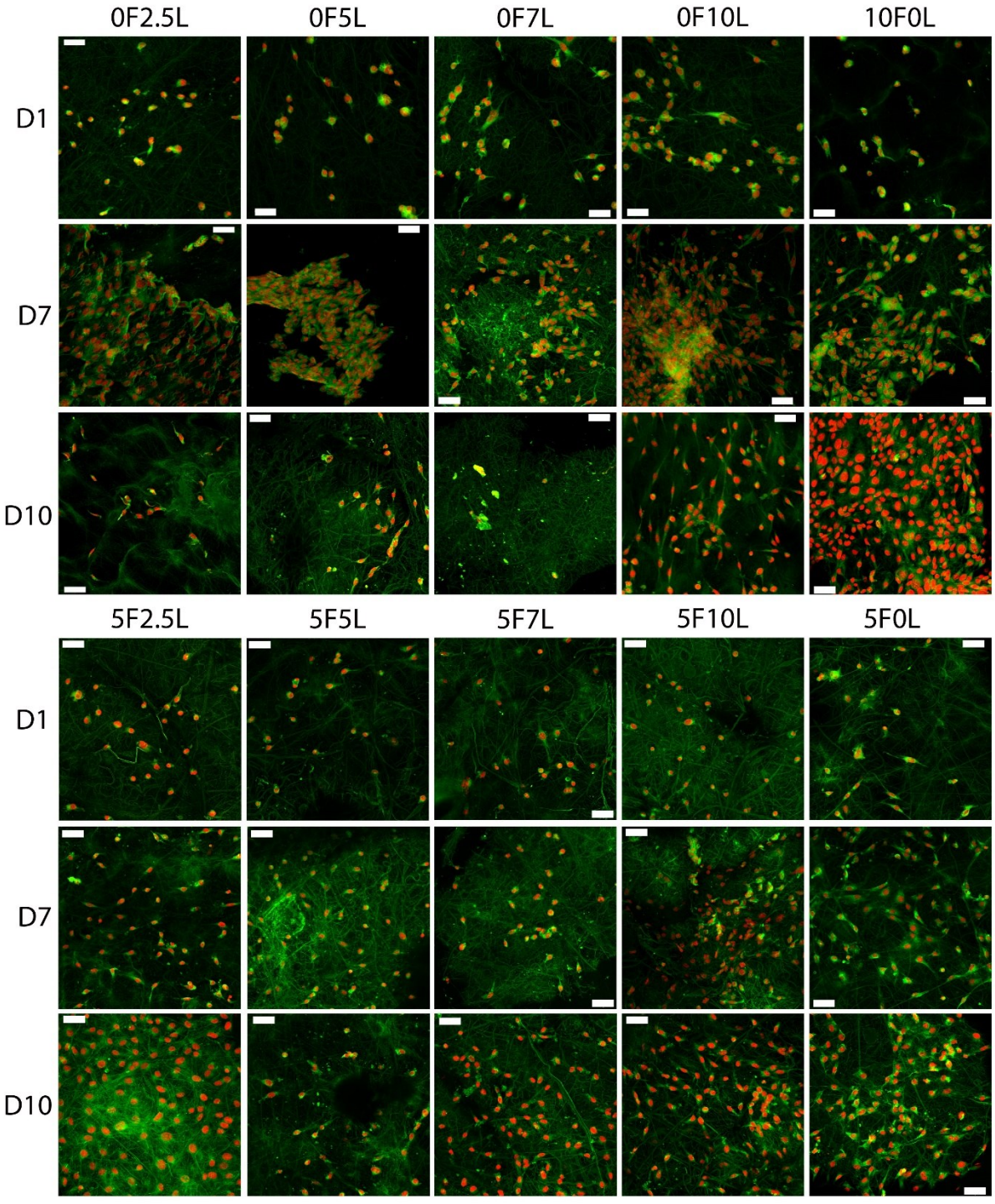

Figure 11 **Confocal microscopy images of the fibroblasts seeded on the PCL scaffolds**. The fibroblasts were observed on day 1, 7 and 10. Green colour depicts cellular biologic membranes (staining by DiOC6(3)), red colour cell nuclei (propidium iodide staining). Magnification 200x, scale bar 50 μm. The sample name (XFYL) codes the supplement concentration in the medium; X stands for concentration of FBS (v/v), Y for concentration of PL (v/v)[172].

The obtained data indicate that the concentration of PL higher than 7% (v/v) promoted cell metabolic activity and proliferation and thus was suitable as an FBS replacement. However, the combination of FBS and the platelet lysate resulted in inhibition of the cultured fibroblasts. The effect of different concentrations of PL in a serum free-medium was investigated, in comparison with medium supplemented with the FBS for fibroblasts expansion. The study showed that the attachment of the cells to the plastic surface of a culture plate was faster in the case of FBS, however, the population doubling time was longer than in the PL-supplemented medium[188]. Another study investigated the effect of various concentrations of PL when added to a medium containing FBS and a serum-free medium. The results showed a dose-dependent effect of the PL, with a more pronounced stimulatory effect in the serum-free medium[189]. The dose-dependent effect of PL was confirmed also by our data showing dose-dependent proliferation of fibroblasts cultured in a medium supplemented with PL only and with combination of FBS and PL. The positive effect in the serum free-medium was increasing with the increasing PL concentration, while increasing concentration of the PL in the medium containing FBS resulted in decrease in the cell metabolic activity and proliferation.

6.1.4 In vitro activity of keratinocytes supplemented with platelet lysate

To investigate the effect of platelet lysate in keratinocytes culture, keratinocytes were seeded on PCL scaffolds and the culture was supplemented with platelet lysate and/or FBS. The metabolic activity and proliferation of keratinocytes was determined (Figure 12).

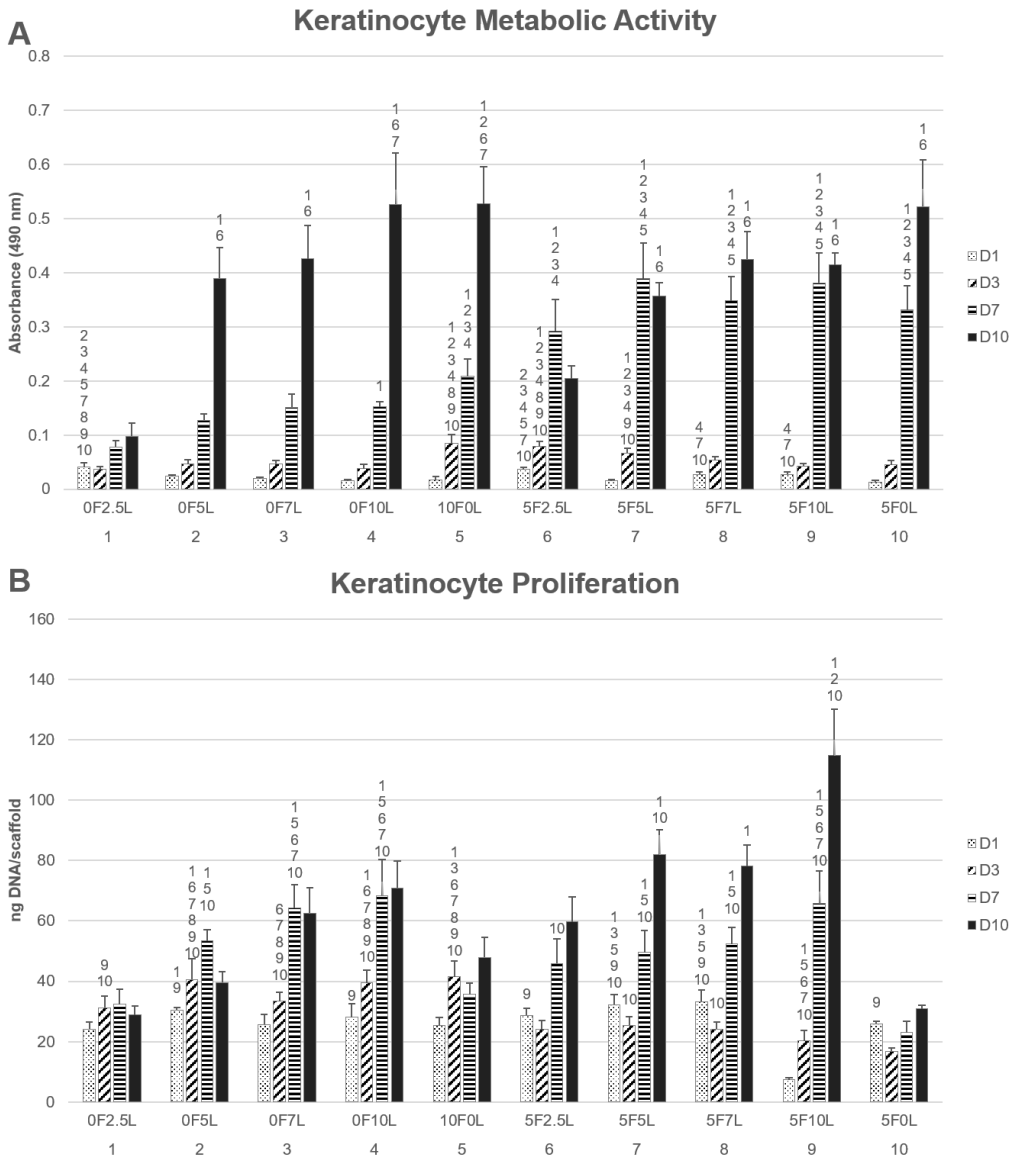

Figure 12 **Metabolic activity and proliferation of keratinocytes**. A – Metabolic activity of keratinocytes was measured by MTS assay (statistical analysis $p < 0.05$), B – Proliferation of keratinocytes was determined by PicoGreen® assay (statistical analysis $p < 0.05$). The sample name (XFYL) codes the supplement concentration in the medium; X stands for concentration of FBS (v/v), Y for concentration of PL (v/v). The numbers above the bars indicate statistical significance[172].

The metabolic activity was significantly increasing in groups supplemented with both the FBS and PL from day 3 to day 7 (Figure 12B). However, we did not observe a further increase in the metabolic activity between days 7 and 10. In the groups where only PL was added, a dose-dependent increase in metabolic activity and a high increase from day 7 to day 10 was

observed. The cells responded well to the cell culture conditions, and the 7% concentration of lysate (0F7L) was sufficient to replace the FBS.

The amount of DNA was continuously increasing throughout the experiment (Figure 12B). The highest amount of DNA was detected in the group with the highest FBS and PL concentration (5F10L). Moreover, with the increasing concentration of the PL samples supplemented with PL and FBS (5F5L, 5F7L, 5F10L), statistically significant differences were observed on day 7. These differences were significantly improved not only in comparison with the group supplemented with 5% FBS, but even with the group with 10% FBS.

The data obtained by the metabolic activity and proliferation testing were confirmed by visualization of keratinocytes via confocal microscopy (Figure 13). The samples showed almost confluent cell layers in the groups containing both the PL and FBS. The number of cells cultured in the serum-free medium supplemented with the PL only was increasing with the PL concentration. The presence of FBS stimulated cell contact and cells formed large clusters on the scaffolds, suggesting a rather stimulatory effect of the supplement mixture, in contrast to the fibroblast culture.

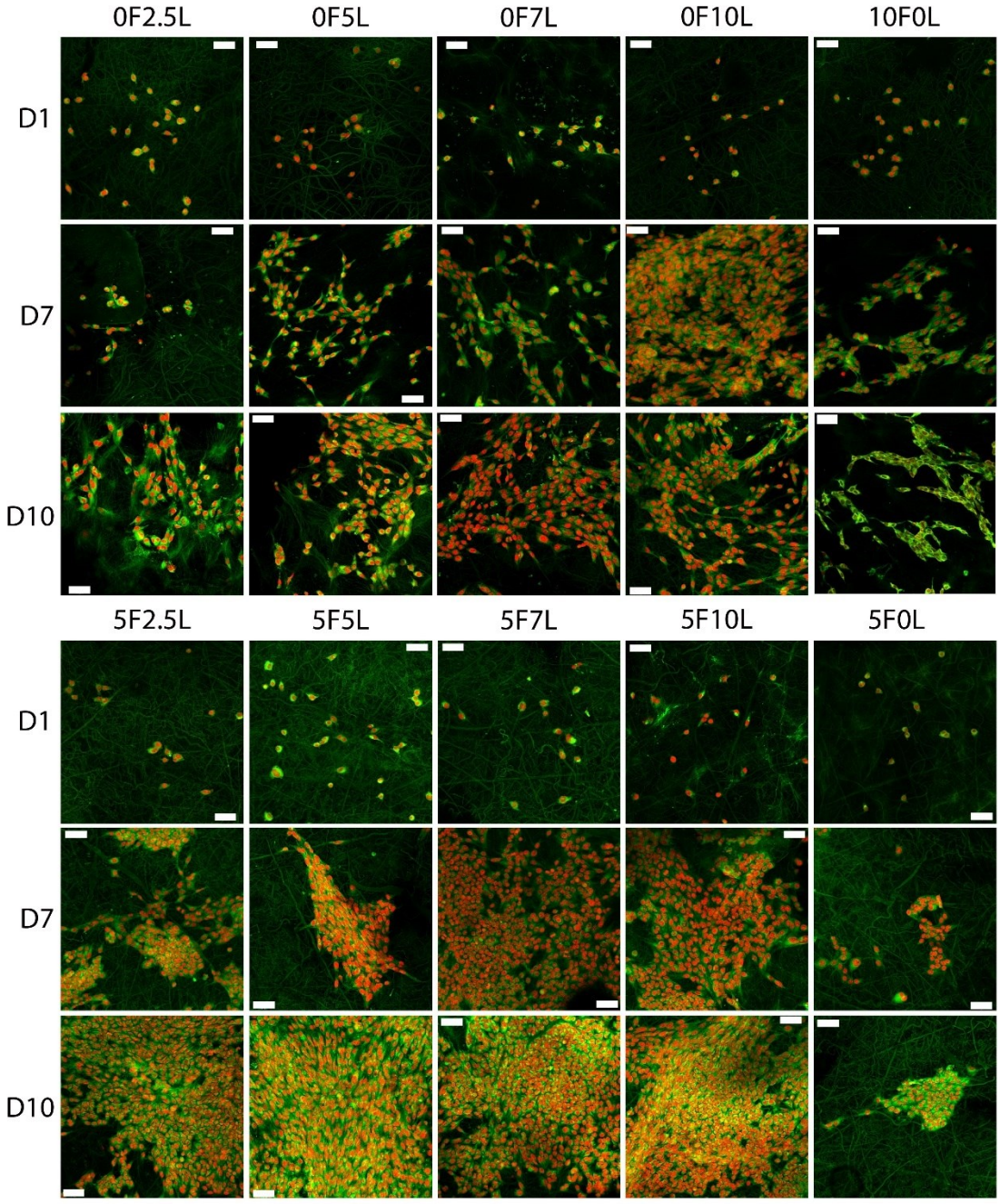

Figure 13 **Confocal microscopy images of the keratinocytes seeded on the PCL scaffolds**. The keratinocytes were observed on day 1, 7 and 10. Green colour depicts cellular biological membranes (staining by DiOC6(3)), red colour cell nuclei (propidium iodide staining). Magnification 200x, scale bar 50 μm. The sample name (XFYL) codes the supplement concentration in the medium; X stands for concentration of FBS (v/v), Y for concentration of PL (v/v)[172].

According to obtained data, the bioactive substances released from the PL positively influenced the proliferation and viability of the cultured keratinocytes. The dose-dependent effect of PL on cell proliferation was observed in both types of media (in media supplemented

with the PL only and in media supplemented with the combination of FBS and PL). However, PL concentration of 5% or higher was able to replace FBS in the serum-free conditions. The observed stimulatory effect was dose-dependent, which was in concordance with findings of a study evaluating primary human keratinocyte culture with different concentrations of PRP. The best proliferation rate was reached when using 10% PRP[190]. In contrast with the behaviour of fibroblasts, a positive dose-dependent effect of combination of both supplements, and thus higher concentration of the bioactive molecules, was observed.

6.1.5 Summary

The study evaluating the effect of bioactive molecules contained in the platelet lysate on skin cells showed, that 7% platelet lysate was able to replace FBS in both cultures of fibroblasts and keratinocytes. However, there were differences in cell behaviour when the cell culture medium was supplemented with both the FBS and platelet lysate (increased concentration of bioactive molecules). The cultured fibroblasts responded to the increasing concentration of bioactive molecules negatively, showing rather inhibition of their metabolic activity and proliferation. On the other hand, the increased concentration of bioactive molecules stimulated cell contact and resulted in improvement of keratinocyte metabolic activity and proliferation.

6.2 Functionalization of electrospun PCL nanofibres with native platelets

To improve the retention of bioactive molecules released from platelet at the site of application, a simple delivery system was proposed. The system consisted of PCL nanofibrous mesh and platelets adhered to the surface of the mesh. The PCL nanofibrous scaffolds were prepared by needleless electrospinning. Furthermore, they were functionalized with native human leucocyte-poor buffy coat-derived platelets at concentration P1 (the maximum platelet

concentration 1,030x10^9 platelet/L), P0.5 (half the maximum concentration 515x10^9 platelets/L) and P0.25 (quarter the maximum concentration 258x10^9 platelets/L). The effect of the released platelet-derived molecules was investigated using murine keratinocytes XB2, fibroblasts 3T3-A31, and melanocytes melan-a. The composition of the samples is summarized in Table 6.

Table 6 **Composition of the electrospun samples functionalized with platelets in the Experiment 6.2**.

Sample	Platelet concentration
P1	1,030x10^9 platelets/L
P0.5	515x10^9 platelets/L
P0.25	258x10^9 platelets/L

6.2.1 Characterization of the scaffold

The architecture of the fabricated electrospun scaffolds was investigated using scanning electron microscopy (Figure 14). The samples showed architecture typical for PCL nanofibers. The analysis showed nano-/microarchitecture with a minimum of non-fibrous defects. The mean diameter of the thin nanofibrous fraction was 241.6 ± 90.6 nm, the thicker fibres had a mean diameter of 748 ± 147.4 nm. In addition, a less abundant microfibrous fraction was detected with a mean diameter of 1486.8 ± 419.1 nm. The mean pore size was 10.28 ± 12.1 μm. On the platelet-functionalized samples, platelets were activated due to their contact with the nanotopography of the prepared nanofibrous layer and subsequently changed their morphology. Furthermore, a clear thick fibrin layer was observed on the platelet-functionalized PCL samples (Figure 14A-C).

Similar architecture of the prepared fibrous samples was observed[191]. The nano-/microstructure combines the advantages of larger pore size between the microfibers with the

high adhesion capacity of the nanofibrous part[192]. Importantly, we have demonstrated efficient adhesion of the platelets to the surface of PCL nanofibers.

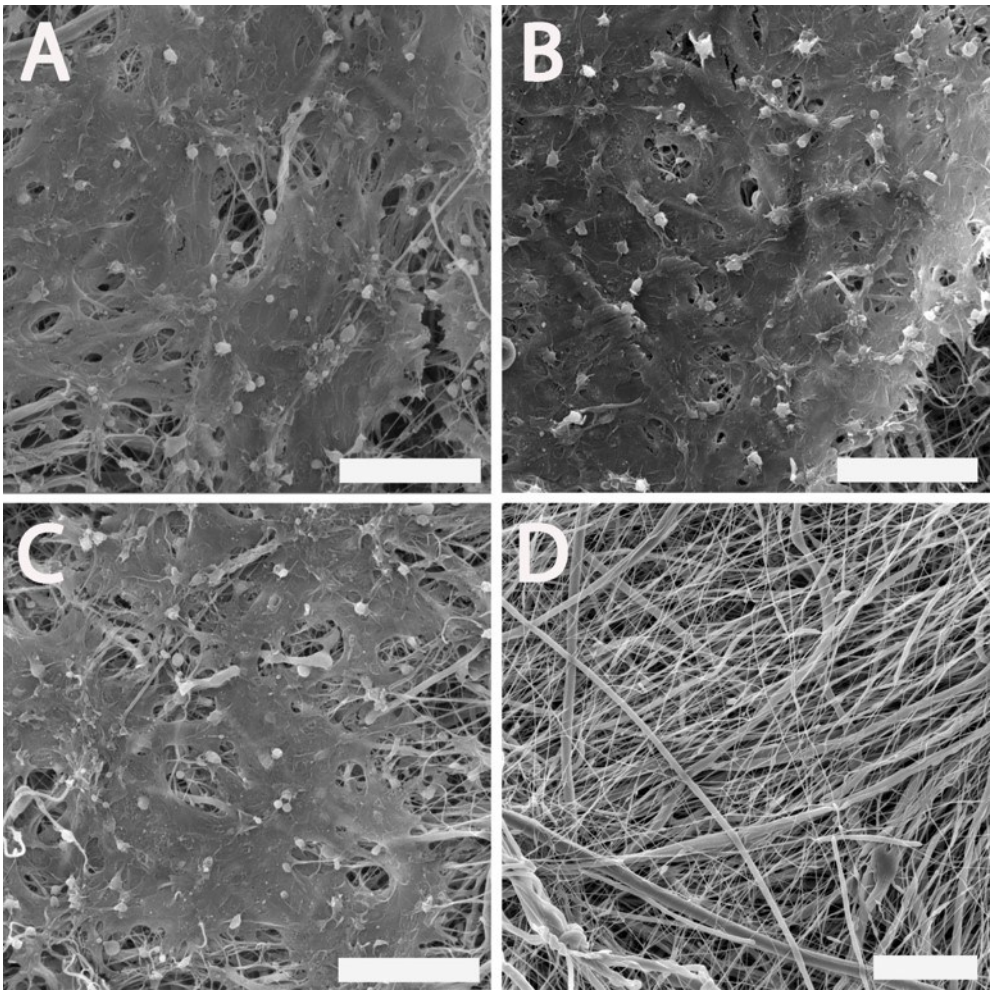

Figure 14 **Scanning electron microscopy of the PCL nanofibrous samples with adhered native platelets after a two-hour incubation**. A – P1 sample: PCL nanofibrous scaffold functionalized with the maximum platelet concentration, scale bar 20 μm, magnification 4,000x. B – P0.5 sample: PCL scaffold functionalized with half the maximum platelet concentration, scale bar 20 μm, magnification 4,000x. C – P0.25 sample: PCL scaffold functionalized with quarter the maximum concentration of platelets, scale bar 20 μm, magnification 4,000x. D – PCL control sample, scale bar 20 μm, magnification 2,940x[193].

Scanning electron microscopy images revealed that the platelets were activated upon adhesion to the scaffold surface and a thick fibrin network was formed. Such findings are in agreement with another study[194]. The study showed that platelets undergo activation upon adhesion to nanofibers thanks to their specific surface topography. The natural character of fibrin has been widely used in various tissue engineering applications. The fibrin network fosters

adhesion of cells via integrin and non-integrin receptors[195]. Such biomimetic motives are crucial for the enhancement of cellular adhesion and proliferation on the rather hydrophobic surface of PCL scaffolds. A similar system composed of platelets adhered to PCL nanofibrous mesh was tested by[191,196]. Jakubova et al. (2011) investigated optimum duration of the incubation period of nanofibre with platelet-rich solution, showing that prolonging the incubation period beyond two hours did not significantly increase the platelet adhesion efficiency. Furthermore, the study investigated the effect of surface adhesion of platelets to primary chondrocytes. Plencner et al. (2015) utilized such a system in ventral hernia regeneration. Both studies showed a significant improvement of cell metabolic activity and proliferation due to the bioactive substances released from platelets.

Platelets are anucleated cells, however, they still possess mitochondria and thus could misrepresent the collected data. Therefore, the viability of the platelets adhered to the surface of nanofibres was evaluated on day 1, 3, and 7 (Figure 15).

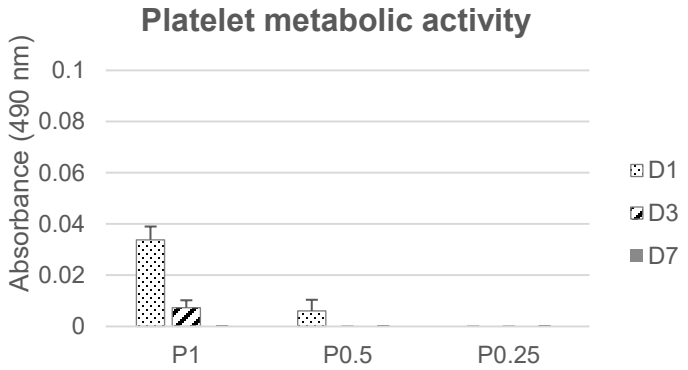

Figure 15 **Metabolic activity of the platelets adsorbed to the surface of nanofibres**. The MTS assay was performed on day 1, 3, and 7.

The acquired data showed that the metabolic activity of the platelets adsorbed to the surface of PCL nanofibres is almost negligible. Some metabolic activity was detected on the samples P1 and P0.5 on day 1 and on the sample P1 on day 3. On the sample containing the

lowest tested platelet concentration (P0.25), there was no metabolic activity of platelets detected. Still, the acquired values were subtracted from the values acquired from the cell-seeded samples to prevent misrepresentation of the data.

6.2.2 Release characteristics of the bioactive molecules

To characterize the release of bioactive molecules from the functionalized samples, levels of EGF as a model molecule were detected, as the EGF plays a key role in the wound healing process. The obtained data are shown as cumulative (Figure 16) and relative (Figure 17) release of the EGF, with cumulative graphs illustrating the absolute concentrations of the EGF detected in the culture media of the respective cell types and relative graphs illustrating the rate of release of the EGF from the platelet-functionalized samples. The cell culture media were collected on day 1, 3, 7, and 14 of the experiment and the EGF concentration was determined using ELISA.

The cumulative release of EGF showed similar patterns among the three types of the cultured cells. The highest EGF concentration was detected in the P1 sample and the EGF concentration was accordingly lower at the samples P0.5 and P0.25. During the experiment, synthesis of EGF was observed in the keratinocyte culture (since day 7, Figure 16A) and fibroblast culture (since day 1, Figure 16B). However, the levels of EGF detected in the control samples were significantly lower than the concentration of EGF delivered by the adhered platelets in the platelet-functionalized samples.

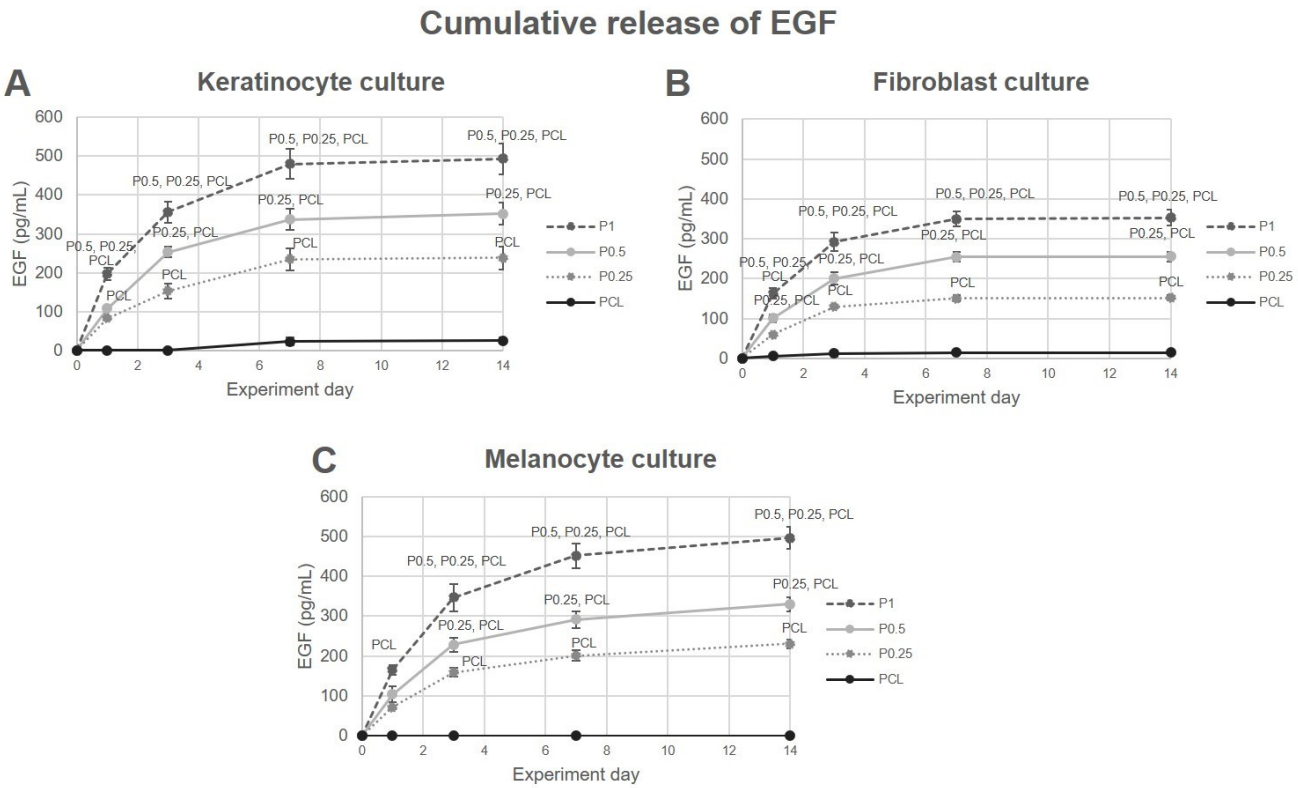

Figure 16 **Cumulative release of EGF from the platelet-functionalized PCL samples**. The levels of EGF in the cell culture media were detected using ELISA on day 1, 3, 7, and 14. A –The cumulative release of EGF detected in the keratinocyte culture. B – The cumulative release of EGF detected in the fibroblast culture. C – The cumulative release of EGF detected in the melanocyte culture. The name of the sample above the time-points in the graph denotes statistical significance; $p<0.05$[193].

EGF has been shown to stimulate proliferation of keratinocytes and fibroblasts[197]. Furthermore, it has been reported that sufficiently high concentrations of EGF result in keratinocyte differentiation, promoting wound healing in diabetic mice[95]. In the melanocyte culture, no synthesis of EGF was detected.

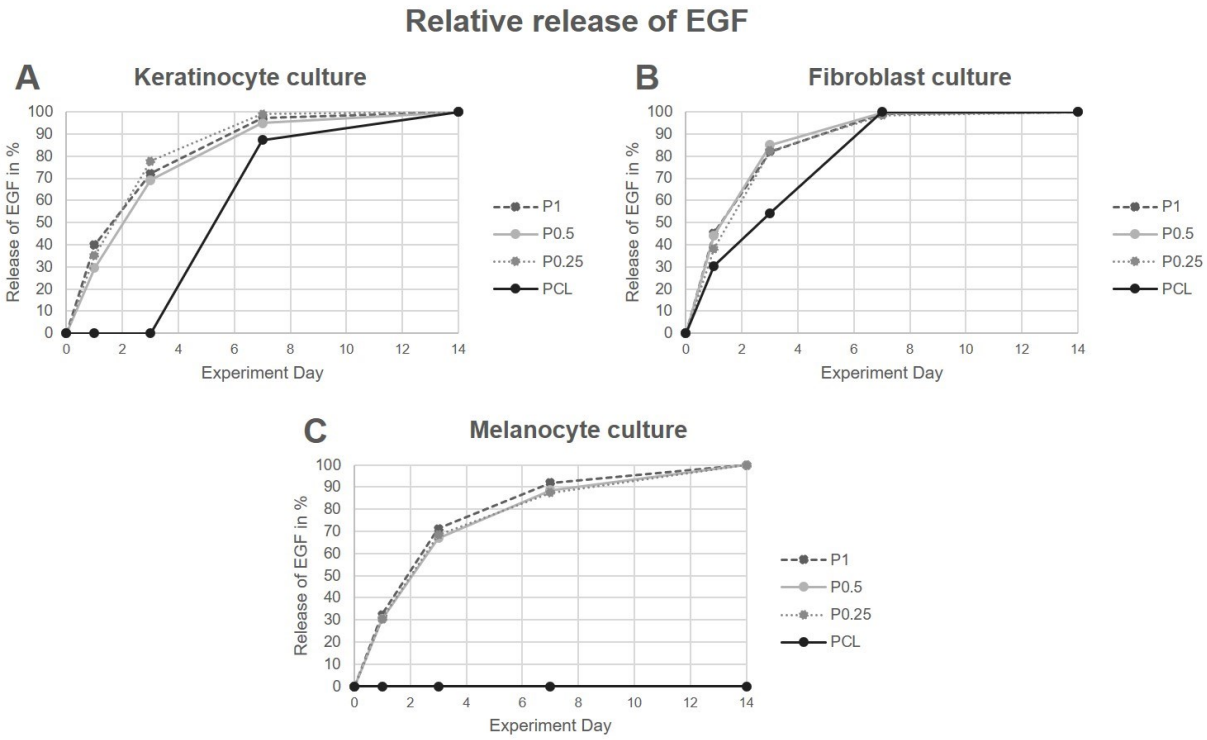

Figure 17 **Relative release of EGF from the platelet-functionalized PCL samples**. The levels of EGF in the cell culture media were detected using ELISA on day 1, 3, 7, and 14. A –The relative release of EGF detected in the keratinocyte culture. B – The relative release of EGF detected in the fibroblast culture. C – The relative release of EGF detected in the melanocyte culture[193].

The relative release of EGF in the platelet-functionalized samples was very similar in all the platelet-functionalized samples, regardless of the initial platelet concentration. The median half-time of release of the EGF (i.e. the time point, when 50% of the EGF was released) was 1.7 days (range 1.3 to 2.1 days; Table 7).

Table 7 **Half-time of EGF release from the platelet-functionalized samples**. The table represents the time to release of 50% of the contained EGF in days in the various cell cultures.

Sample	Keratinocytes (days)	Fibroblasts (days)	Melanocytes (days)
P1	1.6	1.3	1.9
P0.5	2.0	1.3	2.1
P0.25	1.7	1.5	2.0

Several similar systems for delivery of platelet-derived bioactive molecules have been developed. A system composed of PCL nanofibres coated with platelet lysate was described[198].

The PCL scaffolds were incubated with the platelet lysate and then the PRP-coated PCL scaffold was freeze-dried. The performed release characteristics showed a significant burst release of the total protein (86% of the total protein released within 4 hours) and VEGF. The release of PDGF-BB and TGF-β1 was slower, however, 50% of the enclosed PDGF-BB and TGF-β1 were released by the system in less than the first 24 hours. Similar results (with release of GFs ranging from 75% to 85% within the first hour) were observed in a study evaluating titanium surfaces of implants covered with activated (thrombin, calcium chloride) or non-activated platelet-poor plasma and plasma rich in growth factors[199].

The more sustained release of the growth factors observed in our study may be due to the thick fibrin network formed on the surface of the PCL scaffolds. The native platelets were activated due to the contact with the topography of the nanofibres and the 2-hour incubation allowed the fibrin network to be formed. It has been shown fibrin serves as a reservoir of several growth factors, including bFGF, TGF-β1, PDGF or IGF-1[200–203]. The fibrin-GF interaction could slow down the release of the captured growth factors.

6.2.3 Keratinocytes seeded on the platelet-functionalized scaffolds

To test the biocompatibility of the scaffolds, the metabolic activity of the seeded cells on platelet-functionalized scaffolds was determined. The Figure 18A shows the metabolic activity of keratinocytes. During the experiment there was no clear tendency in the acquired data. On day 14 the metabolic activity of keratinocytes was significantly higher on the P0.25 sample (quarter the maximum platelet concentration) in comparison to the PCL control.

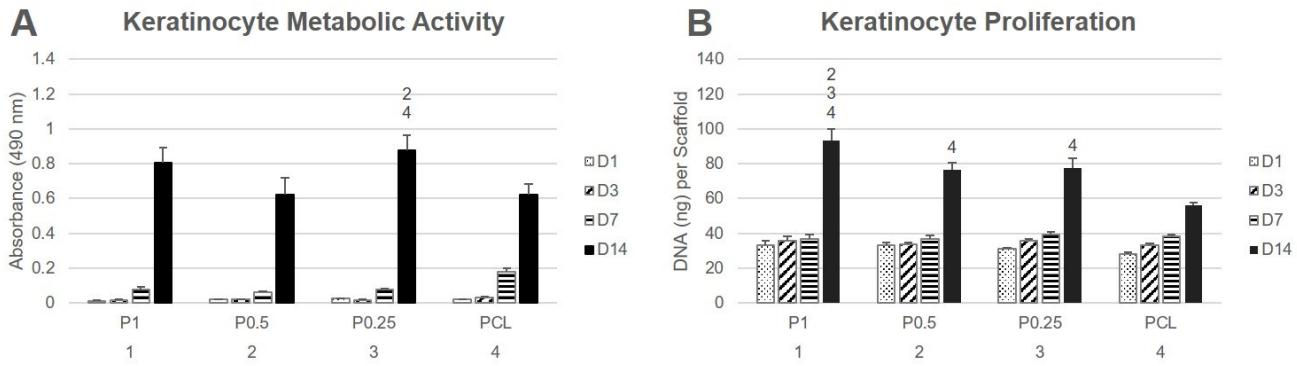

Figure 18 **Keratinocyte metabolic activity and proliferation**. A – Metabolic activity of keratinocytes measured by MTS assay (statistical analysis $p<0.05$). B – Proliferation of keratinocytes determined by dsDNA fluorescence assay (statistical analysis $p<0.05$). The level of significance is denoted by the numbers above the bars in the graph, number 1 representing the P1 scaffold, 2 the P0.5 scaffold, 3 the P0.25 scaffold and 4 the PCL control scaffold.

Proliferation of keratinocytes seeded on nanofibrous scaffolds is shown in Figure 18B. Until the day 14, there were no significant differences in keratinocyte proliferation among the samples. On day 14, all the samples containing platelets exhibited a significant increase in cell proliferation in comparison to the plain PCL. Furthermore, there were significant differences among the platelet-functionalized samples. On the P1 sample, the amount of the synthetized DNA was significantly larger in comparison to the P0.5 and P0.25 samples.

The keratinocytes seeded on the samples were visualized using laser scanning confocal microscopy on day 1, 7, and 14 (Figure 19).

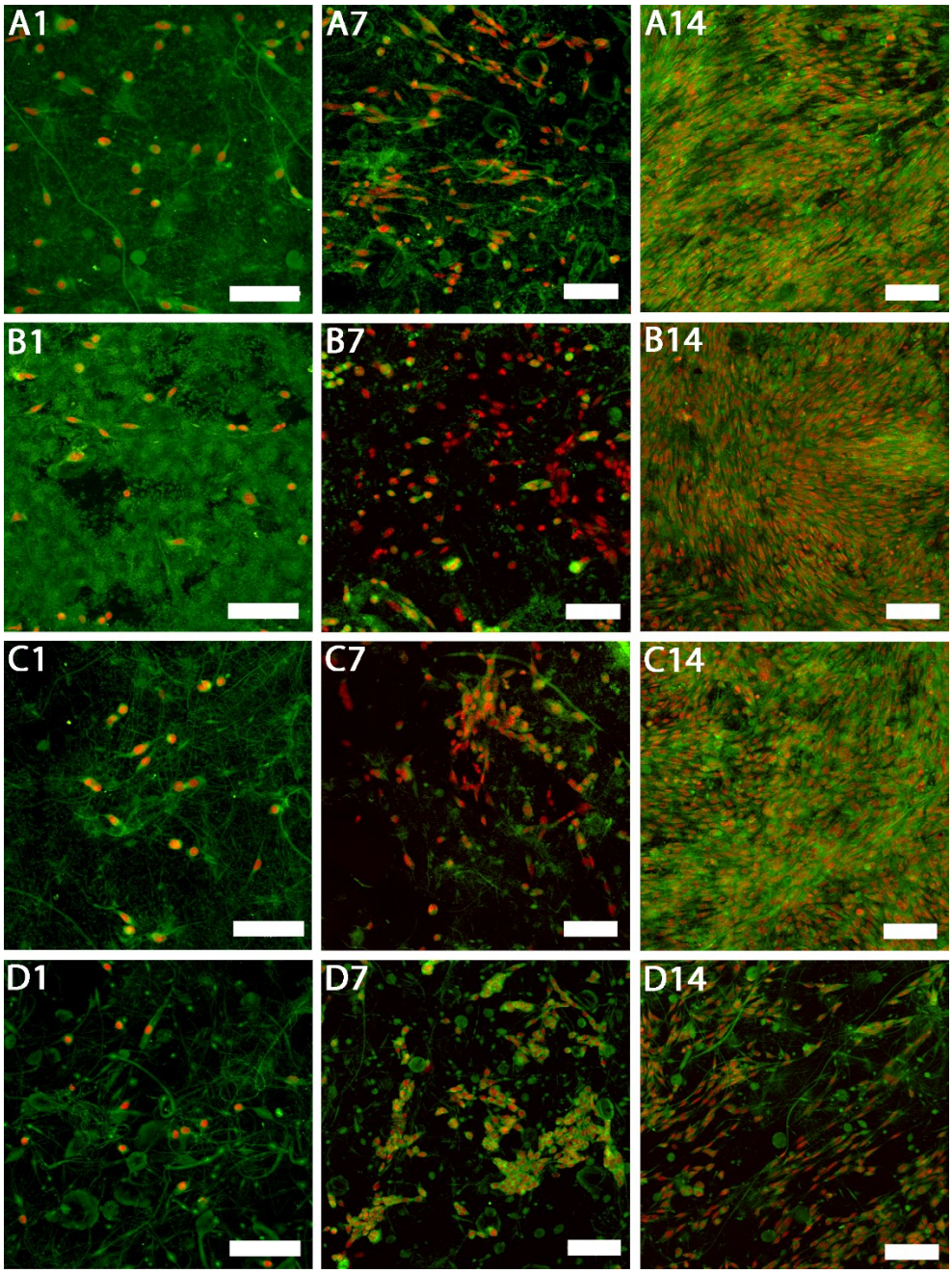

Figure 19 **Confocal images of keratinocytes seeded on the platelet-functionalized samples**. Cellular membranes were stained by DiOC6(3) (green colour), cell nuclei using propidium iodide (red colour). A1 – P1 scaffold on day 1, A7 – P1 scaffold on day 7, A14 – P1 scaffold on day 14, B1 – P0.5 scaffold on day 1, B7 – P0.5 scaffold on day 7, B14 – P0.5 scaffold on day 14, C1 – P0.25 scaffold on day 1, C7 – P0.25 scaffold on day 7, C14 – P0.25 scaffold on day 14, D1 –PCL scaffold on day 1, D7 –PCL scaffold on day 7, D14 –PCL scaffold on day 14. A1, B1, C1, D1 – scale bar 100 μm, magnification 200x, A7, A14, B7, B14, C7, C14, D7, D14 – scale bar 100 μm, magnification 150×[193].

On day 14, the keratinocyte monolayers were confluent on all the samples containing platelets. On the contrary, the number of cells on the plain PCL control sample did not increase so dramatically between day 7 and 14 of the experiment.

The results indicate that the released growth factors stimulated metabolic activity and proliferation on the platelet-functionalized samples in comparison to the plain PCL scaffold. However, the stimulatory effect on keratinocytes seemed to be independent of the initial platelet concentration. Our confocal microscopy studies of the morphology of the keratinocytes showed confluent layers of cells on all the platelet-containing samples.

6.2.4 Fibroblasts seeded on the platelet-functionalized scaffolds

The metabolic activity of fibroblasts seeded on platelet-functionalized samples is shown in Figure 20A.

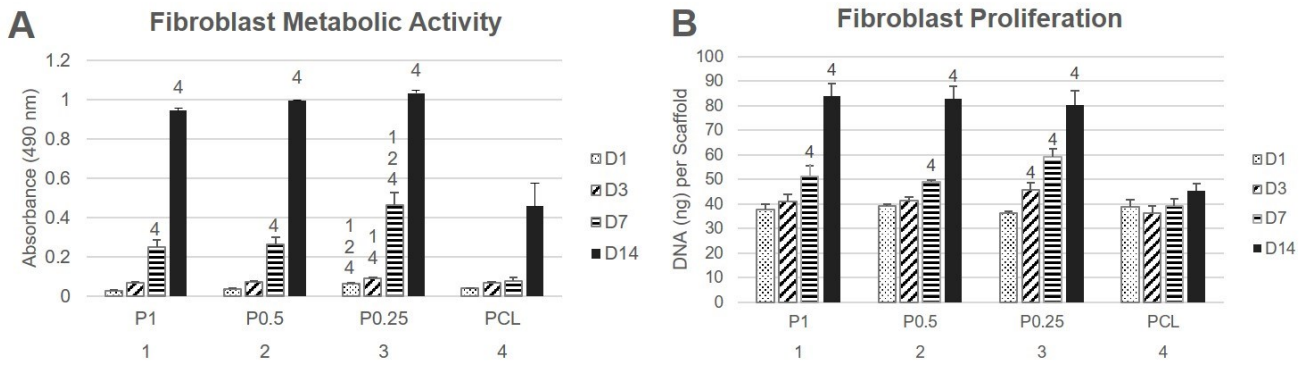

Figure 20 **Fibroblast metabolic activity and proliferation**. A – Metabolic activity of fibroblasts measured by MTS assay (statistical analysis $p<0.05$). B – Proliferation of fibroblasts determined by dsDNA fluorescence assay (statistical analysis $p<0.05$). The level of significance is denoted by the numbers above the bars in the graph, number 1 representing the P1 scaffold, 2 the P0.5 scaffold, 3 the P0.25 scaffold and 4 the PCL control scaffold[193].

Through the entire experiment the metabolic activity of fibroblasts on the P0.25 scaffold was significantly higher in comparison to the PCL scaffold. In addition to that, on day 1, 3 and 7, the metabolic activity of fibroblasts seeded on the P0.25 scaffold was significantly higher than the metabolic activity of cells on scaffolds P1 and P0.5. From day 7, the metabolic activity of cells on the platelet-functionalized samples was significantly improved in comparison to the plain PCL control. On day 14, there were no statistically significant differences in the cell metabolic activity on the scaffolds functionalized with platelets.

Proliferation of fibroblasts (Figure 20B) was determined on day 1, 3, 7, and 14. There were no significant differences in the amount of the synthetized DNA between the samples with platelets and the PCL control until day 7 of the experiment. On day 7 and 14, there was a significantly larger amount of DNA on the scaffolds with platelets in comparison to the control PCL sample. There were no significant differences among the platelet-functionalized samples.

Stimulation of fibroblast proliferation and ECM production in the presence of platelets was described by[204]. The positive effect of platelet-derived bioactive molecules on the 3T3 fibroblasts observed in our study is in concordance with the results observed in a study focused on strategies for outcomes improvement in incisional hernia, where polypropylene (PP) mesh with or without PCL nanofibers coated with platelet-rich solution was evaluated[191]. Our study confirmed that the adhered platelets stimulated the cell metabolic activity and proliferation from day 1 of the experiment. It has been shown that during the first half of the experiment, the fibroblast responded the most in terms of proliferation and metabolic activity to the lowest concentration of platelets (sample P0.25). However, the differences among the platelet-functionalized samples were levelled by the end of the experiment.

Visualization of the fibroblasts can be seen in Fig. 5. On day 14, the fibroblast monolayers on samples containing platelets were almost confluent, in contrary to the control sample, where the increase in cell number was during the experiment only subtle. There were no significant differences among the samples with platelets.

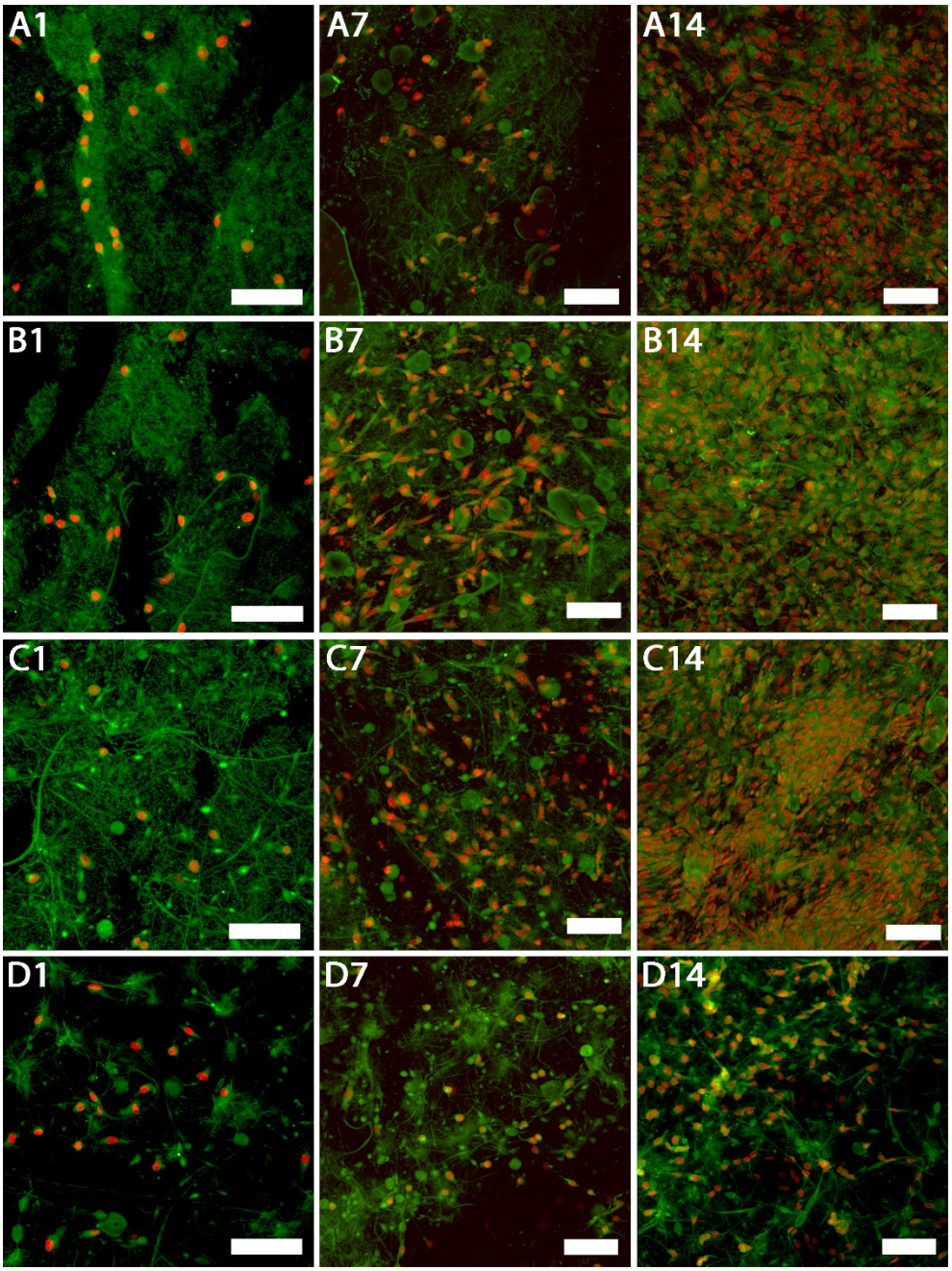

Figure 21 **Confocal images of fibroblasts seeded on the platelet-functionalized samples**. Cellular membranes were stained by DiOC6(3) (green colour), cell nuclei using propidium iodide (red colour). A1 – P1 scaffold on day 1, A7 – P1 scaffold on day 7, A14 – P1 scaffold on day 14, B1 – P0.5 scaffold on day 1, B7 – P0.5 scaffold on day 7, B14 – P0.5 scaffold on day 14, C1 – P0.25 scaffold on day 1, C7 – P0.25 scaffold on day 7, C14 – P0.25 scaffold on day 14, D1 –PCL scaffold on day 1, D7 –PCL scaffold on day 7, D14 –PCL scaffold on day 14. A1, B1, C1, D1 – scale bar 100 μm, magnification 200x, A7, A14, B7, B14, C7, C14, D7, D14 – scale bar 100 μm, magnification 150×[193].

We have shown that the bioactive substances released from platelets stimulate both fibroblasts and keratinocytes. Interactions between keratinocytes and fibroblasts gradually shift the wound healing process from inflammation to the proliferative phase and granulation tissue

synthesis [33]. Both cell types are essential to reduce the wound volume and to facilitate proper wound closure. Currently, there are very few drugs stimulating both cell types simultaneously and the development of such a system for deep wound healing would be very beneficial[205].

6.2.5 Melanocytes seeded on the platelet-functionalized scaffolds

The metabolic activity of melanocytes seeded on the platelet-functionalized samples is shown in Figure 22A.

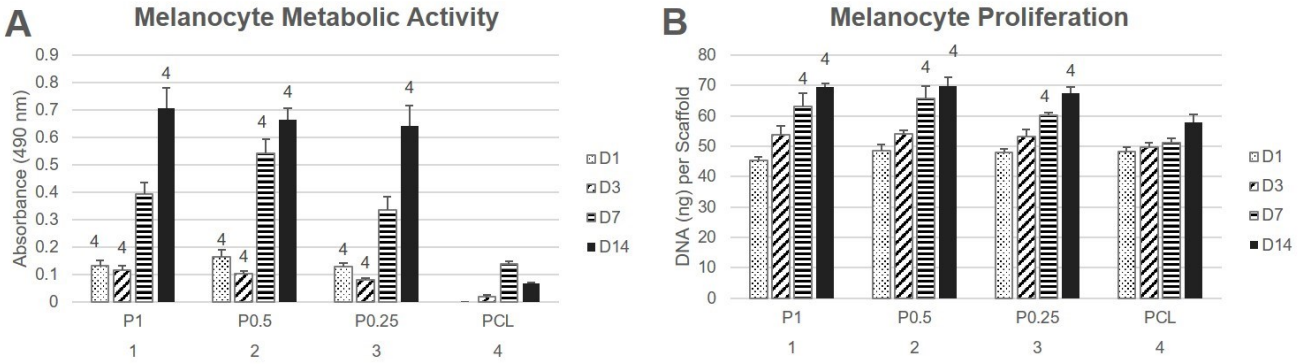

Figure 22 **Melanocyte metabolic activity and proliferation**. A – Metabolic activity of melanocytes measured by MTS assay (statistical analysis $p<0.05$). B – Proliferation of melanocytes determined by dsDNA fluorescence assay (statistical analysis $p<0.05$). The level of significance is denoted by the numbers above the bars in the graph, number 1 representing the P1 scaffold, 2 the P0.5 scaffold, 3 the P0.25 scaffold and 4 the PCL control scaffold[193].

During the entire experiment the metabolic activity of melanocytes on the samples containing platelets was significantly higher in comparison to plain PCL. However, there were no statistically significant differences among the platelet-containing samples.

The amount of synthetized DNA by melanocytes was determined as described above (Figure 22B). The data show the proliferation of melanocytes was increasing through the entire experiment. Platelets significantly promoted melanocyte proliferation on all the platelet-functionalized scaffolds from day 7 in comparison to the PCL control. There were no significant differences among the platelet-functionalized samples in melanocyte proliferation.

The amount of melanin synthetized by melanocytes on the nanofibrous scaffolds (Figure 23) was increasing throughout the entire experiment.

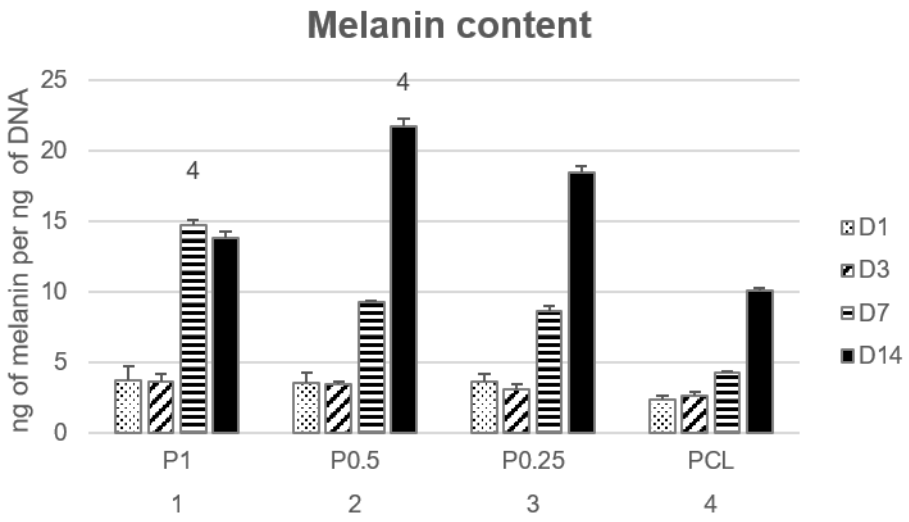

Figure 23 **Melanin synthesis on the platelet-functionalized scaffolds**. The amount of the synthesized melanin was normalized to the amount of DNA contained on the scaffolds. The level of significance ($p<0.05$) is denoted by the numbers above the bars in the graph, number 1 representing the P1 scaffold, 2 the P0.5 scaffold, 3 the P0.25 scaffold and 4 the PCL control scaffold[193].

On day 7, there was a significantly larger amount of melanin on scaffold P1 containing the highest concentration of platelets in comparison to plain PCL nanofibers, indicating the higher concentration of the platelet-derived growth factors resulted in faster synthesis of melanin. However, on day 14, the amount of synthetized melanin was significantly larger on the P0.5 scaffold in comparison to PCL control. The results suggest the lower concentrations of platelet-derived molecules could result in more sustained melanin synthesis in the long-term.

The Figure 24 shows melanocyte proliferation during the experiment. The observed increase in number of melanocytes seeded on the scaffolds with platelets between day 1 and day 7 was more pronounced in comparison to the PCL control. On day 7, the monolayers of the cells on the platelet-containing samples were almost confluent and no differences were observed on day 14.

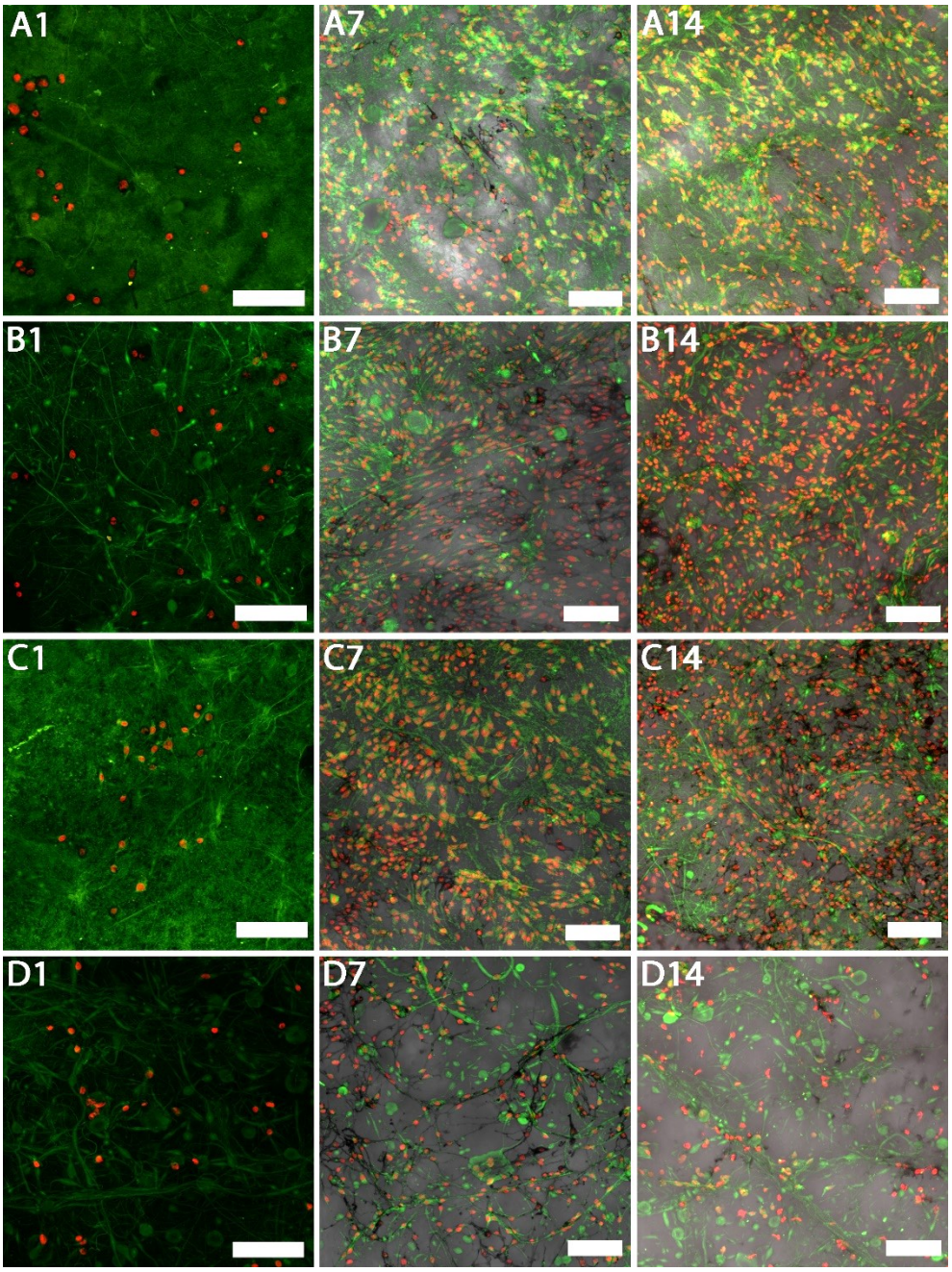

Figure 24 **Confocal images of melanocytes seeded on the platelet-functionalized samples**. Cellular membranes were stained by DiOC6(3) (green colour), cell nuclei using propidium iodide (red colour). The black colour depicts the deposited melanin obtained by merge with images in visible light. A1 – P1 scaffold on day 1, A7 – P1 scaffold on day 7, A14 – P1 scaffold on day 14, B1 – P0.5 scaffold on day 1, B7 – P0.5 scaffold on day 7, B14 – P0.5 scaffold on day 14, C1 – P0.25 scaffold on day 1, C7 – P0.25 scaffold on day 7, C14 – P0.25 scaffold on day 14, D1 –PCL scaffold on day 1, D7 – PCL scaffold on day 7, D14 –PCL scaffold on day 14. A1, B1, C1, D1 – scale bar 100 μm, magnification 200x, A7, A14, B7, B14, C7, C14, D7, D14 – scale bar 100 μm, magnification 150×[193].

On the PCL control sample, the overall number of melanocytes was lower than on the platelet-functionalized samples and the cell monolayers were not confluent even by day 14 of

the experiment. In addition to that, the synthesized melanin was clearly visible on the scaffolds. In the confocal images merged with images in visible light, the melanin is depicted by the black colour. The absorption characteristics of melanin may interfere with the fluorescence-based cell proliferation assay, resulting in discrepancy of the results obtained via the proliferation assay and via confocal microscopy.

Melanocytes are cells responsible for proper pigmentation of the skin. The lack of pigmentation (and thus UV protection) is a common issue in tissue-engineered skin substitutes[53,54]. Furthermore, there are several pigmentation disorders with vitiligo being the most common, characterized by white lesions due to the loss of functional melanocytes[206]. The concept of a cellular patch has been proposed for vitiligo therapy[207]. Using a suitable biomaterial, healthy melanocytes are expanded. The biomaterial further provides the cells with mechanical support during the transplantation to the site of lesion. As such material, several polymers in the form of films have been studied (polylactic acid, polyvinyl chloride and silicone or chitosan coated polystyrene[207–209]). Some of the materials have been used in clinical practice, for example polylactic acid or human amniotic membrane[210,211]. We have shown the PCL nanofibers are suitable biomaterial for melanocyte culture. These results were further supported by a study evaluating PCL nanofibres for culture and differentiation of melanocytes isolated from the outer root sheath of a hair follicle, suggesting the suitability of PCL nanofibres for split-thickness epidermal models[212]. Furthermore, the functionalization of nanofibers with platelets led to a significant increase in cell proliferation, metabolic activity and melanin synthesis. According to the confocal microscopy images, the colonization of the scaffolds by melanocytes was extremely effective.

The results of the study showed that the system was able to stimulate fibroblasts, keratinocytes and melanocytes and could serve as a viable system for tissue engineering. It combines the mechanical stability of PCL nanofibers with the bioactive action of platelets. Our proposed system could serve as a cell-free scaffold that promotes fibroblast and keratinocyte proliferation, migration and angiogenesis via VEGF released from the adhered platelets[195,213]. The stimulation of keratinocyte and fibroblast growth on scaffolds should foster the healing process and may decrease the healing times as a crucial complication in chronic wounds. Additionally, the melanocytes could improve pigmentation outcomes of skin substitutes or the system could serve as a scaffolding system for melanocyte transplantation in vitiligo therapy.

No significant concentration-dependent effect of the platelets was found, thus even the lowest tested concentration was able to stimulate the skin cells. In addition, the simple adhesion method enables fast and convenient on-site preparation and rapid translation to clinical practice.

6.2.6 Summary

The aim of the sub-study was to develop a simple drug delivery system that would prolong the presence of bioactive molecules with short half-time at the site of delivery. The results of the study showed that the morphology of the PCL nanofibres promoted platelet activation and resulted in formation of a thick fibrin network. The median half-time of EGF release was 1.7 days. The metabolic activity and proliferation of keratinocytes was improved on the platelet-functionalized PCL samples in a dose-dependent manner. In contrary, the best metabolic activity and proliferation of fibroblasts was achieved on the PCL sample containing the lowest tested platelet concentration, which was in accordance with our previous platelet lysate study.

Furthermore, the metabolic activity of melanocytes seeded on the platelet-functionalized samples was significantly stimulated regardless the platelet concentration. Therefore, even the lowest tested platelet concentration was able to achieve comparable results as the highest tested platelet concentration. Similarly, the presence of platelets resulted in stimulation of melanin synthesis.

6.3 Comparison of PCL scaffolds functionalized with native platelets

To compare the efficacy of platelet adhesion to the surface of nanofibres prepared by different fibre-fabricating techniques, PCL meshes were prepared using electrospinning (ES) and centrifugal spinning (CS). The scaffolds were functionalized with native human leucocyte-poor buffy coat-derived platelets at varying concentrations. The effect of the released platelet-derived molecules was investigated using murine melanocytes melan-a. The composition of the samples is summarized in Table 8.

Table 8 **Composition of the electrospun and centrifugal samples functionalized with platelets in the Experiment 6.3.**

	Sample	Platelet concentration
Electrospun scaffolds		
10x physiological concentration	E10PC	3,000x10^9 platelets/L
3x physiological concentration	E3PC	900x10^9 platelets/L
Physiological concentration	EPC	300x10^9 platelets/L
3x diluted physiological concentration	E0.3PC	100x10^9 platelets/L
10x diluted physiological concentration	E0.3PC	30x10^9 platelets/L
Centrifugal spun scaffolds		
10x physiological concentration	C10PC	3,000x10^9 platelets/L
3x physiological concentration	C3PC	900x10^9 platelets/L
Physiological concentration	CPC	300x10^9 platelets/L
3x diluted physiological concentration	C0.3PC	100x10^9 platelets/L
10x diluted physiological concentration	C0.1PC	30x10^9 platelets/L

6.3.1 Characterization of the scaffold

Nano-/microfibrous scaffolds were prepared using the two fibre-forming techniques; electrospinning and centrifugal spinning. Generally, both types of scaffolds mimic the native ECM thanks to their porosity, pore interconnection and fibrous structure. However, the electrospun fibrous layer is more planar, forming rather a 2D-like structure in comparison to the centrifugal spun 3D-like scaffolds. The morphology of the layers was in accordance. In the electrospun samples, the mean fibre diameter was found to be 581 ± 522 nm. The fibre diameter of the dominant nanofibrous fraction was 203 nm. The diameter of the less represented microfibrous fraction was up to 2,500 nm. The morphology of the electrospun mesh was more compact, with a mean pore size of 1.5 ± 2 μm^2 and a maximum pore size of 37.2 μm^2. The porosity of electrospun fibres was 55.0 ± 4.2%. The mean fibre diameter in the centrifugal spun samples was 701 ± 494 nm, with the maximum fibre diameter of 2,785 nm and the

minimum fibre diameter of 126 nm. However, the pore size was distinctly improved to 15.2 ± 22.7 μm^2, with a maximum pore size of 239 μm^2. The porosity of the centrifugal spun fibres, 64.6 ± 3.25%, was significantly improved in comparison to the electrospun samples. It has been shown that the more open morphology of the centrifugal spun samples fosters cell penetration into the deeper layers of the scaffold[214].

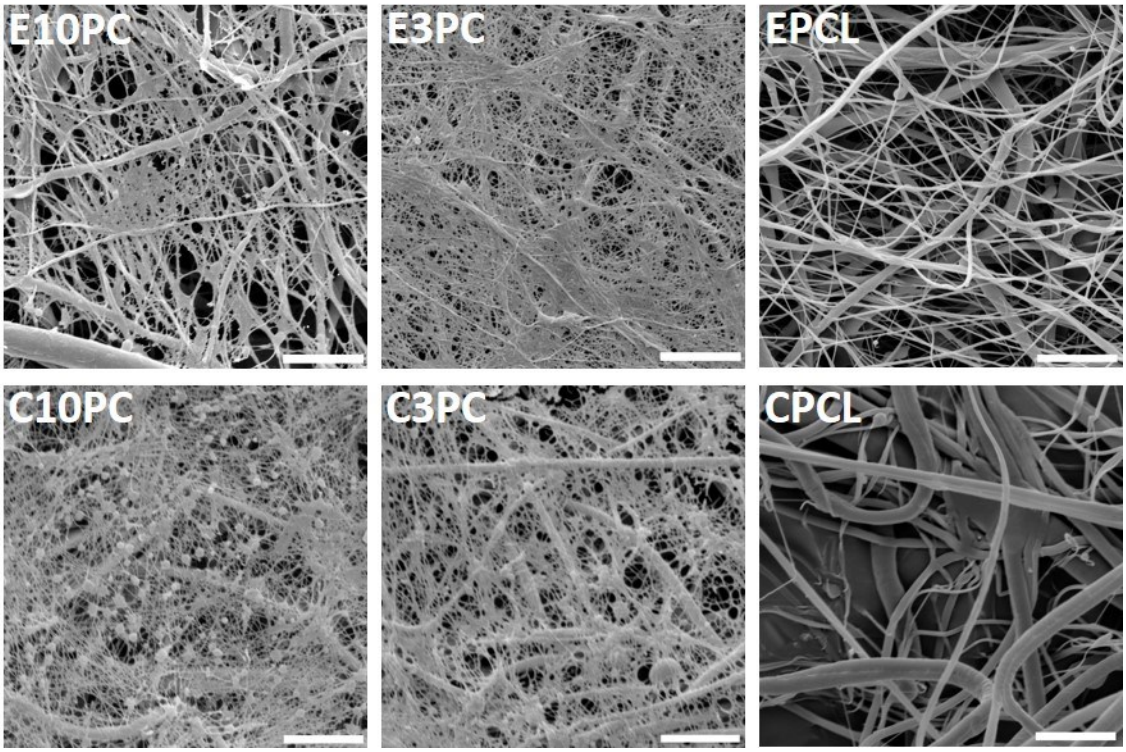

Figure 25 **Scanning electron microscopy of the electrospun and centrifugal spun PCL nanofibrous samples with adhered platelets**. The images acquired on day 1 illustrate the fibrin network formed on the surface of the two samples with the highest platelet concentrations (E10PC, C10PC, E3PC, and C3PC) and the electrospun (EPCL) and centrifugal spun (CPCL) control samples. Magnification 6,000x; scale bar 10 µm.

The platelets adhered to the surface of the nanofibres were visualized using SEM (Figure 25). The acquired images showed clear fibrin network formed on the two highest concentrations of the electrospun and centrifugal spun scaffolds (samples E10PC, C10PC, E3PC and C3PC). On the samples with the lower platelet concentrations, the fibrin network was very scarce. The presence of the fibrin network was decreasing with the decreasing platelet concentration, and on the samples E0.1PC and C0.1PC, no fibrin network was detected.

On the centrifugal spun samples, there were more platelets embedded within the fibrin network. The platelets showed morphology typical for their activated state. Another study that used centrifugal spun PCL nanofibers with adhered platelets for stimulation of proliferation and viability of MG-63 cells, showed, that platelets of circular shape were present on the surface of the nanofibres even after 14 days[215].

The viability of platelets adsorbed to the surface of nanofibers was determined using the MTS assay on days 1, 3, 7 and 14 (Figure 26).

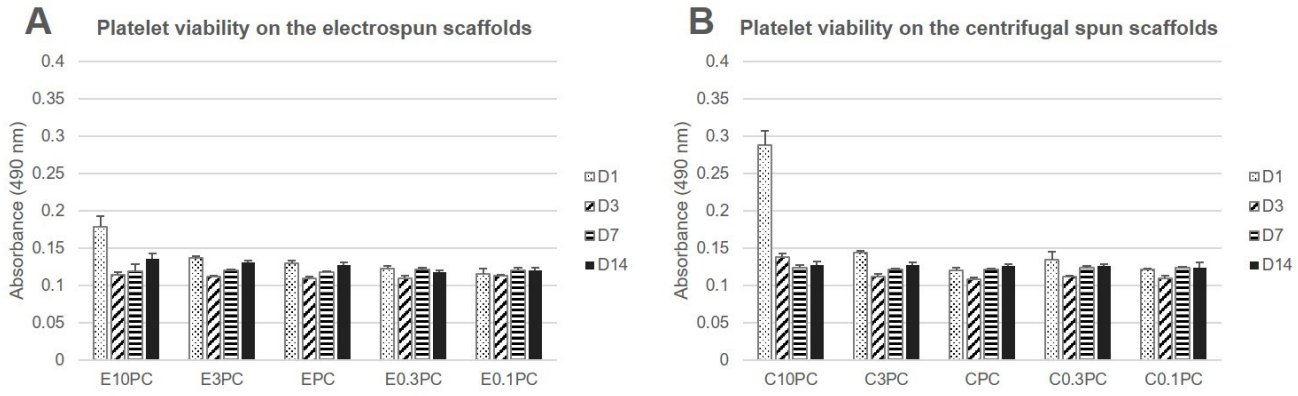

Figure 26 **Viability of platelets seeded on the electrospun and centrifugal spun PCL scaffolds**. The viability of platelets was determined using and MTS assay. A – Viability of platelets seeded on the electrospun scaffolds. B – Viability of platelets seeded on the centrifugal spun scaffolds.

The viability of the highest concentration of platelets seeded on the centrifugal spun scaffolds (C10PC) was almost 2 times higher in comparison to the corresponding electrospun scaffolds (E10PC) on day 1, indicating adsorption of more platelets to the centrifugal spun scaffolds. Otherwise, the metabolic activity of the adsorbed platelets on the electrospun and centrifugal scaffolds was almost negligible throughout the experiment.

6.3.2 Characterization of the platelets

The concentrations of bioactive molecules contained in the platelets were determined using the X-MAP technology. The summary of the obtained results is shown in Table 9.Table 9 Concentration of the determined analytes in the platelet concentrate.

Table 9 Concentration of the determined analytes in the platelet concentrate.

Pro-inflammatory cytokines		
	IL-1b	1.6 ± 0.1 pg/mL
	IL-2	7.7 ± 0.4 pg/mL
	IL-6	15.6 ± 3.5 pg/mL
	IL-7	14.8 ± 0.9 pg/mL
	IL-8	19.2 ± 1.1 pg/mL
	IL-9	95.4 ± 2.7 pg/mL
	IL-12	<LOQ
	IL-15	239.7 ± 15.1 pg/mL
	IL-17	17.7 ± 1.0 pg/mL
	IFN-γ	9.1 ± 0.4 pg/mL
	TNF-α	57.2 ± 3.0 pg/mL
Anti-inflammatory cytokines		
	IL-1ra	214 ± 11.3 pg/mL
	IL-4	1.2 ± 0.1 pg/mL
	IL-5	41.2 ± 2.8 pg/mL
	IL-10	<LOQ
	IL-13	<LOQ
Chemokines		
	Eotaxin	23.3 ± 0.7 pg/mL
	IP-10	225.0 ± 4.6 pg/mL
	MCP-1	12.3 ± 1.1 pg/mL
	MIP-1a	1.3 ± 0.1 pg/mL
	MIP-1b	1,427.1 ± 91.1 pg/mL
	RANTES	16,082.4 ± 1,498 pg/mL
Growth factors		
	IGF-1	32.4 ng/mL
	TGF-β1	17,569.9 ± 1,507.8 pg/mL
	bFGF	67.6 ± 4.1 pg/mL
	G-CSF	79.0 ± 5.9 pg/mL
	GM-CSF	6.5 ± 0.4 pg/mL
	PDGF-BB	1,125.8 ± 48.1 pg/mL
	VEGF	275.0 ± 29.8 pg/mL

The concentrations of the measured analytes corresponded to the values observed in our other studies[215] and to the values observed by other groups[118,178].

6.3.3 Release characteristics of the bioactive molecules

To characterize the release of bioactive molecules from the functionalized samples, levels of thrombospondin-1 and TGF-β1 released from the electrospun and centrifugal spun scaffolds were detected. TSP-1 is a bioactive molecule abundant in the platelet, fostering the proliferative processes during wound healing. The obtained data for TSP-1 are shown as cumulative (Figure 27A) and relative (Figure 27B) release.

Detectable amounts of thrombospondin were present only in the samples with the three highest concentrations of TSP-1 (10-fold physiological concentration of platelets E10PC and C10PC, 3-fold physiological concentration of platelets E3PC and C3PC, and physiological concentration of platelets EPC and CPC). The cumulative release of TSP-1 (Figure 27A) showed that the adhesion of platelets to the centrifugal spun scaffolds resulted in an approximately two-fold increase of the TSP-1 amount when compared to the electrospun scaffolds. In the centrifugal spun sample with the highest concentration of platelet (C10PC), a significant amount of TSP-1 was detected even on day 14. On the contrary, all the TSP-1 was released from all the electrospun samples by day 3 of the experiment.

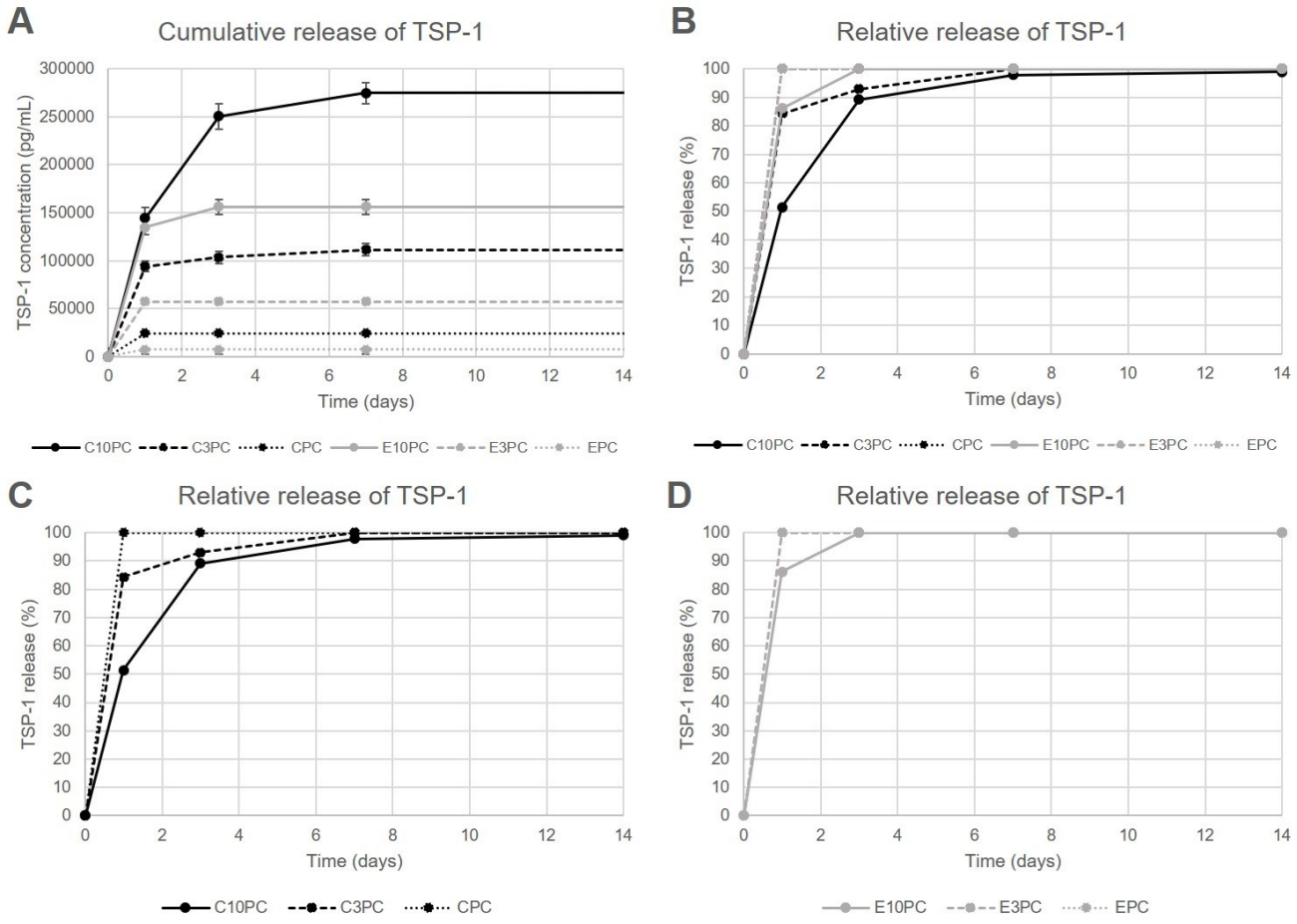

Figure 27 **Cumulative and relative release of thrombospondin-1 from the platelet functionalized electrospun and centrifugal spun samples**. Data for the samples with the three highest concentrations (E/C 10PC, 3PC, and PC) are shown; the lower concentrations were below the detection limit of the assay. A – Cumulative release of TSP-1 from the electrospun (E10PC, E3PC, EPC) and centrifugal spun (C10PC, C3PC, CPC) samples. B – Relative release of TSP-1 from the electrospun and centrifugal spun samples. The release characteristics of the CPC, E3PC and EPC samples were identical, therefore, they overlap in the graph. C – Relative release of TSP-1 from the centrifugal spun samples. D – Relative release of TSP-1 from the electrospun samples; the release characteristics of the E3PC and EPC samples were identical.

Furthermore, the release of TGF-β1 from the platelet-functionalized scaffolds was investigated (Figure 28).

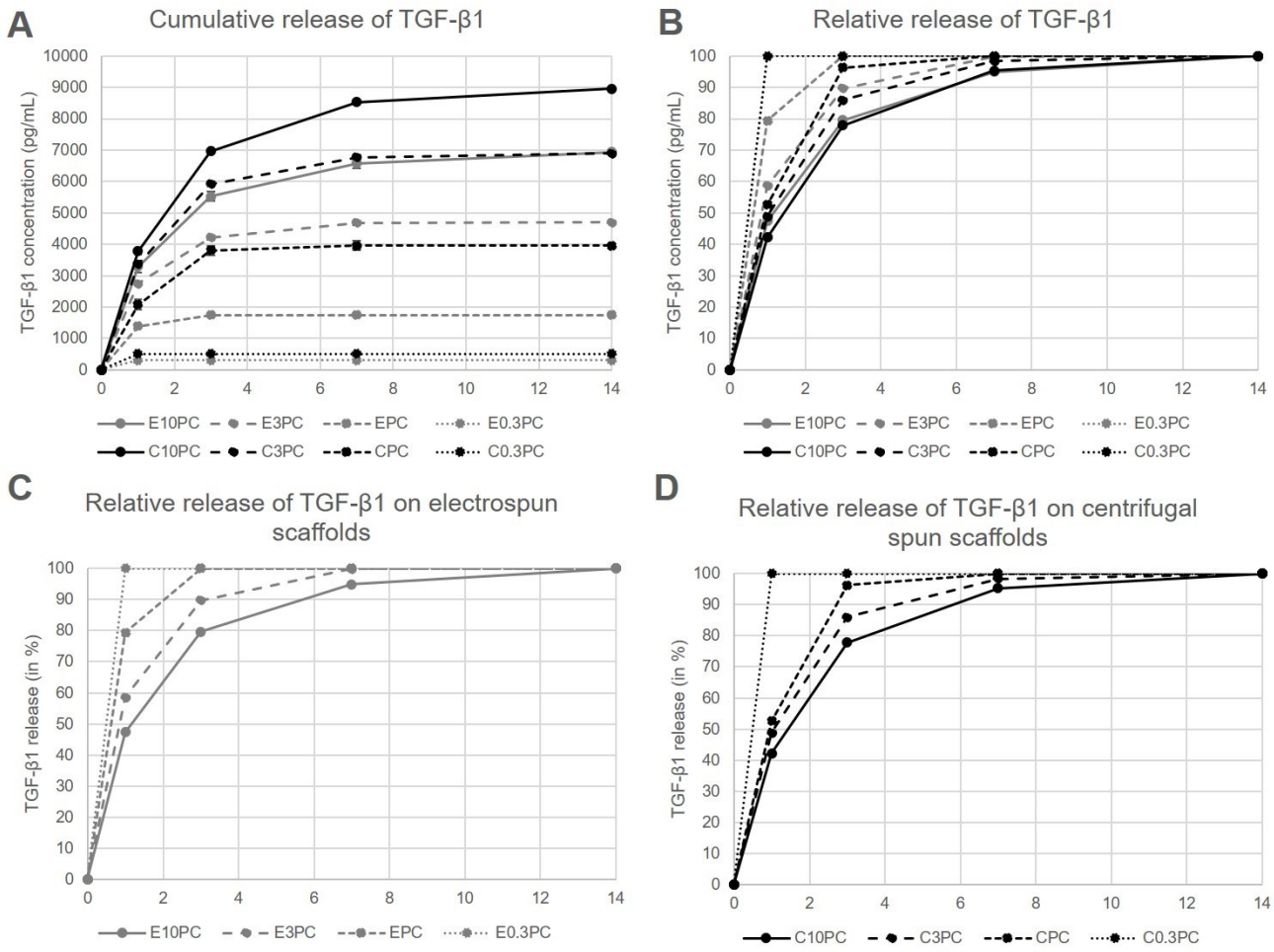

Figure 28 **Cumulative and relative release of TGF-β1 from the platelet functionalized electrospun and centrifugal spun samples**. Data for the samples with the four highest concentrations (E10PC, E3PC, EPC, E0.3PC, C10PC, C3PC, CPC, and C0.3PC) are shown; the lower concentrations were below the detection limit of the assay. A – Cumulative release of TGF-β1 from the electrospun (E10PC, E3PC, EPC, and E0.3PC) and centrifugal spun (C10PC, C3PC, CPC, and C0.3PC) samples. B – Relative release of TGF-β1 from the electrospun and centrifugal spun samples. The release characteristics of the CPC, E3PC and EPC samples were identical, therefore, they overlap in the graph. C – Relative release of TGF-β1 from the centrifugal spun samples. D – Relative release of TGF-β1 from the electrospun samples; the release characteristics of the E3PC and EPC samples were identical.

The Figure 28A shows cumulative release of TGF-β1. The data followed similar trend when compared to the TSP-1 data. There was significantly higher concentration of detected TGF-β1 on the centrifugal spun scaffolds when compared to the respective electrospun scaffolds, however with the higher concentrations (10PC, 3PC), the 2-fold increase seen in TSP-1 was not observed.

The relative release characteristics revealed that the release of TSP-1 and TGF-β1 was faster when compared to the release of EGF in the Experiment 6.2. The half-time release of TSP-1 from the platelet-functionalized samples ranged from 0.5 days to almost 1 day and is shown in Table 10.

Table 10 **Half-time of TSP-1 and TGF-β1 release from the platelet-functionalized samples**. The table represents the time to release of 50% of the contained TSP-1 and TGF-β1 in days.

Sample	Half-time of TSP-1 release (days)	Half-time of TGF-β1 release (days)
C10PC	0.98	1.46
C3PC	0.59	1.11
CPC	0.5	0.96
E10PC	0.57	1.19
E3PC	0.5	0.86
EPC	0.5	0.63

The half-time of release of TGF-β1 (Table 10) was longer when compared with the detected levels of TSP-1, and the half-time decreased with the decreasing platelet concentration. These findings indicated stronger interaction of TGF-β1 with the fibrin matrix formed on the surface of the nanofibres. This is in accordance with the findings of a study that investigated binding of several growth factors (TGF-β1 included). In the study, the growth factors were combined with fibrinogen solution; the fibrinogen was polymerized using thrombin and factor XIII. The concentration of growth factors released from the fibrin matrix was determined. The study showed strong interaction of TGF-β1 with fibrinogen via its heparin-binding domain. In the study, 50% of the contained TGF-β1 was released after 1.5 days, which is in accordance with our results[216].

6.3.4 Melanocytes seeded on the platelet-functionalized samples

To test the biocompatibility of the scaffolds, the metabolic activity melanocytes seeded on platelet-functionalized scaffolds was determined. The metabolic activity of the melanocytes is shown in the Figure 29. The Figure 29A shows the metabolic activity of melanocytes seeded on the electrospun scaffolds and the Figure 29B shows the metabolic activity of melanocytes seeded on the centrifugal spun scaffolds. The acquired data showed a clear tendency of a dose-dependent effect of the platelet concentration adsorbed to the scaffolds. On the electrospun scaffolds, the bioactive compounds released from the platelets significantly improved the melanocyte metabolic activity in comparison to the plain PCL control from day 3 of the experiment. By the end of the experiment, the three highest platelet concentrations (samples EPC10, EPC3, and EPC) significantly improved melanocyte metabolic activity in comparison to the below-physiologic platelet concentration, with the sample EPC3 showing the highest metabolic activity. Furthermore, even the below-physiologic platelet concentrations (E.03PC and E0.1PC) resulted in improved melanocyte metabolic activity when compared to the PCL control.

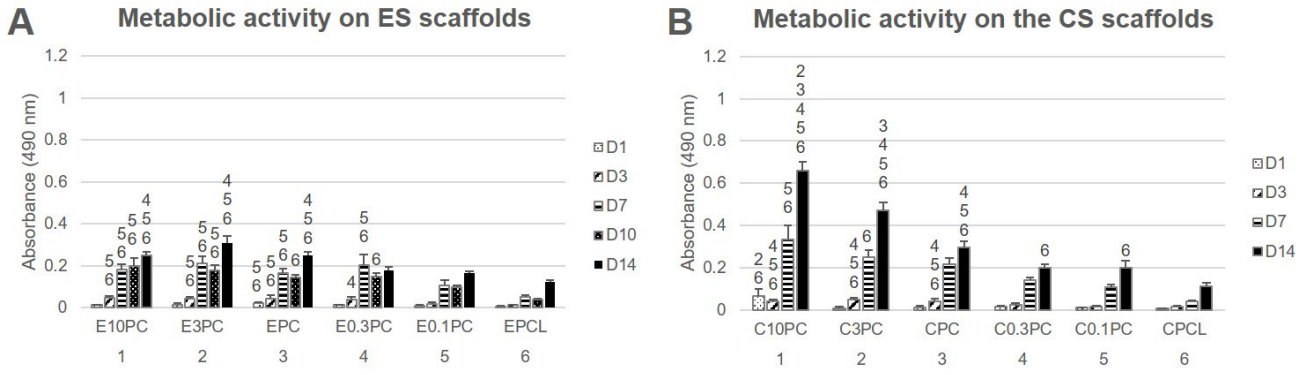

Figure 29 **Metabolic activity of melanocytes seeded on the electrospun and centrifugal spun scaffolds**. A – Metabolic activity of melanocytes seeded on the electrospun PCL scaffolds measured by MTS assay (statistical analysis $p<0.05$). B – Metabolic activity of melanocytes seeded on the centrifugal spun PCL scaffolds measured by MTS assay (statistical analysis $p<0.05$). The level of significance is denoted by the numbers above the bars in the graph. ES stands for electrospun, CS stands for centrifugal spun.

The metabolic activity of melanocytes seeded on the centrifugal spun scaffolds is shown in the Figure 29B. Similarly, as in the case of the electrospun scaffolds, the metabolic activity of melanocytes seeded on the centrifugal spun scaffolds was platelet concentration-dependent. In contrary to the below-physiological platelet concentrations (C0.1PC and C0.3PC), the melanocyte metabolic activity was significantly improved in comparison to the PCL control from day 3. By the end of the experiment, the highest melanocyte metabolic activity was detected on the scaffold with the highest platelet concentration (C10PC), followed by the second highest concentration (C3PC) and the physiological platelet concentration (CPC).

The overall statistical analysis of the all obtained data (data not shown in the graphs) showed there were no statistically significant differences between the electrospun and centrifugal spun samples on day 1, 3, and 7. However, on day 14, the metabolic activity of melanocytes seeded on the C10PC scaffolds (centrifugal spun scaffolds seeded with the highest tested platelet concentration) was significantly improved not only in comparison to all the other tested centrifugal spun scaffolds, but in comparison to the all tested electrospun scaffolds as well. Furthermore, even the metabolic activity of melanocytes seeded on the second highest tested concentration of platelets adhered to the centrifugal scaffold (C3PC) was significantly improved in comparison to all the tested electrospun samples. These differences were levelled out at the physiological platelet concentration, as there was no significant difference in the metabolic activity of melanocytes seeded on the CPC and EPC samples. Furthermore, the morphology of the electrospun and centrifugal spun nanofibrous samples did not seem to affect the melanocyte metabolic activity, as there were no significant differences detected on the plain PCL controls.

A similar trend was observed in the melanocyte proliferation data shown in Figure 30. The Figure 30A shows proliferation of melanocytes seeded on the electrospun scaffolds, the Figure 30B shows proliferation of melanocytes seeded on the centrifugal spun scaffolds.

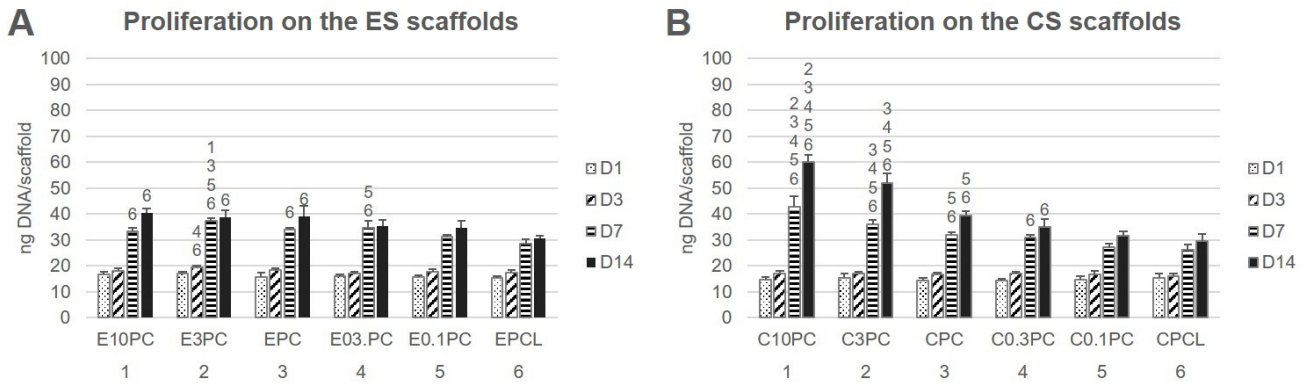

Figure 30 **Proliferation of melanocytes seeded on the electrospun and centrifugal spun scaffolds**. A – Proliferation of melanocytes seeded on the electrospun PCL scaffolds (statistical analysis $p<0.05$). B – Proliferation of melanocytes seeded on the centrifugal spun PCL scaffolds (statistical analysis $p<0.05$). The level of significance is denoted by the numbers above the bars in the graph. ES stands for electrospun, CS stands for centrifugal spun.

There were only mild statistically significant differences in proliferation of melanocytes seeded on the electrospun scaffolds, with the E3PC scaffold achieving the highest proliferation on day 7 of the experiment. Furthermore, the scaffolds with the three highest platelet concentrations (E10PC, E3PC, and EPC) reached a significantly improved proliferation in comparison to the plain PCL control on day 14. The differences in melanocyte proliferation were more pronounced on the centrifugal spun samples. In the first half of the experiment, there were no statistically significant differences in melanocyte proliferation. However, on day 7, the proliferation of melanocytes seeded on the centrifugal spun scaffolds with the highest platelet concentration (C10PC) was significant higher when compared to the all other centrifugal spun scaffolds, followed in the trend by the second highest platelet concentration (C3PC). The same trend was observed on day 14 of the experiment. The melanocyte proliferation on samples CPC and C0.3PC was improved compared to the plain PCL control. However, on the sample

functionalized with the lowest platelet concentration (C0.1PC), no improvement in melanocyte proliferation was achieved. The overall statistical analysis (data not shown in the graphs) confirmed the trend observed in the metabolic activity data. On day 7, the metabolic activity of melanocytes seeded on the centrifugal spun C10PC scaffold showed the highest proliferation when compared to all the centrifugal spun and electrospun scaffolds as well. Furthermore, the response was observed on day 14 as well, when the C10PC and the C3PC samples showed a superior proliferation when compared to all the electrospun samples (in addition to the centrifugal spun samples). Similarly, there was no difference in proliferation of melanocytes seeded on the plain electrospun or centrifugal spun PCL control, suggesting the sole effect of the platelet-derived molecules on the behaviour of melanocytes, regardless of the scaffold morphology.

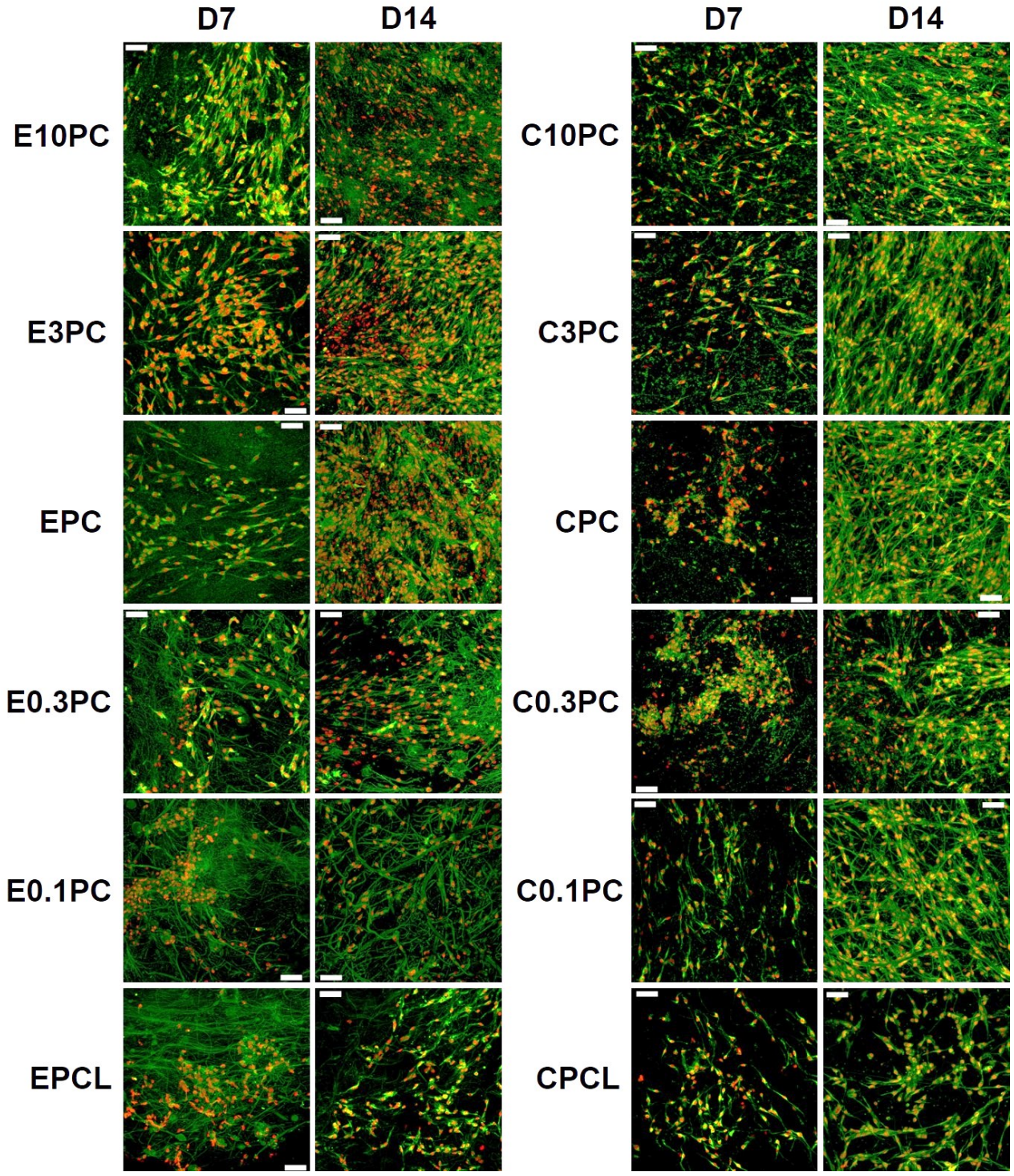

Figure 31 **Confocal images of melanocytes seeded on the platelet-functionalized electrospun or centrifugal spun samples**. Cellular membranes were stained by DiOC6(3) (green colour), cell nuclei using propidium iodide (red colour). For each sample, a representative image from day 7 and day 14 is given. Magnification 200x, scale bar 50 µm.

The morphology of melanocytes seeded on the platelet-functionalized samples was visualized using confocal microscopy (Figure 31). The confocal microscopy images confirmed

the other obtained data. A significant increase in cell number was observed from day 7 to day 14 on the electrospun and the centrifugal spun nanofibrous scaffolds. There was an obvious difference in cell numbers on the platelet-functionalized samples and on the PCL control, on both the electrospun and the centrifugal spun scaffolds. Furthermore, the melanocytes cultured on the centrifugal spun scaffolds showed more dendritic morphology and formed a more complex network in comparison to the melanocytes cultured on the more 2D-like electrospun morphology. Similar changes in melanocyte morphology in a platelet lysate-enriched culture medium were observed[172]. These changes may be attributed to the high PDGF-BB contained in the platelets, as the PDGF-BB has been shown to stimulate melanogenesis, dendritogenesis, and differentiation of human melanocytes[217].

6.3.5 Summary

The results of the study showed that surface and more porous structure of the centrifugal spun scaffolds resulted in an almost 2-fold increase in the number of platelets adhered to the surface of the fibrous mesh. Furthermore, the fibrin network formed on top of the nanofibres served as a drug delivery system, slowing down the release of TGF-β1 in comparison to the TSP-1. The biological activity of the system was tested using melanocytes. The obtained data showed a strong dose-dependent behaviour of melanocytes seeded on the platelet-functionalized scaffolds. Furthermore, no significant effect of the morphology of the 2D-like electrospun scaffold and 3D-like centrifugal spun scaffold was shown, however, based on the confocal images, the melanocytes seeded on the centrifugal spun scaffolds exhibited more pronounced dendritogenesis.

6.4 Comparison of platelet lyophilizate-loaded scaffolds

As systems containing native platelets have rather short-term lifespan, the aim of the study was to develop a system delivering platelet-derived growth factors in a long-term manner. The nanofibrous scaffolds were prepared by needleless electrospinning and centrifugal spinning technique. The aim of the study was to compare two coaxial fibre formation techniques. Platelet lyophilizate was embedded into the coaxial nanofibres as a natural source of growth factors and cytokines, the precise composition of the samples is given in Table 2. The effect of differing stereology of the electrospun and centrifugal spun scaffolds, as well as of the released platelet-derived molecules, was investigated using murine keratinocytes XB2 and fibroblasts 3T3-A31.

6.4.1 Characterization of the fibrous scaffolds

Proper choice of scaffold is one of the major factors influencing the repair of a tissue function. Stereological measurements of the prepared electrospun and centrifugal spun nanofibrous layers showed morphology typical for PCL (Figure 32). The electrospun layer consisted of a population of nano- and microfibers with a minimum of non-fibrous defects. The mean diameter of the thin nanofibrous fraction was 384 ± 196 nm. Furthermore, a fraction of less abundant microfibre was identified with a mean diameter of 1,207 ± 284 nm.

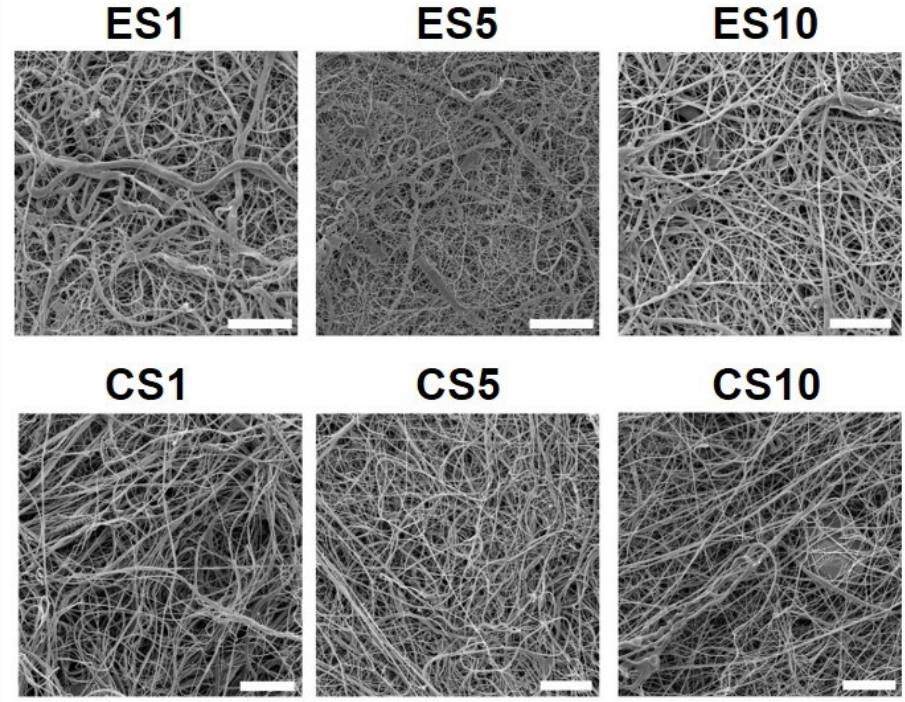

Figure 32 **Scanning electron microscopy of the electrospun (ES) and centrifugal spun (CS) PCL nanofibrous samples**. Electrospun samples containing 1% PF-68, 5% PF-68 and 10% PF-68 (ES1, ES5 and ES10, respectively); magnification 2,000x and scale bar 20 μm. Centrifugal spun samples 1% PF-68, 5% PF-68 and 10% PF-68 (CS1, CS5 and CS10, respectively); magnification 650x and scale bar 50 μm[218].

According to the stereological measurements of the centrifugal spun layers, the samples contained thicker microfibres with a mean diameter of 1,390 ± 626 nm. The measurement of the pore size of the prepared fibrous mats showed a statistically significant increase in the pore size in all the centrifugal spun samples when compared to the electrospun samples. The median pore size of the electrospun samples ranged from 2.5–2.8 μm^2 and of the centrifugal samples 4.2–5.8 μm^2. The electrospun samples contained 0 to 22 % of pores larger than 4 μm^2; however, in the centrifugal spun samples, 57–67% of the pores were larger than 4 μm^2.

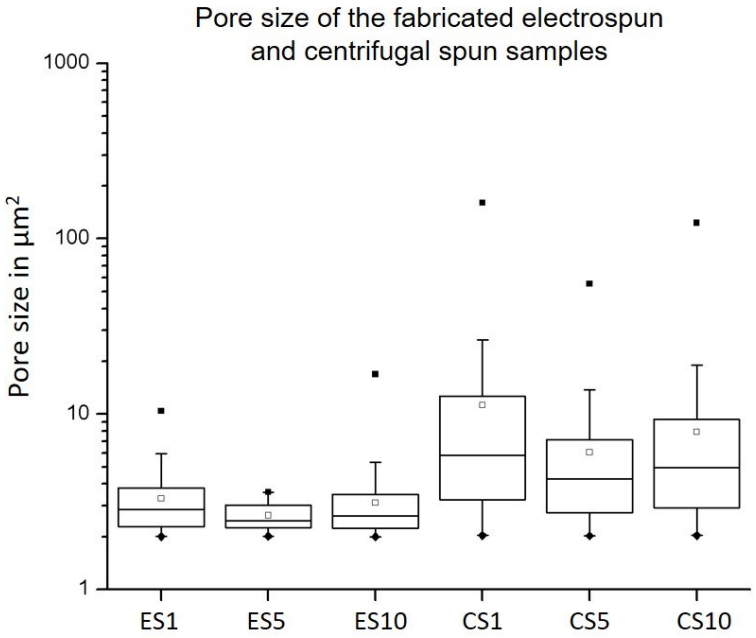

Figure 33 **Pore size of the fabricated fibrous scaffolds**. The pore sizes measured in the fabricated electrospun and centrifugal spun core-shell scaffolds. ES PCL-1% PF-68 (ES1), ES PCL-5% PF-68 (ES5), ES PCL-10% PF-68 (ES10), CS PCL-1% PF-68 (CS1), CS PCL-5% PF-68 (CS5), CS PCL-10% PF-68 (CS10). The data are presented in box plots with whiskers. ♦ denotes the minimum, ■ denotes the maximum and □ denotes the mean value[218].

The morphology of the electrospun scaffolds was shown to promote keratinocyte, melanocyte and fibroblast growth[172,191]. The nanofibres in the microfibrous network supported cell adhesion. Pham et al. described higher cellular spreading on nanofibrous scaffolds with when compared to microfibrous layers[219]. The structure of the electrospun scaffolds was rather planar with a tightly packed fibre network. The sheet-like structure of the electrospun scaffolds did not allow cell penetration through the scaffold, and the cells were growing in the superficial 50 µm of the scaffold[214,219,220]. The planar structure may be favourable for skin tissue engineering applications. The nanofibrous sheet acts as a barrier-like scaffold. The seeded cells are localised on the basal part of the wound and the scaffold protects them from the outer environment. In contrast to that, the centrifugal spun scaffolds are more 3D structures. This was caused mainly by to the dominant presence of microfibres. The fibres were more loosely organized, and the mean pore size was significantly larger. The scaffolds showed a median

pore size ranging from 4.2 to 5.8 μm^2, with dominant presence of pores larger than 4 μm^2. The common migration protocols for fibroblasts used an 8 μm pore size for migration testing [221]. Furthermore, the mean pore size for cell penetration in vivo was much smaller than the predicted in vitro value. This could relate to individual fibres pushing apart during cell movement[222]. Our previous study showed improved penetration of cells through the PCL scaffolds prepared by centrifugal spinning compared to electrospinning[91,214].

The scaffolds were enriched by platelet-derived bioactive molecules to stimulate cell proliferation. The presence of the PF-68 core micelles containing the platelet lyophilizate proteins in the fibrous meshes was confirmed by FTIR-ATR spectroscopy. The control PCL fibres showed a typical FTIR spectra with a dominant C=O stretch band at 1,750 cm^{-1} and a typical fingerprinting zone. The control PF-68 sample showed strong absorption in 2,750–3,000 cm^{-1}, corresponding to the resonance of C-H groups and resonance in 3,500 cm^{-1} region corresponding to the O-H stretch. In the case of both electrospun and centrifugal spun PCL-PF-68 nanofibres with the PF-68 as a core phase, the band corresponding to the O-H stretch band at 3,200–3,600 cm^{-1} was present. The band has a broad shape and the absorbance increased with PF-68 concentration from 1% to 10% (Figure 34).

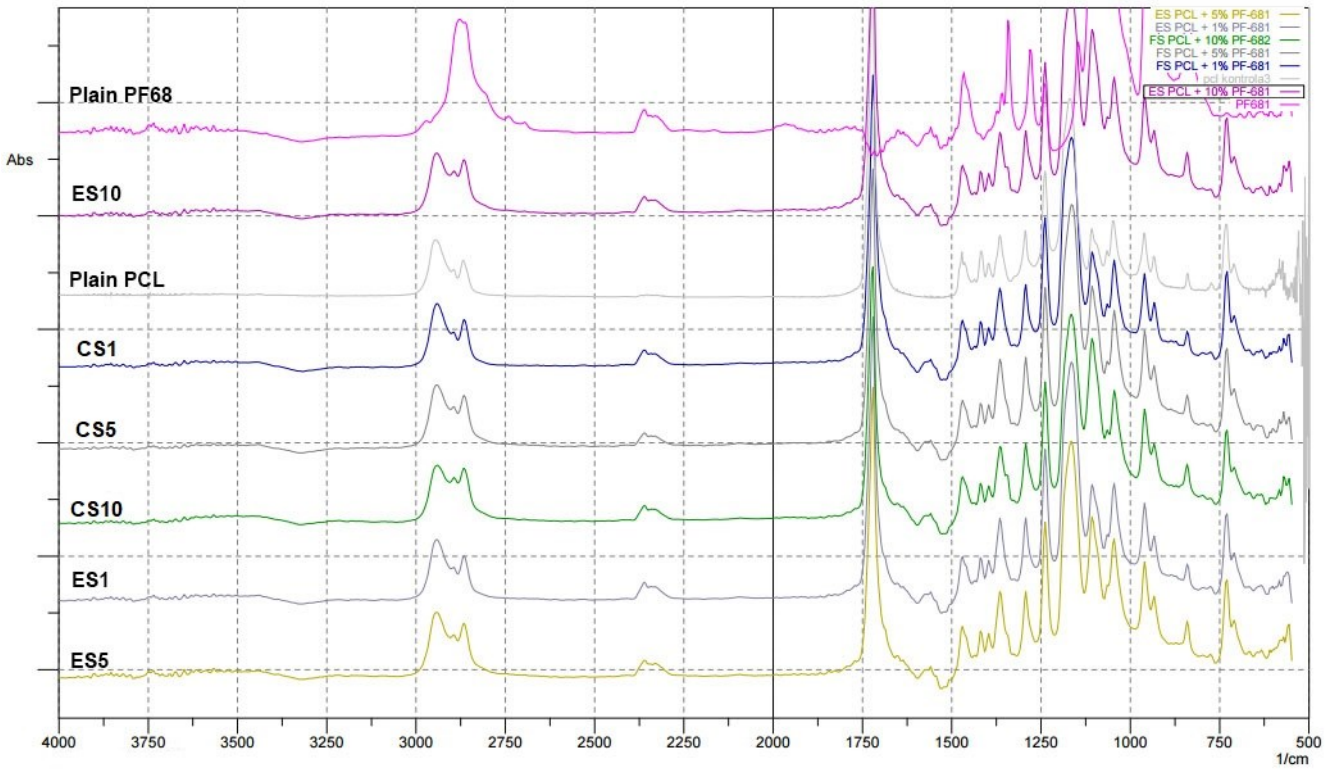

Figure 34 **FTIR-ATR spectra of electrospun and centrifugal spun PCL and PCL-PF-68 nanofibres**. Spectra of PCL, PF-68, ES PCL-1% PF-68 (ES1), CS PCL-1% PF-68 (CS1), ES PCL-5% PF-68 (ES5), CS PCL-5% PF-68 (CS5), ES PCL-10% PF-68 (ES10), CS PCL-10% PF-68 (CS10). The difference in spectra indicate the resonance of PF-68 groups at 3200-3600 cm^{-1} (O-H stretch), 2775-3000 cm^{-1} (C-H stretch) and 1600 cm^{-1} (C-N stretch)[218].

In the case of both electrospun and centrifugal spun samples containing core of 10% PF-68, an increased C-H stretch peak (2,850–3,000 cm^{-1}) was observed. The change in spectra was in accordance with the PF-68 composition consisting of polyethylene oxide and polypropylene oxide units. Nevertheless, the presence of the platelet lyophilizate resulted in an increased absorbance at 1,600 cm^{-1} corresponding to a C-N stretch of proteins in all samples containing the platelet lyophilizate.

6.4.2 Characterization of the platelet lyophilizate

The total protein content in the platelet lyophilizate was determined to be 0.48 mg/mL. The BioPlex multiplex assay was performed to assay the concentrations of specific mediators contained in the platelet lyophilizate (Figure 35).

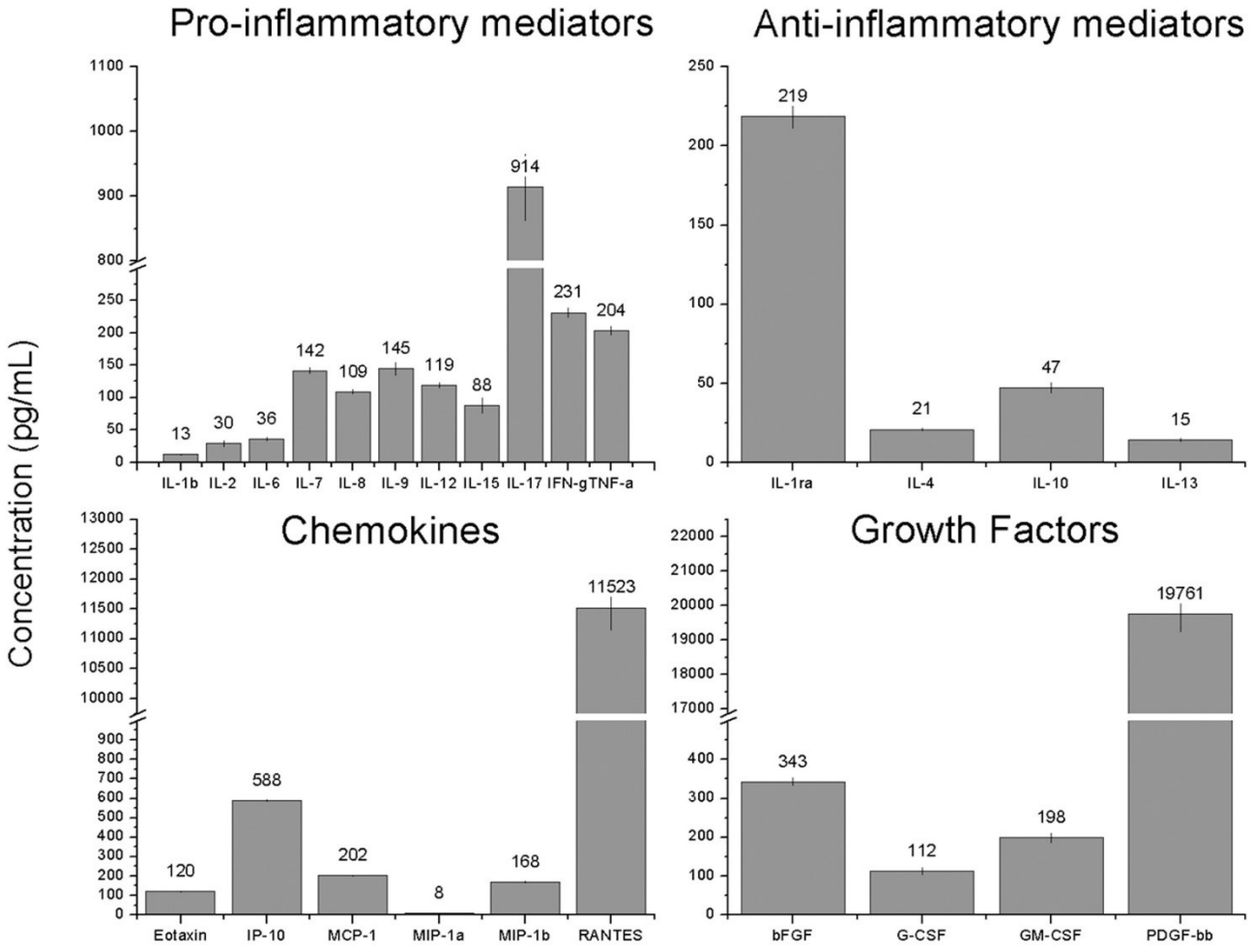

Figure 35 **Concentration of the assayed mediators in the platelet lyophilizate**[218].

According to the obtained data, the lyophilizate contained various pro- and anti-inflammatory mediators; the most abundant pro-inflammatory mediator was IL-17. Furthermore, chemokines and growth factors were found in the platelet lyophilizate, which are of great importance in tissue engineering applications. The most represented chemokine and growth factor were RANTES and PDGF-BB, respectively.

Comparable levels of cytokines, chemokines and growth factors were detected by the XMAP assay in platelet lyophilizate encapsulated into centrifugal spun nanofibres, native platelets adhered to the surface of centrifugal spun PCL nanofibers and the platelet lysate used

in cell culture in the Experiment 6.1 (Buzgo et al. 2017; Rampichova et al. 2017). The data demonstrated the preservation of the growth factors during the freeze-drying process of the platelets. Such preparation provides a significant improvement in shelf-life. It is possible to keep the freeze/dried platelets functional for up to two years[223]. Additionally, by lyophilization of the platelets, their loading into nanofibres in the powder form is facilitated during the fabrication processes. The concentration of the platelet lyophilizate in the solutions used for spinning can be tailored to the requirements of the particular application, and, furthermore, the lyophilizate is soluble in suitable solvents.

6.4.3 Release characteristics of the bioactive molecules

The release profiles of platelet lyophilizate encapsulated into the core-shell electrospun and centrifugal spun nanofibres were determined and are shown in Figure 36. The Figure 36A, illustrating the cumulative release, shows the dependence of the absolute amount of the bioactive molecules contained in the platelet lyophilizate on the concentration of the core polymer PF-68 (1 to 10%), whereas the Figure 36B, illustrating the relative release, shows the release rate of the bioactive molecules and its dependence on the PF-68 core concentration. The data obtained during measuring the relative total protein release from the electrospun and centrifugal spun samples, the embedded proteins were released in a higher rate (a burst) during the first days of the experiment.

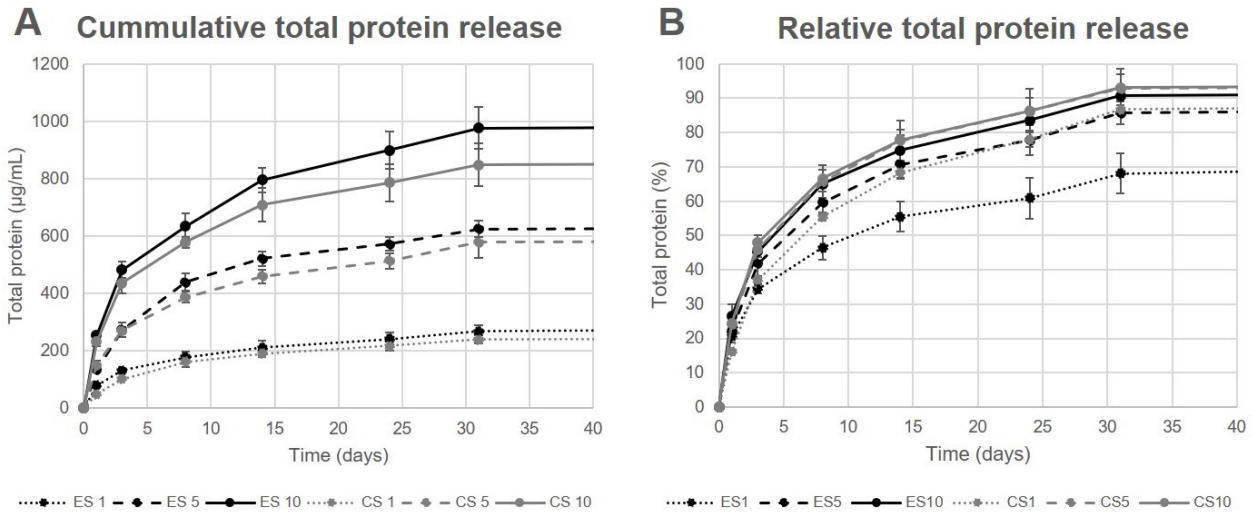

Figure 36 **Total protein release from the electrospun and centrifugal spun fibrous scaffolds**. A – Cumulative total protein release, B – Relative total protein release. ES PCL-1% PF-68 (ES1), CS PCL-1% PF-68 (CS1), ES PCL-5% PF-68 (ES5), CS PCL-5% PF-68 (CS5), ES PCL-10% PF-68 (ES10), CS PCL-10% PF-68 (CS10). Lines in black colour represent the protein release from the electrospun scaffolds, lines in grey colour represent the centrifugal spun scaffolds.

The amount of the protein released on day 1 ranged from 20 to 24 percent in all the tested samples. The burst release was followed by a sustained release continuing for 30 days. In electrospun fibres, the release rate increased with increasing PF-68 core concentration. The half-time of release for the ES1 sample (1% PF-68 fibres) was determined to be 10.4 days. In the case of the higher core concentrations, the release was faster and half-time was shifted to 5.3 days for ES5 (5% PF-68) and 4.2 days for ES10 (10% PF-68). Similar pattern was followed by the centrifugal spun scaffolds; the half-time of the release was decreasing with the increasing PF-68 concentration. In the case of the sample CS1 (1% PF-68), it was 6.5 days and in CS5 (5% PF-68) and CS10 (10% PF-68) it decreased to 4 and 3.6 days, respectively. The faster release from the samples correlates with the behaviour observed in our previous studies. The emulsion electrospinning prepares fibres for long-term delivery of active molecules [98]. In the case of centrifugal spinning, the fibres showed a similar release pattern and the mean release time was shorter than in the studies with electrospun fibres[91,224–226]. This may be caused by better encapsulation of molecules and more homogenous core droplet distribution in

electrospun fibres. In centrifugal spun fibres due to high centrifugal forces, the droplets are shifted closer to the surface of the fibres resulting in faster release.

The highest total protein release (Figure 36A) was detected in the groups containing 10% PF-68 as a core phase, for both electrospun and centrifugal spun fibres. With a decreasing PF-68 concentration, the amount of the released proteins decreased and was lowest for the samples containing 1% PF-68. The higher total cumulative release of protein in samples with a higher PF-68 concentration may relate to the higher presence of PF-68 core micelles in the structure of the fibre. This hypothesis is confirmed by the higher number of PF-68 core droplets observed during the emulsion centrifugal spinning process[91]. The higher number of core droplets results in a higher droplet interconnection and a lower number of the isolated droplets, forming a more continuous core in the core/shell-like structure. Upon interaction of fibres with high PF-68 concentration with an aqueous solvent, the water diffuses into these droplet pores and dissolves the core droplets, resulting in a higher and faster release. The droplet interconnection enables further diffusion and desorption from deeper droplets without the need for fibre degradation. In the case of scaffolds with a lower PF-68 concentration, the number of interconnected droplets available for release is lower, resulting in a more sustained, yet less intensive release. A long-term release is in the case of fibres driven both by diffusion and degradation mechanisms[227]. The PCL fibre degradation is slow and plays a less dominant role[228]. The surface degradation of the fibres was observed on the SEM images taken on day 1 and 17 of the experiment (Figure 37).

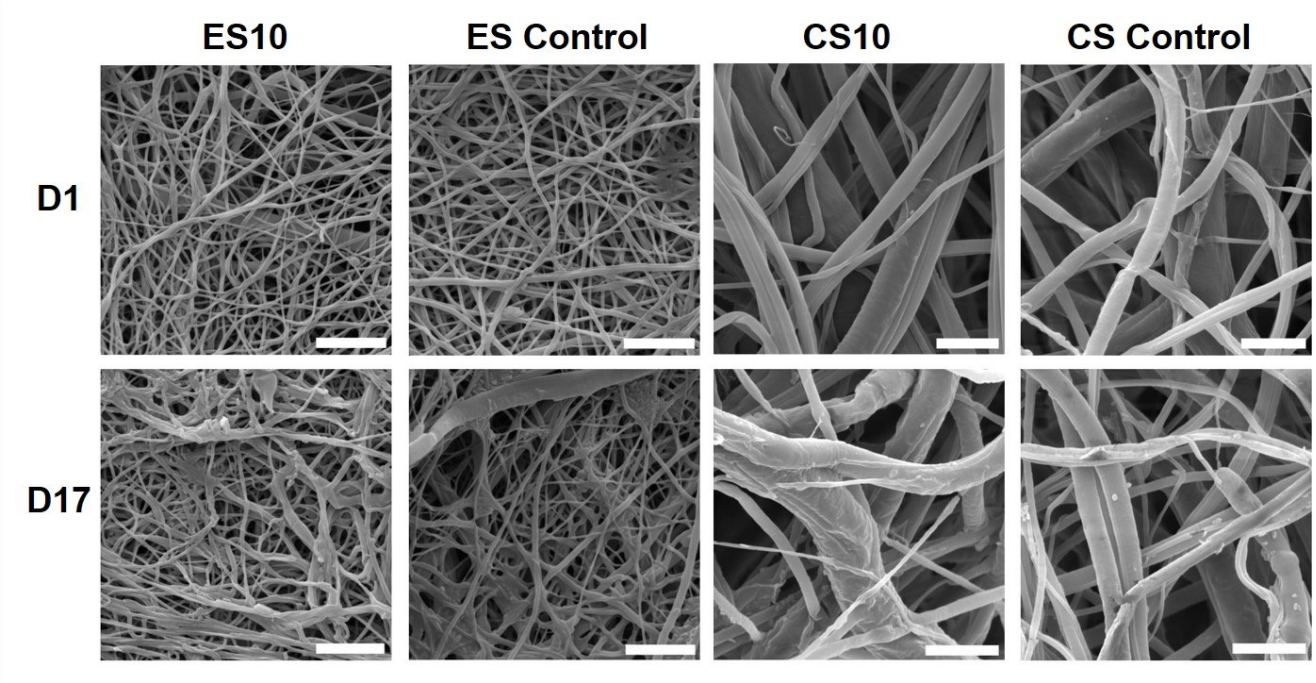

Figure 37 **Scanning electron images showing the degradation of the electrospun and centrifugal spun scaffolds**. The SEM images were taken after 1 and 17 days of incubation in an aqueous solution. Control scaffolds and scaffolds containing 10% PF-68 (ES10 and CS10) were used to illustrate the changes. After the 17-day immersion of the scaffolds in the aqueous solution, the scaffolds were fixed using glutaraldehyde and dehydrated. On day 17, degradation changes of the surface of the fibres were observed. Magnification 8000x, scale bar 5 μm[218].

After a short-term (1-day) incubation in the aqueous solvent, the samples showed smooth surface indicating tight polymer chain interconnection. On the other hand, after 17 days of incubation, the changes in fibre surface morphology were apparent. The fibres showed more structured surface connected with changes in polymer chain organization. Such changes resulted in more porous structure of the fibres and may play role in release from the scaffolds. Besides erosion of the fibre surface, the release is regulated by the rate of drug and water diffusion. The diffusion is driven via the interconnected droplets and through nanopores in the PCL fibre structure, observed previously[84]. The hypothesis correlates both with the release half-times and the amount of the total protein released from our scaffolds.

The molecular mechanisms behind wound healing highlight the suitability of platelets as a source of growth factors. The release from the fibres correlates with the time frame of skin

regeneration. The cytokines contained in platelets stimulate the healing processes, and after their incorporation into the fibrous meshes, the scaffolds stimulate progress through the wound healing phases. The pattern of the protein release from our scaffolds correlates with the duration of the wound healing phases. The half-time of release from 3 to 5 days for samples with 5% and 10% PF-68 provides an optimal stimulation for the early and middle phases of wound healing. Nevertheless, the prolonged release enables the extension of wound dressing exchange intervals and helps to decrease the economic burden related to the successful healing of wounds.

6.4.4 Fibroblasts seeded on the fibrous scaffolds

The platelet lyophilizate embedded into the scaffolds was used for stimulation of fibroblast proliferation and their metabolic activity (Figure 38). The biocompatibility of the fibrous meshes was tested using 3T3 fibroblasts. The metabolic activity of the seeded fibroblasts was evaluated using the MTS assay on days 1, 3, 7, 14 and 17. The data showed similar results for stimulation of metabolic activity of the seeded fibroblasts on the electrospun (Figure 38A) and centrifugal spun scaffolds (Figure 38B). In both the electrospun and centrifugal spun samples, the samples containing the highest amount of the platelet lyophilizate (ES10 or CS10) were superior in terms of stimulation of fibroblast metabolic activity. Furthermore, the performed overall statistical analysis of all the acquired data confirmed, that the metabolic activity of the seeded fibroblasts on the centrifugal spun sample CS10 (highest loading capacity) was significantly higher in comparison to all the tested samples (electrospun and centrifugal spun) on day 14 and higher than the electrospun samples on day 17.

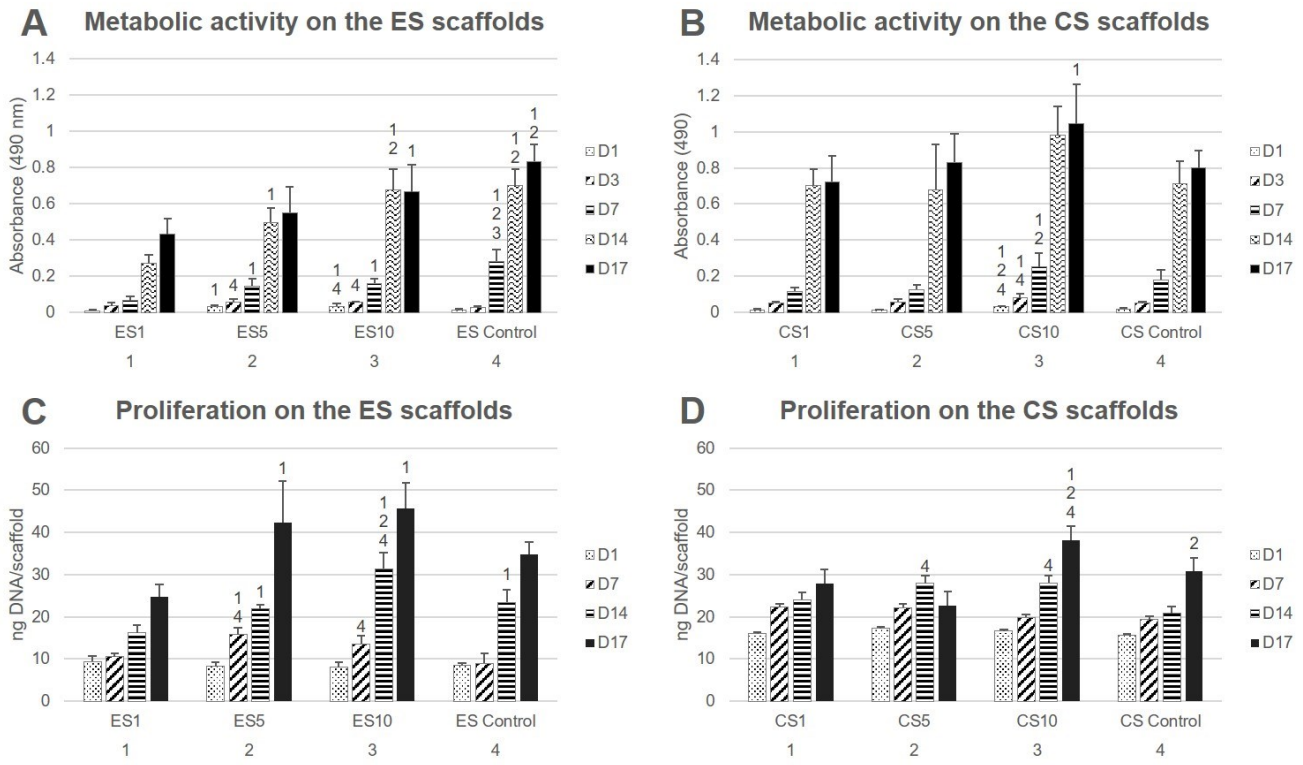

Figure 38 **Metabolic activity and proliferation of fibroblasts seeded on the electrospun and centrifugal spun scaffolds**. A – Metabolic activity of fibroblasts seeded on the electrospun scaffolds, B – Metabolic activity of fibroblasts seeded on the centrifugal spun scaffolds, C – Proliferation of fibroblasts seeded on the electrospun scaffolds, D – Proliferation of fibroblasts seeded on the centrifugal spun scaffolds. ES PCL-1% PF-68 (ES1), ES PCL-5% PF-68 (ES5), ES PCL-10% PF-68 (ES10), ES PCL Control, CS PCL-1% PF-68 (CS1), CS PCL-5% PF-68 (CS5), CS PCL-10% PF-68 (CS10), CS PCL Control. D1 – D17 denote experimental days. The level of significance is denoted by the numbers above the bars in the graph, number 1 representing the E/CS1 scaffold, 2 the E/CS5 scaffold, 3 the E/CS10 scaffold and 4 the E/CS control scaffold Statistical significance was set at $p<0.05$[218].

The proliferation data for the days corresponding to the MTS assay showed a similar pattern (Figure 38C-D). The statistical analysis of all samples showed a significantly improved initial adhesion of fibroblasts to all the centrifugal spun samples on day 1 when compared to the electrospun samples. Such trend was maintained until day 14 of the experiment. On day 14, all the differences between the centrifugal spun and electrospun samples were levelled out. The samples with the highest loading capacity (ES10, CS10) yielded the most promising results in stimulation of the fibroblast proliferation.

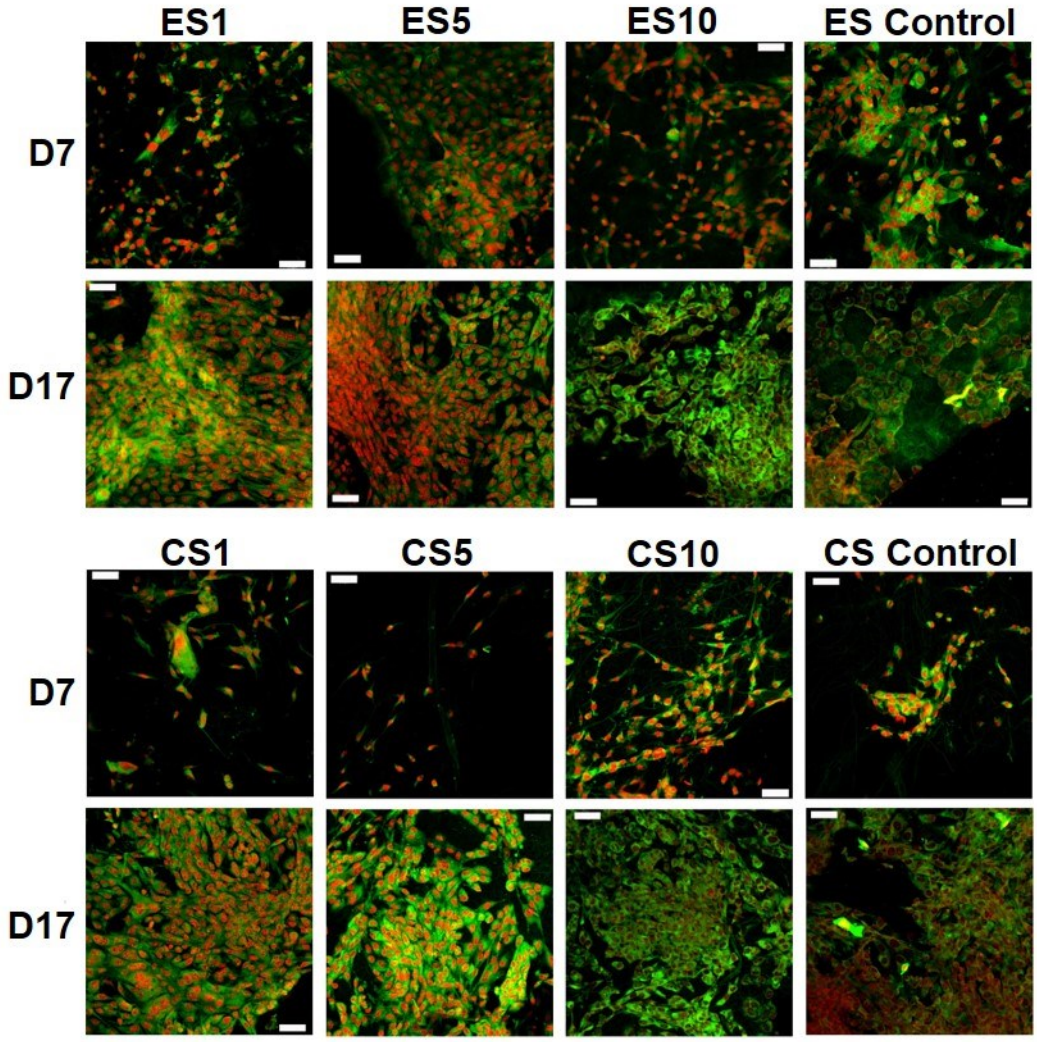

Figure 39 **Confocal microscopy images of the fibroblasts seeded on the electrospun and centrifugal spun scaffolds**. The fibroblasts seed on the scaffolds were scanned on day 7 and day 17. ES PCL-1% PF-68 (ES1), ES PCL-5% PF-68 (ES5), ES PCL-10% PF-68 (ES10), ES PCL Control, CS PCL-1% PF-68 (CS1), CS PCL-5% PF-68 (CS5), CS PCL-10% PF-68 (CS10), CS PCL Control. Green colour depicts the cellular biologic membranes (staining by DiOC6(3)), red colour cell nuclei (propidium iodide staining). Magnification 200x, scale bar 50 μm[218].

The data were confirmed by confocal microscopy. The fibroblast morphology detected on day 7 was similar on all the tested scaffolds. However, after a longer culture, the cell morphology among the scaffolds began to differ. On the scaffolds with the lower concentrations of PF-68, the cells were overlapped and more stratified. On the other hand, the cells on the scaffolds containing more of the platelet lyophilisate were more isolated and the boundaries between the cells were more pronounced (Figure 39).

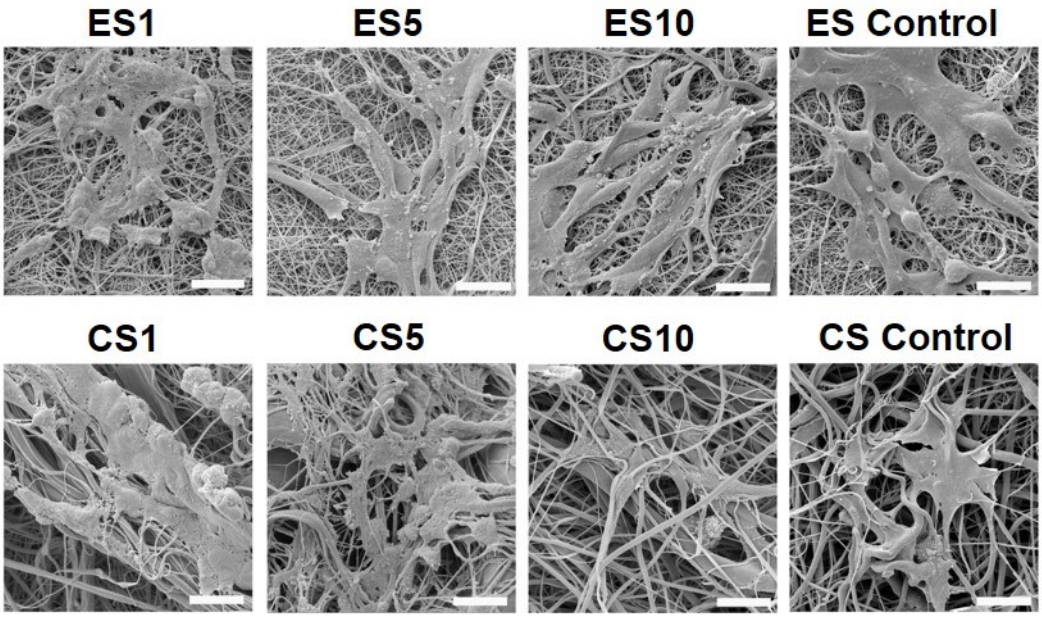

Figure 40 **SEM images of fibroblast morphology on the electrospun and the centrifugal spun scaffolds**. The samples with the seeded cells were fixed and dehydrated on day 7 of the experiment. ES PCL-1% PF-68 (ES1), ES PCL-5% PF-68 (ES5), ES PCL-10% PF-68 (ES10), ES PCL Control, CS PCL-1% PF-68 (CS1), CS PCL-5% PF-68 (CS5), CS PCL-10% PF-68 (CS10), CS PCL Control. Magnification 3000x, scale bar 20 μm[218].

Furthermore, the morphology of the seeded fibroblasts was visualised using scanning electron microscopy on day 7 (Figure 40). On the scaffolds with the lower platelet lyophilizate content, the cells formed clusters. However, with the increasing concentration of the platelet lyophilizate, the cells were well spread and exhibited morphology typical for the culture of fibroblasts on PCL scaffolds. To emphasize and more accurately observe the effect of the released platelet lyophilizate, the seeded cells were cultured under serum-reduced conditions (5% FBS), suggesting that the growth factors contained in scaffolds with lower concentration of platelet lyophilizate were not enough to properly stimulate fibroblast proliferation.

The results indicate that the fibroblasts showed a similar growth pattern on both the electrospun and centrifugal spun scaffolds. Polycaprolactone in the form of fibrous scaffolds was shown to stimulate fibroblast proliferation and metabolic activity[81,191]. The results indicated a similar affinity of fibroblasts to both the nano-/microfibrous and microfibrous scaffolds. The

structure of both scaffolds resembled the structure of the ECM of the connective tissues and the fibroblasts showed good adhesion and proliferation on the scaffolds. In addition, the platelet lyophilizate stimulated cell metabolic activity in a rather dose-dependent manner, which was in accordance with our previous study[91]. The samples containing PF-68 and the lowest concentration of the growth factors did not significantly stimulate the cell metabolic activity. This may relate to the altered release characteristics or the dominant inhibitory effect of the released chemokines. The 1% PF-68 fibres showed the slowest release rate and the lowest total protein content. The most dominant chemokines in platelet lyophilizate were IL-17 and RANTES. At low concentrations, these proteins were the most abundant chemokines released from the fibres. IL-17 was shown to stimulate the production of pro-angiogenic factors in fibroblasts and thus mediate fibroblast-induced angiogenesis[229]. In the groups with higher PF-68 concentrations, the amount of the total released protein was higher. With the increasing total protein concentration, the bioavailability of the growth factors, which act as fibroblast mitogens, increased as well (i.e. PDGF, EGF). Therefore, their proliferation and metabolic activity were improved. Such findings are in accordance with our previous study that revealed a dose-dependent effect of human platelet lysate on fibroblasts cultured on plain electrospun PCL scaffolds[172]. Additionally, the positive effect of growth factors released from the platelets adhered to the PCL nanofibrous scaffold, was observed in fibroblast culture.

6.4.5 Keratinocytes seeded on the fibrous scaffolds

Additionally, keratinocytes were used to evaluate the biocompatibility of the prepared fibrous scaffolds. On days 1, 3, 7, 14 and 17, the MTS assay was performed (Figure 41).

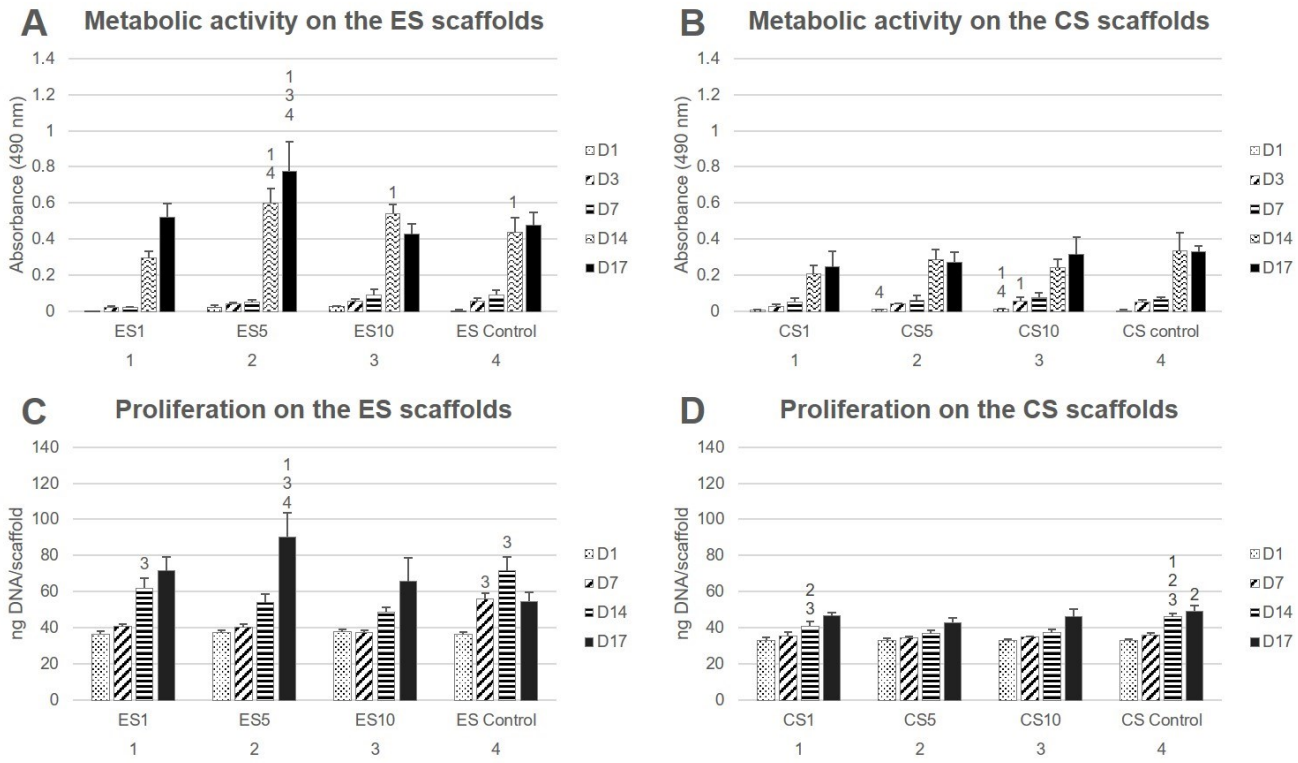

Figure 41 **Metabolic activity and proliferation of keratinocytes seeded on the electrospun and centrifugal spun scaffolds**. A – Metabolic activity of keratinocytes seeded on the electrospun scaffolds, B – Metabolic activity of keratinocytes seeded on the centrifugal spun scaffolds, C – Proliferation of keratinocytes seeded on the electrospun scaffolds, D – Proliferation of keratinocytes seeded on the centrifugal spun scaffolds. ES PCL-1% PF-68 (ES1), ES PCL-5% PF-68 (ES5), ES PCL-10% PF-68 (ES10), ES PCL Control, CS PCL-1% PF-68 (CS1), CS PCL-5% PF-68 (CS5), CS PCL-10% PF-68 (CS10), CS PCL Control. D1 – D17 denote experimental days. The level of significance is denoted by the numbers above the bars in the graph, number 1 representing the E/CS1 scaffold, 2 the E/CS5 scaffold, 3 the E/CS10 scaffold and 4 the E/CS control scaffold Statistical significance was set at $p<0.05$[218].

The data acquired from keratinocytes seeded on the electrospun scaffolds (Figure 41A) showed improved metabolic activity on the ES5 and ES10 and ES Control samples, when compared to the ES1 scaffold through the first 14 days of the experiment. On day 14, the keratinocytes seeded on the ES5 sample showed improved metabolic activity when compared to the ES Control sample. Additionally, on day 17, the metabolic activity of keratinocytes seeded on the ES5 sample was significantly higher than all the other electrospun samples (ES1, ES10 and ES Control). No such trend was observed on the centrifugal spun samples (Figure 41B). The samples CS5 and CS10 showed improved metabolic activity of the cells on days 1 and 3, however, all the differences were levelled out by day 7 and no statistically significant difference

in metabolic activity was observed until the end of the experiment. The performed overall statistical analysis of the metabolic activity of keratinocytes seeded on the fibrous samples showed, that on day 14 of the experiment the electrospun samples ES5, ES10 and the control sample exhibited higher metabolic activity of the seeded keratinocytes when compared to all the centrifugal spun samples (CS1, CS5, CS10 and CS Control). However, on the last day of the experiment, improved metabolic activity was found on the electrospun samples ES1 and ES5.

Furthermore, keratinocyte proliferation was evaluated. The data showed increasing proliferation on the platelet lyophilisate-enriched electrospun scaffolds through the entire experiment (Figure 41C). On day 17, keratinocytes seeded on the ES5 scaffold showed superior proliferation to all the other electrospun samples. The proliferation of keratinocytes seeded on the centrifugal spun samples (Figure 41D) was not as pronounced as on the electrospun samples, and the stimulatory effect of platelet lyophilizate was not observed.

The optimal concentration of the released bioactive molecules for keratinocyte culture seemed to follow the release pattern of fibrous scaffolds prepared with 5% PF-68. Keratinocytes cultured on such scaffolds showed a statistically significantly higher metabolic activity and cell proliferation, not only in comparison to the PCL control, but to the other platelet lyophilizate-enriched samples as well. In our previous study with the platelets adhered to the surface of the nanofibres, all the platelet-functionalised PCL samples showed improved keratinocyte metabolic activity and proliferation without significant differences among them, suggesting the other concentrations of the platelet-derived bioactive molecules in the current study were either too high (ES10) and rather inhibited the keratinocyte proliferation, or too low (ES1) and, in terms of improved cellular proliferation, insufficient. The dose-dependent effect of platelet lyophilizate

in keratinocyte culture was also observed in culture on blend PCL nanofibers[168]. Correspondingly, we have investigated the optimal composition of cell culture media supplemented with platelet lysate (PL) in keratinocytes. According to our results, the stimulation of proliferation of keratinocytes was achieved with increasing PL concentration, with the optimal concentration being determined as 7% (v/v) PL[172].

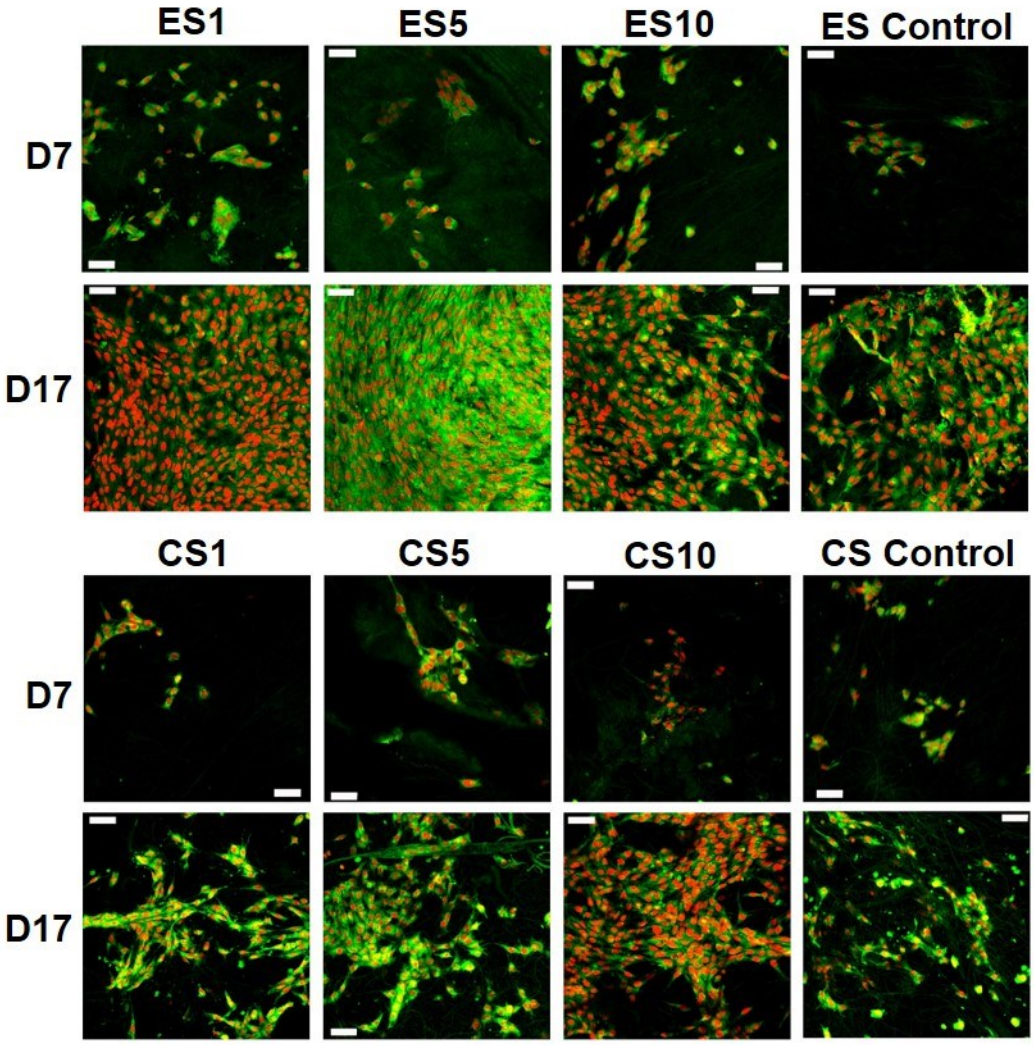

Figure 42 **Confocal microscopy images of the keratinocytes seeded on the electrospun and centrifugal spun scaffolds**. The keratinocytes seed on the scaffolds were scanned on day 7 and day 17. ES PCL-1% PF-68 (ES1), ES PCL-5% PF-68 (ES5), ES PCL-10% PF-68 (ES10), ES PCL Control, CS PCL-1% PF-68 (CS1), CS PCL-5% PF-68 (CS5), CS PCL-10% PF-68 (CS10), CS PCL Control. Green colour depicts the cellular biologic membranes (staining by DiOC6(3)), red colour cell nuclei (propidium iodide staining). Magnification 200x, scale bar 50 μm[218].

The data obtained in the proliferation assay were confirmed by confocal microscopy (Figure 42). The images acquired on day 17 showed significantly improved proliferation of keratinocytes on the ES5 sample, where the keratinocytes formed confluent layers and exhibited stratified morphology. Although the increase in cell numbers from day 7 to day 17 was not so pronounced on the other samples (ES1, ES10, CS1, CS5, CS10 and controls), the proliferation of keratinocytes was clearly detectable.

On the 2D-like electrospun samples, the cultured keratinocytes formed confluent layers. The most promising composition of the prepared fibres, in terms of promotion of stratified epithelium formation, was shown by the ES5 sample. Such findings confirmed that in favourable conditions, keratinocytes tend to mature, and form stratified layers. However, on all the centrifugal spun samples, islands varying in number of the cultured cells were found, regardless of the presence and/or concentration of the platelet-derived bioactive molecules. This indicates suboptimal morphology of the tested centrifugal spun fibrous layers for the stimulation of keratinocyte epithelium formation. Such findings are in concordance with the findings of study investigating the influence of fibre diameter and pore size of denatured collagen microfiber scaffolds on keratinocyte adhesion, proliferation, migration and penetration into the scaffold[230]. The results showed that the porous scaffold promoted cell adhesion and survival, however hampered keratinocyte migration and penetration. Thus, the data suggest suitability of the morphology of the electrospun layers for keratinocyte stimulation.

Additionally, scanning electron microscopy was used to visualise the cells adhered to the nanofibrous scaffolds on day 7 (Figure 43). The images showed well spread cells with morphology characteristic for keratinocytes.

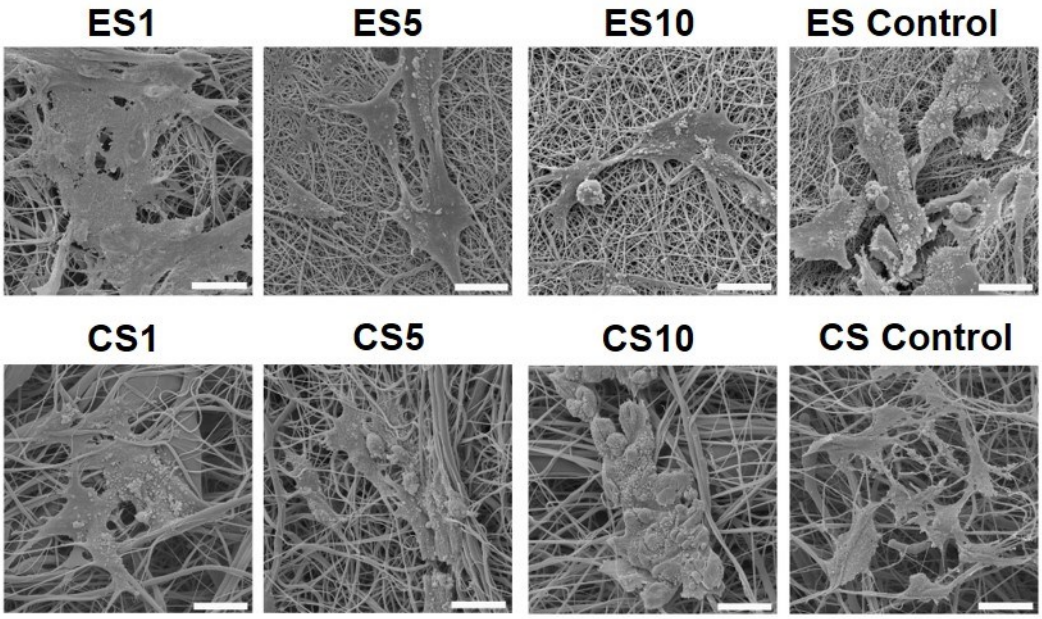

Figure 43 **SEM images of keratinocyte morphology on the electrospun and the centrifugal spun scaffolds**. The samples with the seeded cells were fixed and dehydrated on day 7 of the experiment. ES PCL-1% PF-68 (ES1), ES PCL-5% PF-68 (ES5), ES PCL-10% PF-68 (ES10), ES PCL Control, CS PCL-1% PF-68 (CS1), CS PCL-5% PF-68 (CS5), CS PCL-10% PF-68 (CS10), CS PCL Control. Magnification 3000x, scale bar 20 μm[218].

On the electrospun scaffolds, the cells were observed on the surface of the fibres. The structure of the scaffold was mimicking the basal lamina. On the other hand, in the case of centrifugal spun scaffolds, the bigger pore size lead to formation of clusters and spheroid like structures. The cells were less spread, and the colonisation of the scaffold was relatively slower. This phenomenon was associated with the different structure of the scaffold. The scaffold with a smaller pore size supported cell adhesion but did not allow cell penetration into its deeper layers, stimulating only cell interaction on superficial layers and pushing the cells to more epithelial tissue formation.

The superior morphological properties of the nanofibres compared to microfibres were shown in chitin electrospun fibrous scaffolds and silk fibroin matrices[231,232]. The submicron diameters of the nanofibrous scaffolds significantly promoted cell adhesion and spreading, compared to the microfibres. Additionally, the dependency of keratinocyte proliferation on the

strand diameter of 3D-plotted collagen fibres was investigated. With the increasing strand diameter, the proliferation rate of keratinocytes decreased[233]. This indicates the importance of proper morphology of the fibrous scaffolds in skin tissue engineering constructs.

Besides morphological mimicking, the release of growth factors stimulated cell proliferation. Human keratinocytes were cultured on PCL and PCL/collagen blend electrospun nanofibrous matrices with immobilised EGF on their surface. The nanofibrous texture of the scaffolds affected the cultured cells. Furthermore, the drug delivery of the immobilised EGF to the surface of the nanofibres resulted in rapid proliferation of keratinocytes in comparison to the control samples containing no EGF[79]. Another study showed that the bioavailability of EGF in an animal diabetic wound model was prolonged by its conjugation to the surface of the PCL/PEG nanofibrous scaffolds in comparison to the PCL/PEG nanofibres soaked in the EGF solution. Such treatment accelerated the wound closure, especially in its early stages[95]. These studies have illustrated the necessity of a sustained release of the growth factors, as most of the GFs administered as exogenous additives failed in clinical practice, mainly due to the high proteolytic activities in the wound.

6.4.6 Summary

The developed drug delivery system enabled long-term delivery of susceptible molecules; significant levels of proteins were detected even after a period of 1 month. Furthermore, a comparable loading efficiency was achieved with the electrostatic and centrifugal spinning techniques. By alteration of the concentration of the core polymer, the release rate may be adjusted to the particular application. The prepared systems were tested in vitro. The data

showed both the 3D- and 2D-like systems were able to foster fibroblast culture, however, keratinocytes clearly preferred the surface of the 2D-like electrospun fibrous scaffolds.

7 CONCLUSION

Tissue engineering is a rapidly evolving field, flexibly responding to the unmet needs of the current medicine. The presented thesis aimed to explore the possibilities of utilization of platelet derivatives in the tissue engineering of the skin.

Firstly, the skin cell culture conditions were optimized, as there is a need for FBS replacement in clinical applications, to prevent xenogeneic immunization. It was shown that 7% platelet lysate sufficiently replaced the effects of 10% FBS. Interestingly, different cells responded to increased or decreased concentrations of bioactive molecules in a different way. While fibroblasts preferred lower concentrations with rather inhibitory effects of combination of FBS and platelet lysate, keratinocytes responded positively to the increasing concentrations of bioactive molecules. This finding highlights the necessity for optimization of cell culture conditions in clinical settings.

Furthermore, a drug delivery system suitable as a wound dressing was developed and optimized. The surface adhesion of autologous platelets in combination with the unique properties of nanofibres enables the translation of such system into clinical practice for topical applications. By adjusting the properties of the system, a scaffold delivering bioactive molecules crucial for fostering the healing process for up to 2 weeks was developed. Achieving such time frame for bioactive molecule delivery is remarkable, considering the simplicity of the system enabling its on-site preparation. The system represents a bridge between basic research and clinical application.

The short life span of native platelet derivatives was overcome by using the platelet lyophilisate. Lyophilisation of the platelets prolongs their life span from five days to up to two

years. Furthermore, it facilitates loading of the platelet content into drug delivery systems, ranging from surface modifications to encapsulation. Given the contained growth factors and their distinct role in the healing process, it is a versatile system that could find broader application in tissue engineering, not only in tissue engineering of the skin. The improved storage conditions may allow its commercialization.

8 SUMMARY

Platelet derivatives are an attractive source of natural growth factors and they are widely used in various tissue engineering and regenerative medicine applications.

The aim of this study was to optimize cell culture conditions using platelet lysate and to develop platelet-functionalized fibrous scaffolds as a controlled drug delivery system for native growth factors. Fibrous scaffolds were prepared by electrostatic and centrifugal spinning of PCL and they were functionalized by the platelets by surface adhesion or their encapsulation using emulsion spinning techniques.

The cell culture study determined the 7% platelet lysate to be the optimum concentration as a medium supplement in keratinocyte and fibroblast culture. Additionally, following surface adhesion of the platelets to PCL electrospun nanofibres, the platelets were activated due to their contact with the nanofibre nanotopography, resulting in formation of fibrin network. Fibrin served as a reservoir of the growth factors, prolonging the half-time of EGF release to 1.7 days. Such platelet-functionalized samples fostered proliferation of keratinocytes, fibroblasts and melanocytes. Furthermore, adhesion of platelets to centrifugally spun nanofibrous scaffolds resulted in almost two-fold increase in the amount of immobilized platelet-derived bioactive molecules, further promoting metabolic activity of the seeded melanocytes. Thanks to encapsulation of the platelet lyophilisate into emulsion electrospun and centrifugal spun coaxial nanofibres, a drug delivery system enabling long-term delivery of platelet-derive biomolecules was developed and optimized. The system was successfully tested in vitro using keratinocytes and fibroblasts, however, its versatility suggests broader application.

9 SOUHRN

Krevní deriváty jsou výborným zdrojem přirozených růstových faktorů. V tkáňovém inženýrství a regenerativní medicíně již našly řadu uplatnění.

Cílem této práce bylo optimalizovat podmínky buněčné kultury za použití destičkového lyzátu, a dále vyvinout mikro- a nanovlákenné nosiče funkcionalizované krevními destičkami, které by mohly sloužit jako systém řízeného dodávání přírodních růstových faktorů. Mikro- a nanovlákenné nosiče byly připraveny elektrostatickým a centrifugačním zvlákňováním PCL. Připravené nosiče byly funkcionalizovány povrchovou adhezí krevních destiček nebo jejich enkapsulací do vnitřní části nanovláken emulzní technikou.

V rámci studie kultivačních podmínek kožních buněk bylo zjištěno, že suplementace media 7% destičkovým lyzátem je dostačující pro nahrazení 10% FBS v kultuře keratinocytů a fibroblastů. Dále byl povrch PCL nanovláken připravených elektrostatickým zvlákňováním funkcionalizován krevními destičkami. Při kontaktu s nanotopografií nanovlákenného povrchu došlo k aktivaci destiček a následně k vytvoření fibrinové sítě, která sloužila jako rezervoár růstových faktorů. Díky tomu došlo k prodloužení poločasu uvolnění EGF až na 1.7 dní. Takto funkcionalizované nanovlákenné nosiče podporovaly proliferace a metabolickou aktivitu keratinocytů, fibroblastů a melanocytů. Při adhezi krevních destiček na mikro-/nanovlákna vytvořená centrifugačním zvlákňováním došlo k dvounásobnému nárůstu množství růstových faktorů zachycených na nosiči, a následně k další stimulaci metabolické aktivity nasazených melanocytů. Díky enkapsulaci destičkového lyofilizátu do koaxiálních nanovláken byl vytvořen systém dlouhodobého dodávání, který byl otestován pomocí fibroblastů a keratinocytů. Díky své univerzálnosti by však mohl hrát roli i v jiných odvětvích tkáňového inženýrství.

10 REFERENCES

1. Marieb, E., Wilhelm, P. & Mallat, J. *Human Anatomy*. (Pearson, 2017).
2. McLafferty, E., Hendry, C. & Farley, A. The integumentary system: anatomy, physiology and function of skin. *Nurs. Stand.* **27,** 35–42 (2012).
3. Tortora, G. J. & Derrickson, B. *Principles of anatomy and physiology*. (2009).
4. Kolarsick, P., Kolarsick, M. & Goodwin, C. Anatomy and Physiology of the Skin. *J. Dermatol. Nurses. Assoc.* **3,** 203–213 (2011).
5. Hirobe, T. Keratinocytes regulate the function of melanocytes. *Dermatologica Sin.* **32,** 200–204 (2014).
6. Shin, Y.-H., Seo, Y.-K., Yoon, H.-H., Song, K.-Y. & Park, J.-K. Effect of keratinocytes on regulation of melanogenesis in culture of melanocytes. *Biotechnol. Bioprocess Eng.* **17,** 203–210 (2012).
7. Boateng, J. & Catanzano, O. Advanced Therapeutic Dressings for Effective Wound Healing—A Review. *J. Pharm. Sci.* **104,** 3653–3680 (2015).
8. Velnar, T., Bailey, T. & Smrkolj, V. The wound healing process: an overview of the cellular and molecular mechanisms. *J. Int. Med. Res.* **37,** 1528–42 (2009).
9. Sen, C. K. *et al.* Human skin wounds: a major and snowballing threat to public health and the economy. *Wound Repair Regen.* **17,** 763–71 (2009).
10. Bitsch, M. *et al.* Standardised method of surgical treatment of chronic leg ulcers. *Scand. J. Plast. Reconstr. Surg. Hand Surg.* **39,** 162–169 (2005).
11. Sinno, H. & Prakash, S. Complements and the wound healing cascade: an updated review. *Plast. Surg. Int.* **2013,** 146764 (2013).
12. Clark, R. A. F., Ghosh, K. & Tonnesen, M. G. Tissue Engineering for Cutaneous Wounds. *J. Invest. Dermatol.* **127,** 1018–1029 (2007).
13. Gurtner, G. C., Werner, S., Barrandon, Y. & Longaker, M. T. Wound repair and regeneration. *Nature* **453,** 314–321 (2008).

14. Demidova-Rice, T. N., Hamblin, M. R. & Herman, I. M. Acute and Impaired Wound Healing: Pathophysiology and Current Methods for Drug Delivery, Part 1: Normal and Chronic Wounds: Biology, Causes, and Approaches to Care. *Adv. Skin Wound Care* **25,** 304–314 (2012).

15. Pospisilova, A. Bercovy vred. *Dermatologie pro praxi* **2,** 79–84 (2008).

16. Beanes, S. R., Dang, C., Soo, C. & Ting, K. Skin repair and scar formation: the central role of TGF-beta. *Expert Rev. Mol. Med.* **5,** 1–22 (2003).

17. Cheresh, D. A. Human endothelial cells synthesize and express an Arg-Gly-Asp-directed adhesion receptor involved in attachment to fibrinogen and von Willebrand factor. *Proc. Natl. Acad. Sci. U. S. A.* **84,** 6471–5 (1987).

18. Gailit, J. *et al.* Human fibroblasts bind directly to fibrinogen at RGD sites through integrin alpha(v)beta3. *Exp. Cell Res.* **232,** 118–26 (1997).

19. Heher, P., Mühleder, S., Mittermayr, R., Redl, H. & Slezak, P. Fibrin-based delivery strategies for acute and chronic wound healing. *Adv. Drug Deliv. Rev.* **129,** 134–147 (2018).

20. Zhao, R., Liang, H., Clarke, E., Jackson, C. & Xue, M. Inflammation in Chronic Wounds. *Int. J. Mol. Sci.* **17,** (2016).

21. Fager, G., Camejo, G., Olsson, U., Ostergren-Lundén, G. & Bondjers, G. Heparin-like glycosaminoglycans influence growth and phenotype of human arterial smooth muscle cells in vitro. II. The platelet-derived growth factor A-chain contains a sequence that specifically binds heparin. *In Vitro Cell. Dev. Biol.* **28A,** 176–80 (1992).

22. Caley, M. P., Martins, V. L. C. & O'Toole, E. A. Metalloproteinases and Wound Healing. *Adv. wound care* **4,** 225–234 (2015).

23. Lazaro, J. L. *et al.* Elevated levels of matrix metalloproteinases and chronic wound healing: an updated review of clinical evidence. *J. Wound Care* **25,** 277–287 (2016).

24. Sorg, H., Tilkorn, D. J., Hager, S., Hauser, J. & Mirastschijski, U. Skin Wound Healing: An Update on the Current Knowledge and Concepts. *Eur. Surg. Res.* **58,** 81–94 (2017).

25. Singer, A. J. & Clark, R. A. F. Cutaneous Wound Healing. *N. Engl. J. Med.* **341,** 738–746

(1999).

26. Xue, M. & Jackson, C. J. Extracellular Matrix Reorganization During Wound Healing and Its Impact on Abnormal Scarring. *Adv. wound care* **4,** 119–136 (2015).

27. Lazarus, G. S. *et al.* Definitions and guidelines for assessment of wounds and evaluation of healing. *Wound Repair Regen.* **2,** 165–170 (1994).

28. Dreifke, M. B., Jayasuriya, A. A. & Jayasuriya, A. C. Current wound healing procedures and potential care. *Mater. Sci. Eng. C* **48,** 651–662 (2015).

29. Barrientos, S., Stojadinovic, O., Golinko, M. S., Brem, H. & Tomic-Canic, M. PERSPECTIVE ARTICLE: Growth factors and cytokines in wound healing. *Wound Repair Regen.* **16,** 585–601 (2008).

30. Rheinwald, J. G. & Green, H. Epidermal growth factor and the multiplication of cultured human epidermal keratinocytes. *Nature* **265,** 421–424 (1977).

31. Brem, H. *et al.* Molecular markers in patients with chronic wounds to guide surgical debridement. *Mol. Med.* **13,** 30–9 (2007).

32. Mast, B. A. & Schultz, G. S. Interactions of cytokines, growth factors, and proteases in acute and chronic wounds. *Wound Repair Regen.* **4,** 411–420 (1996).

33. Werner, S. & Grose, R. Regulation of Wound Healing by Growth Factors and Cytokines. *Physiol. Rev.* **83,** 835–870 (2003).

34. Ornitz, D. M. FGFs, heparan sulfate and FGFRs: complex interactions essential for development. *BioEssays* **22,** 108–112 (2000).

35. Demidova-Rice, T. N., Hamblin, M. R. & Herman, I. M. Acute and Impaired Wound Healing: Pathophysiology and Current Methods for Drug Delivery, Part 2: Role of Growth Factors in Normal and Pathological Wound Healing: Therapeutic Potential and Methods of Delivery. *Adv. Skin Wound Care* **25,** 349–370 (2012).

36. Robson, M. C. The role of growth factors in the healing of chronic wounds. *Wound Repair Regen.* **5,** 12–17 (1997).

37. Raja, Sivamani, K., Garcia, M. S. & Isseroff, R. R. Wound re-epithelialization: modulating

keratinocyte migration in wound healing. *Front. Biosci.* **12,** 2849–68 (2007).

38. Niu, J. *et al.* Keratinocyte Growth Factor/Fibroblast Growth Factor-7-regulated Cell Migration and Invasion through Activation of NF-κB Transcription Factors. *J. Biol. Chem.* **282,** 6001–6011 (2007).

39. Clark, R. A. *The molecular and cellular biology of wound repair*. (Plenum Press, 1996).

40. Mitra, R. & Khar, A. Suppression of macrophage function in AK-5 tumor transplanted animals: role of TGF-β1. *Immunol. Lett.* **91,** 189–195 (2004).

41. Tsunawaki, S., Sporn, M., Ding, A. & Nathan, C. Deactivation of macrophages by transforming growth factor-β. *Nature* **334,** 260–262 (1988).

42. Heldin, C.-H. & Westermark, B. Mechanism of Action and In Vivo Role of Platelet-Derived Growth Factor. *Physiol. Rev.* **79,** 1283–1316 (1999).

43. Uutela, M. *et al.* PDGF-D induces macrophage recruitment, increased interstitial pressure, and blood vessel maturation during angiogenesis. *Blood* **104,** 3198–3204 (2004).

44. Edelberg, J. M. *et al.* PDGF mediates cardiac microvascular communication. *J. Clin. Invest.* **102,** 837–43 (1998).

45. Ando, Y. & Jensen, P. J. Epidermal growth factor and insulin-like growth factor I enhance keratinocyte migration. *J. Invest. Dermatol.* **100,** 633–9 (1993).

46. Krishnaswami, S., Ly, Q. P., Rothman, V. L. & Tuszynski, G. P. Thrombospondin-1 promotes proliferative healing through stabilization of PDGF. *J. Surg. Res.* **107,** 124–30 (2002).

47. Jinnin, M. *et al.* Regulation of fibrogenic/fibrolytic genes by platelet-derived growth factor C, a novel growth factor, in human dermal fibroblasts. *J. Cell. Physiol.* **202,** 510–517 (2005).

48. Boateng, J. S., Matthews, K. H., Stevens, H. N. E. & Eccleston, G. M. Wound Healing Dressings and Drug Delivery Systems: A Review. *J. Pharm. Sci.* **97,** 2892–2923 (2008).

49. Queen, D., Orsted, H., Sanada, H. & Sussman, G. A dressing history. *Int. Wound J.* **1,**

59–77 (2004).

50. Shevchenko, R. V, James, S. E. L. & James, S. E. L. A review of tissue-engineered skin bioconstructs available for skin reconstruction. *J. R. Soc. Interface* **7,** 229–58 (2010).

51. Fonder, M. A. *et al.* Treating the chronic wound: A practical approach to the care of nonhealing wounds and wound care dressings. *J. Am. Acad. Dermatol.* **58,** 185–206 (2008).

52. Han, G. & Ceilley, R. Chronic Wound Healing: A Review of Current Management and Treatments. *Adv. Ther.* **34,** 599–610 (2017).

53. Vig, K. *et al.* Advances in Skin Regeneration Using Tissue Engineering. *Int. J. Mol. Sci.* **18,** 789 (2017).

54. Böttcher-Haberzeth, S., Biedermann, T. & Reichmann, E. Tissue engineering of skin. *Burns* **36,** 450–460 (2010).

55. Falanga, V. Wound healing and its impairment in the diabetic foot. *Lancet (London, England)* **366,** 1736–43 (2005).

56. Robson, M. *et al.* Recombinant human platelet-derived growth factor-BB for the treatment of chronic pressure ulcers. *Ann. Plast. Surg.* **29,** 193–201 (1992).

57. Rees, R. S., Robson, M. C., Smiell, J. M. & Perry, B. H. Becaplermin gel in the treatment of pressure ulcers: a phase II randomized, double-blind, placebo-controlled study. *Wound Repair Regen.* **7,** 141–7 (1999).

58. Steed, D. L. Clinical evaluation of recombinant human platelet-derived growth factor for the treatment of lower extremity diabetic ulcers. Diabetic Ulcer Study Group. *J. Vasc. Surg.* **21,** 71-8; discussion 79-81 (1995).

59. MacNeil, S. Progress and opportunities for tissue-engineered skin. *Nature* **445,** 874–880 (2007).

60. Vacanti, C. A. The history of tissue engineering. *J. Cell. Mol. Med.* **10,** 569–76 (2006).

61. Langer, R. & Vacanti, J. P. Tissue engineering. *Science* **260,** 920–6 (1993).

62. Howard, D., Buttery, L. D., Shakesheff, K. M. & Roberts, S. J. Tissue engineering:

strategies, stem cells and scaffolds. *J. Anat.* **213,** 66–72 (2008).

63. Lutolf, M. P. & Hubbell, J. A. Synthetic biomaterials as instructive extracellular microenvironments for morphogenesis in tissue engineering. *Nat. Biotechnol.* **23,** 47–55 (2005).

64. Supp, D. M. & Boyce, S. T. Engineered skin substitutes: Practices and potentials. *Clin. Dermatol.* **23,** 403–412 (2005).

65. Alrubaiy, L. & Al-Rubaiy, K. K. Skin Substitutes: A Brief Review of Types and Clinical Applications. *Oman Med. J.* **24,** 6–8 (2009).

66. Límová, M. Active Wound Coverings: Bioengineered Skin and Dermal Substitutes. *Surg. Clin. North Am.* **90,** 1237–1255 (2010).

67. Uccioli, L. A Clinical Investigation on the Characteristics and Outcomes of Treating Chronic Lower Extremity Wounds using the TissueTech Autograft System. *Int. J. Low. Extrem. Wounds* **2,** 140–151 (2003).

68. Ho, W. S. Skin substitutes: An overview. *Ann. Coll. Surg. Hong Kong* **6,** 102–108 (2002).

69. Rieger, K. A., Birch, N. P. & Schiffman, J. D. Designing electrospun nanofiber mats to promote wound healing – a review. *J. Mater. Chem. B* **1,** 4531 (2013).

70. Ma, Z., Kotaki, M., Inai, R. & Ramakrishna, S. Potential of Nanofiber Matrix as Tissue-Engineering Scaffolds. *Tissue Eng.* **11,** 101–109 (2005).

71. Hassiba, A. J. *et al.* Review of recent research on biomedical applications of electrospun polymer nanofibers for improved wound healing. *Nanomedicine* **11,** 715–737 (2016).

72. von der Mark, K. & Park, J. Engineering biocompatible implant surfaces: Part II: Cellular recognition of biomaterial surfaces: Lessons from cell–matrix interactions. *Prog. Mater. Sci.* **58,** 327–381 (2013).

73. Dhandayuthapani, B., Yoshida, Y., Maekawa, T. & Kumar, D. S. Polymeric scaffolds in tissue engineering application: A review. *Int. J. Polym. Sci.* **2011,** (2011).

74. Pillai, C. K. S. Recent advances in biodegradable polymeric materials. *Mateirals Sci. Technol.* **30,** 558–566 (2014).

75. Cipitria, A., Skelton, A., Dargaville, T. R., Dalton, P. D. & Hutmacher, D. W. Design, fabrication and characterization of PCL electrospun scaffolds - A review. *J. Mater. Chem.* **21,** 9419–9453 (2011).

76. Zhong, S. P., Zhang, Y. Z. & Lim, C. T. Tissue scaffolds for skin wound healing and dermal reconstruction. *Wiley Interdiscip. Rev. Nanomedicine Nanobiotechnology* **2,** 510–525 (2010).

77. Chen, H., Huang, J., Yu, J., Liu, S. & Gu, P. Electrospun chitosan-graft-poly (É›-caprolactone)/poly (É›-caprolactone) cationic nanofibrous mats as potential scaffolds for skin tissue engineering. *Int. J. Biol. Macromol.* **48,** 13–19 (2010).

78. Powell, H. M. & Boyce, S. T. Engineered Human Skin Fabricated Using Electrospun Collagen–PCL Blends: Morphogenesis and Mechanical Properties. *Tissue Eng. Part A* **15,** 2177–2187 (2009).

79. Gümüdereliog, M., Dalkıranog, S., Seda Tıg, R. & Aydın, L. A novel dermal substitute based on biofunctionalized electrospun PCL nanofibrous matrix. *J. Biomed. Mater. Res. Part A* **98A,** 461–472 (2011).

80. Sadeghi-Avalshahr, A., Nokhasteh, S., Mahdi Molavi, A., Khorsand-Ghayeni, M. & Mahdavi-Shahri, M. Synthesis and characterization of collagen/ PLGA biodegradable skin scaffold fibers. *Regen. Biomater.* 309–314 (2017). doi:10.1093/rb/rbx026

81. Dubsky, M. *et al.* Nanofibers prepared by needleless electrospinning technology as scaffolds for wound healing. *J. Mater. Sci. Mater. Med.* **23,** 931–941 (2012).

82. Dahlin, R. L., Kasper, F. K. & Mikos, A. G. Polymeric nanofibers in tissue engineering. *Tissue Eng. Part B. Rev.* **17,** 349–64 (2011).

83. Chew, S. Y., Wen, Y., Dzenis, Y. & Leong, K. W. The role of electrospinning in the emerging field of nanomedicine. *Curr. Pharm. Des.* **12,** 4751–70 (2006).

84. Mickova, A. *et al.* Core/Shell Nanofibers with Embedded Liposomes as a Drug Delivery System. *Biomacromolecules* **13,** 952–962 (2012).

85. Reneker, D. H. & Yarin, A. L. Electrospinning jets and polymer nanofibers. *Polymer (Guildf).* **49,** 2387–2425 (2008).

86. Lukáš, D. *et al.* Physical principles of electrospinning (Electrospinning as a nano-scale technology of the twenty-first century). *Text. Prog.* **41,** 59–140 (2009).

87. Ramakrishna, S., Fujihara, K., Teo, W.-E., Lim, T.-C. & Ma, Z. *An Introduction to Electrospinning and Nanofibers*. (WORLD SCIENTIFIC, 2005). doi:10.1142/5894

88. Li, Z. & Wang, C. Effects of Working Parameters on Electrospinning. in *One-Dimensional Nanostructures* 15–28 (Springer, 2013). doi:10.1007/978-3-642-36427-3

89. Zander, N. E. Formation of melt and solution spun polycaprolactone fibers by centrifugal spinning. *J. Appl. Polym. Sci.* **132,** (2015).

90. Zhang, X. & Lu, Y. Centrifugal Spinning: An Alternative Approach to Fabricate Nanofibers at High Speed and Low Cost. *Polym. Rev.* **54,** 677–701 (2014).

91. Buzgo, M. *et al.* Emulsion centrifugal spinning for production of 3D drug releasing nanofibres with core/shell structure. *RSC Adv.* **7,** 1215–1228 (2017).

92. Rogalski, J., Bastiaansen, C. & Peijs, T. PA6 Nanofibre Production: A Comparison between Rotary Jet Spinning and Electrospinning. *Fibers* **6,** 37 (2018).

93. Meinel, A. J., Germershaus, O., Luhmann, T., Merkle, H. P. & Meinel, L. Electrospun matrices for localized drug delivery: Current technologies and selected biomedical applications. *Eur. J. Pharm. Biopharm.* **81,** 1–13 (2012).

94. Bölgen, N., Vargel, İ., Korkusuz, P., Menceloğlu, Y. Z. & Pişkin, E. In vivo performance of antibiotic embedded electrospun PCL membranes for prevention of abdominal adhesions. *J. Biomed. Mater. Res. Part B Appl. Biomater.* **81B,** 530–543 (2007).

95. Choi, J. S., Leong, K. W. & Yoo, H. S. In vivo wound healing of diabetic ulcers using electrospun nanofibers immobilized with human epidermal growth factor (EGF). *Biomaterials* **29,** 587–596 (2008).

96. Lee, K. Y., Jeong, L., Kang, Y. O., Lee, S. J. & Park, W. H. Electrospinning of polysaccharides for regenerative medicine. *Adv. Drug Deliv. Rev.* **61,** 1020–1032 (2009).

97. Ji, W. *et al.* Fibrous scaffolds loaded with protein prepared by blend or coaxial electrospinning. *Acta Biomater.* **6,** 4199–4207 (2010).

98. Buzgo, M. *et al.* Needleless emulsion electrospinning for the regulated delivery of susceptible proteins. *J. Tissue Eng. Regen. Med.* **12,** (2018).

99. Rice, J. J. *et al.* Engineering the Regenerative Microenvironment with Biomaterials. *Adv. Healthc. Mater.* **2,** 57–71 (2013).

100. Frieden, I. J. Addendum: Commentary on Becaplermin Gel (Regranex) for Hemangiomas. *Pediatr. Dermatol.* **25,** 590–590 (2008).

101. Carragee, E. J., Hurwitz, E. L. & Weiner, B. K. A critical review of recombinant human bone morphogenetic protein-2 trials in spinal surgery: emerging safety concerns and lessons learned. *Spine J.* **11,** 471–491 (2011).

102. Garrison, K. R. *et al.* Clinical effectiveness and cost-effectiveness of bone morphogenetic proteins in the non-healing of fractures and spinal fusion: a systematic review. *Health Technol. Assess.* **11,** 1–150, iii–iv (2007).

103. Masoudi, E., Ribas, J., Kaushik, G., Leijten, J. & Khademhosseini, A. Platelet-Rich Blood Derivatives for Stem Cell-Based Tissue Engineering and Regeneration. *Curr. stem cell reports* **2,** 33–42 (2016).

104. De Pascale, M. R., Sommese, L., Casamassimi, A. & Napoli, C. Platelet Derivatives in Regenerative Medicine: An Update. *Transfus. Med. Rev.* **29,** 52–61 (2015).

105. Dougherty, E. J. An Evidence-Based Model Comparing the Cost-effectiveness of Platelet-Rich Plasma Gel to Alternative Therapies for Patients with Nonhealing Diabetic Foot Ulcers. *Adv. Skin Wound Care* **21,** 568–575 (2008).

106. Sharathkumar, A. A. & Shapiro, A. PLATELET FUNCTION Second Edition. *World Federation of Hemophilia* 22 (2008).

107. Burnouf, T., Goubran, H. A. & Seghatchian, J. Multifaceted regenerative lives of expired platelets in the second decade of the 21st century. *Transfus. Apher. Sci.* **51,** 107–112 (2014).

108. Burnouf, T., Strunk, D., Koh, M. B. C. & Schallmoser, K. Human platelet lysate: Replacing fetal bovine serum as a gold standard for human cell propagation? *Biomaterials* **76,** 371–387 (2016).

109. Fitch-Tewfik, J. L. & Flaumenhaft, R. Platelet Granule Exocytosis: A Comparison with Chromaffin Cells. *Front. Endocrinol. (Lausanne).* **4,** 77 (2013).

110. Foster, T. E., Puskas, B. L., Mandelbaum, B. R., Gerhardt, M. B. & Rodeo, S. A. Platelet-Rich Plasma. *Am. J. Sports Med.* **37,** 2259–2272 (2009).

111. Verma, A. & Agarwal, P. Platelet utilization in the developing world: Strategies to optimize platelet transfusion practices. *Transfus. Apher. Sci.* **41,** 145–149 (2009).

112. Chan, R. K. *et al.* Expired liquid preserved platelet releasates retain proliferative activity. *J. Surg. Res.* **126,** 55–58 (2005).

113. Ross, R., Glomset, J., Kariya, B. & Harker, L. A platelet-dependent serum factor that stimulates the proliferation of arterial smooth muscle cells in vitro. *Proc. Natl. Acad. Sci. U. S. A.* **71,** 1207–10 (1974).

114. Mendes, B. B. *et al.* Blood derivatives awaken in regenerative medicine strategies to modulate wound healing. *Adv. Drug Deliv. Rev.* **129,** 376–393 (2018).

115. Zhou, Y., Zhang, J., Wu, H., Hogan, M. V & Wang, J. H.-C. The differential effects of leukocyte-containing and pure platelet-rich plasma (PRP) on tendon stem/progenitor cells - implications of PRP application for the clinical treatment of tendon injuries. *Stem Cell Res. Ther.* **6,** 173 (2015).

116. Anitua, E., Prado, R., Padilla, S. & Orive, G. Platelet-rich plasma scaffolds for tissue engineering: More than just growth factors in three dimensions. *Platelets* **26,** 281–282 (2015).

117. Dohan Ehrenfest, D. M., Rasmusson, L. & Albrektsson, T. Classification of platelet concentrates: from pure platelet-rich plasma (P-PRP) to leucocyte- and platelet-rich fibrin (L-PRF). *Trends Biotechnol.* **27,** 158–167 (2009).

118. Amable, P. *et al.* Platelet-rich plasma preparation for regenerative medicine: optimization and quantification of cytokines and growth factors. *Stem Cell Res. Ther.* **4,** 67 (2013).

119. Gibble, J. & Ness, P. Fibrin glue: the perfect operative sealant? *Transfusion* **30,** 741–747 (1990).

120. Dohan, D. M. *et al.* Platelet-rich fibrin (PRF): A second-generation platelet concentrate.

Part I: Technological concepts and evolution. *Oral Surgery, Oral Med. Oral Pathol. Oral Radiol. Endodontology* **101,** e37–e44 (2006).

121. Sierra, D. H. Fibrin Sealant Adhesive Systems: A Review of Their Chemistry, Material Properties and Clinical Applications. *J. Biomater. Appl.* **7,** 309–352 (1993).

122. Spicer, P. P. & Mikos, A. G. Fibrin glue as a drug delivery system. *J. Control. Release* **148,** 49–55 (2010).

123. Jeon, O., Ryu, S. H., Chung, J. H. & Kim, B.-S. Control of basic fibroblast growth factor release from fibrin gel with heparin and concentrations of fibrinogen and thrombin. *J. Control. Release* **105,** 249–59 (2005).

124. Wong, C., Inman, E., Spaethe, R. & Helgerson, S. Fibrin-based biomaterials to deliver human growth factors. *Thromb. Haemost.* **89,** 573–82 (2003).

125. Sacchi, V. *et al.* Long-lasting fibrin matrices ensure stable and functional angiogenesis by highly tunable, sustained delivery of recombinant VEGF164. *Proc. Natl. Acad. Sci. U. S. A.* **111,** 6952–7 (2014).

126. Catelas, I., Dwyer, J. F. & Helgerson, S. Controlled Release of Bioactive Transforming Growth Factor Beta-1 from Fibrin Gels In Vitro. *Tissue Eng. Part C Methods* **14,** 119–128 (2008).

127. Mittermayr, R. *et al.* Controlled release of fibrin matrix-conjugated platelet derived growth factor improves ischemic tissue regeneration by functional angiogenesis. *Acta Biomater.* **29,** 11–20 (2016).

128. Zhibo, X. & Miaobo, Z. Effect of Sustained-Release Lidocaine on Reduction of Pain After Subpectoral Breast Augmentation. *Aesthetic Surg. J.* **29,** 32–34 (2009).

129. Ozaki, S. *et al.* Comprehensive evaluation of fibrin glue as a local drug-delivery system—efficacy and safety of sustained release of vancomycin by fibrin glue against local methicillin-resistant Staphylococcus aureus infection. *J. Artif. Organs* **17,** 42–49 (2014).

130. Christman, K. L., Fok, H. H., Sievers, R. E., Fang, Q. & Lee, R. J. Fibrin Glue Alone and Skeletal Myoblasts in a Fibrin Scaffold Preserve Cardiac Function after Myocardial Infarction. *Tissue Eng.* **10,** 403–409 (2004).

131. Tuan, T.-L., Song, A., Chang, S., Younai, S. & Nimni, M. E. In VitroFibroplasia: Matrix Contraction, Cell Growth, and Collagen Production of Fibroblasts Cultured in Fibrin Gels. *Exp. Cell Res.* **223,** 127–134 (1996).

132. Cox, S., Cole, M. & Tawil, B. Behavior of Human Dermal Fibroblasts in Three-Dimensional Fibrin Clots: Dependence on Fibrinogen and Thrombin Concentration. *Tissue Eng.* **10,** 942–954 (2004).

133. Mogford, J. E., Tawil, B., Jia, S. & Mustoe, T. A. Fibrin sealant combined with fibroblasts and platelet-derived growth factor enhance wound healing in excisional wounds. *Wound Repair Regen.* **17,** 405–410 (2009).

134. Horch, R. ., Bannasch, H. & Stark, G. . Transplantation of cultured autologous keratinocytes in fibrin sealant biomatrix to resurface chronic wounds. *Transplant. Proc.* **33,** 642–644 (2001).

135. Kopp, J., Jeschke, M. G., Bach, A. D., Kneser, U. & Horch, R. E. Applied tissue engineering in the closure of severe burns and chronic wounds using cultured human autologous keratinocytes in a natural fibrin matrix. *Cell Tissue Bank.* **5,** 81–87 (2004).

136. Marx, R. E. Platelet-Rich Plasma (PRP): What Is PRP and What Is Not PRP? *Implat Dent* **10,** 225–228 (2001).

137. Tsay, R. C. *et al.* Differential growth factor retention by platelet-rich plasma composites. *J. Oral Maxillofac. Surg.* **63,** 521–528 (2005).

138. Davis, V. L. *et al.* Platelet-Rich Preparations to Improve Healing. Part II: Platelet Activation and Enrichment, Leukocyte Inclusion, and Other Selection Criteria. *J. Oral Implantol.* **40,** 511–521 (2014).

139. Anitua, E., Sánchez, M., Orive, G. & Andía, I. The potential impact of the preparation rich in growth factors (PRGF) in different medical fields. *Biomaterials* **28,** 4551–4560 (2007).

140. Anitua, E. *et al. Autologous preparations rich in growth factors promote proliferation and induce VEGF and HGF production by human tendon cells in culture*. *Journal of Orthopaedic Research* **23,** (2005).

141. Anitua, E. A. Enhancement of Osseointegration by Generating a Dynamic Implant

Surface. *J. Oral Implantol.* **32,** 72–76 (2006).

142. Fernández-Barbero, J. E. *et al.* Flow cytometric and morphological characterization of platelet-rich plasma gel. *Clin. Oral Implants Res.* **17,** 687–693 (2006).

143. O'connell, S. M. *et al.* Autologous platelet-rich fibrin matrix as cell therapy in the healing of chronic lower-extremity ulcers Wound Repair and Regeneration. *Wound Repair Regen.* **16,** 749–756 (2008).

144. Saad Setta, H., Elsahat, A., Elsherbiny, K., Massoud, K. & Safe, I. Platelet-rich plasma versus platelet-poor plasma in the management of chronic diabetic foot ulcers: A comparative study. *Int. Wound J.* **8,** 307–312 (2011).

145. Bernardi, M. *et al.* The production method affects the efficacy of platelet derivatives to expand mesenchymal stromal cells in vitro. *J. Transl. Med.* **15,** 90 (2017).

146. Crespo-Diaz, R. *et al.* Platelet Lysate Consisting of a Natural Repair Proteome Supports Human Mesenchymal Stem Cell Proliferation and Chromosomal Stability. *Cell Transplant.* **20,** 797–811 (2011).

147. Crovetti, G. *et al.* Platelet gel for healing cutaneous chronic wounds. *Transfus. Apher. Sci.* **30,** 145–151 (2004).

148. Moroz, A. *et al.* Platelet lysate 3D scaffold supports mesenchymal stem cell chondrogenesis: An improved approach in cartilage tissue engineering. *Platelets* **24,** 219–225 (2013).

149. Fortunato, T. M., Beltrami, C., Emanueli, C., De Bank, P. A. & Pula, G. Platelet lysate gel and endothelial progenitors stimulate microvascular network formation in vitro: tissue engineering implications. *Nat. Publ. Gr.* (2016). doi:10.1038/srep25326

150. Burnouf, T., Chou, M.-L., Wu, Y.-W., Su, C.-Y. & Lee, L.-W. Antimicrobial activity of platelet (PLT)-poor plasma, PLT-rich plasma, PLT gel, and solvent/detergent-treated PLT lysate biomaterials against wound bacteria. *Transfusion* **53,** 138–146 (2013).

151. Malafaya, P. B., Oliveira, J. T. & Reis, R. L. The Effect of Insulin-Loaded Chitosan Particle-Aggregated Scaffolds in Chondrogenic Differentiation. *Tissue Eng. Part A* **16,** 735–47 (2010).

152. Wang, Z. *et al.* Novel biomaterial strategies for controlled growth factor delivery for biomedical applications. *NPG Asia Mater.* **9,** 435 (2017).

153. Santo, V. E., Gomes, M. E., Mano, J. F. & Reis, R. L. Chitosan-chondroitin sulphate nanoparticles for controlled delivery of platelet lysates in bone regenerative medicine. *J. Tissue Eng. Regen. Med.* **6,** s47–s59 (2012).

154. Doucet, C. *et al.* Platelet Lysates Promote Mesenchymal Stem Cell Expansion: A Safety Substitute for Animal Serum in Cell-Based Therapy Applications. *J. Cell. Physiol.* **205,** 228–236 (2005).

155. Shih, D. T. B. & Burnouf, T. Preparation, quality criteria, and properties of human blood platelet lysate supplements for ex vivo stem cell expansion. *N. Biotechnol.* **32,** 199–211 (2015).

156. Pietramaggiori, G. *et al.* Trehalose lyophilized platelets for wound healing. *Wound Repair Regen.* **15,** 213–220 (2007).

157. Radtke, S., Giebel, B., Wagner, W. & Horn, P. A. Platelet lysates and their role in cell therapy. *ISBT Sci. Ser.* **9,** 193–197 (2014).

158. Muraglia, A. *et al.* Biological activity of a standardized freeze-dried platelet derivative to be used as cell culture medium supplement. *Platelets* **25,** 211–220 (2014).

159. Choukroun, J. *et al.* Platelet-rich fibrin (PRF): A second-generation platelet concentrate. Part IV: Clinical effects on tissue healing. *Oral Surgery, Oral Med. Oral Pathol. Oral Radiol. Endodontology* **101,** e56–e60 (2006).

160. van Hinsbergh, V. W., Collen, A. & Koolwijk, P. Role of fibrin matrix in angiogenesis. *Ann. N. Y. Acad. Sci.* **936,** 426–37 (2001).

161. Danielsen, P., Jørgensen, B., Karlsmark, T., Jorgensen, L. N. & Ågren, M. S. Effect of Topical Autologous Platelet-Rich Fibrin versus No Intervention on Epithelialization of Donor Sites and Meshed Split-Thickness Skin Autografts: A Randomized Clinical Trial. *Plast. Reconstr. Surg.* **122,** 1431–1440 (2008).

162. Gaßling, V. L., Açil, Y., Springer, I. N., Hubert, N. & Wiltfang, J. Platelet-rich Plasma and Platelet-rich fibrin in human cell culture. *YMOE* **108,** 48–55 (2009).

163. He, L., Lin, Y., Hu, X., Zhang, Y. & Wu, H. A comparative study of platelet-rich fibrin (PRF) and platelet-rich plasma (PRP) on the effect of proliferation and differentiation of rat osteoblasts in vitro. *YMOE* **108,** 707–713 (2009).

164. Mitchell, A. C., Briquez, P. S., Hubbell, J. A. & Cochran, J. R. Engineering growth factors for regenerative medicine applications. *Acta Biomater.* **30,** 1–12 (2016).

165. Gainza, G., Villullas, S., Pedraz, J. L., Hernandez, R. M. & Igartua, M. Advances in drug delivery systems (DDSs) to release growth factors for wound healing and skin regeneration. *Nanomedicine Nanotechnology, Biol. Med.* **11,** 1551–1573 (2015).

166. Santo, V. E., Popa, E. G., Mano, J. F., Gomes, M. E. & Reis, R. L. Natural assembly of platelet lysate-loaded nanocarriers into enriched 3D hydrogels for cartilage regeneration. *Acta Biomater.* **19,** 56–65 (2015).

167. Kutlu, B., Tigli Aydin, R. S., Akman, A. C., Gümüsderelioglu, M. & Nohutcu, R. M. Platelet-rich plasma-loaded chitosan scaffolds: preparation and growth factor release kinetics. *J. Biomed. Mater. Res. Part B* **101B,** 28–35 (2013).

168. Bertoncelj, V. *et al.* Development and bioevaluation of nanofibers with blood-derived growth factors for dermal wound healing. *Eur. J. Pharm. Biopharm.* **88,** 64–74 (2014).

169. Sell, S. A., Wolfe, P. S., Ericksen, J. J., Simpson, D. G. & Bowlin, G. L. Incorporating Platelet-Rich Plasma into Electrospun Scaffolds for Tissue Engineering Applications. *Tissue Eng. Part A* **17,** 2723–2737 (2011).

170. Liu, J. *et al.* Construction of PRP-containing nanofibrous scaffolds for controlled release and their application to cartilage regeneration. (2015). doi:10.1039/c4tb00515e

171. Buzgo, M. *et al.* Time-regulated drug delivery system based on coaxially incorporated platelet α-granules for biomedical use. *Nanomedicine* **8,** 1137–1154 (2013).

172. Sovkova, V. *et al.* Platelet lysate as a serum replacement for skin cell culture on biomimetic PCL nanofibers. *Platelets* **29,** (2018).

173. Bieback, K. *et al.* Human Alternatives to Fetal Bovine Serum for the Expansion of Mesenchymal Stromal Cells from Bone Marrow. *Stem Cells* **27,** 2331–2341 (2009).

174. Mohammadi, S. *et al.* Human Platelet Lysate as a Xeno Free Alternative of Fetal Bovine

Serum for the In Vitro Expansion of Human Mesenchymal Stromal Cells. *Int. J. Hematol. stem cell Res.* **10,** 161–71 (2016).

175. Riem Vis, P. W. *et al.* Platelet-lysate as an autologous alternative for fetal bovine serum in cardiovascular tissue engineering. *Tissue Eng. Part A* **16,** 1317–27 (2010).

176. Carducci, A. *et al.* GMP-grade platelet lysate enhances proliferation and migration of tenon fibroblasts. *Front. Biosci. (Elite Ed).* **8,** 84–99 (2016).

177. Horn, P. *et al.* Impact of individual platelet lysates on isolation and growth of human mesenchymal stromal cells. *Cytotherapy* **12,** 888–898 (2010).

178. Mussano, F. *et al.* Cytokine, chemokine, and growth factor profile of platelet-rich plasma. *Platelets* **27,** 467–471 (2016).

179. Miller, C. H., Rice, A. S., Garrett, K. & Stein, S. F. Gender, race and diet affect platelet function tests in normal subjects, contributing to a high rate of abnormal results. *Br. J. Haematol.* **165,** 842–53 (2014).

180. Ishida, Y., Kondo, T., Kimura, A., Matsushima, K. & Mukaida, N. Absence of IL-1 receptor antagonist impaired wound healing along with aberrant NF-kappaB activation and a reciprocal suppression of TGF-beta signal pathway. *J. Immunol.* **176,** 5598–606 (2006).

181. Jin, W. & Dong, C. IL-17 cytokines in immunity and inflammation. *Emerg. Microbes Infect.* **2,** e60 (2013).

182. Wang, C. Q. F. *et al.* IL-17 and TNF synergistically modulate cytokine expression while suppressing melanogenesis: potential relevance to psoriasis. *J. Invest. Dermatol.* **133,** 2741–2752 (2013).

183. Crawford, A., Angelosanto, J. M., Nadwodny, K. L., Blackburn, S. D. & Wherry, E. J. A Role for the Chemokine RANTES in Regulating CD8 T Cell Responses during Chronic Viral Infection. *PLoS Pathog.* **7,** e1002098 (2011).

184. El-Sharkawy, H. *et al.* Platelet-Rich Plasma: Growth Factors and Pro- and Anti-Inflammatory Properties. *J. Periodontol.* **78,** 661–669 (2007).

185. Burnouf, T. *et al.* Blood-derived biomaterials and platelet growth factors in regenerative medicine. *Blood Rev.* **27,** 77–89 (2013).

186. Coppé, J.-P., Kauser, K., Campisi, J. & Beauséjour, C. M. Secretion of Vascular Endothelial Growth Factor by Primary Human Fibroblasts at Senescence. *J. Biol. Chem.* **281,** 29568–29574 (2006).

187. Coppé, J.-P., Desprez, P.-Y., Krtolica, A. & Campisi, J. The Senescence-Associated Secretory Phenotype: The Dark Side of Tumor Suppression. *Annu. Rev. Pathol. Mech. Dis.* **5,** 99–118 (2010).

188. Witzeneder, K. *et al.* Human-derived alternatives to fetal bovine serum in cell culture. *Transfus. Med. Hemotherapy* **40,** 417–423 (2013).

189. Ranzato, E., Mazzucco, L., Patrone, M. & Burlando, B. Platelet lysate promotes *in vitro* wound scratch closure of human dermal fibroblasts: different roles of cell calcium, P38, ERK and PI3K/AKT. *J. Cell. Mol. Med.* **13,** 2030–2038 (2009).

190. Stessuk, T. *et al.* Platelet-rich plasma (PRP) and adipose-derived mesenchymal stem cells: stimulatory effects on proliferation and migration of fibroblasts and keratinocytes in vitro. *Arch. Dermatol. Res.* **308,** 511–520 (2016).

191. Plencner, M. *et al.* Significant improvement of biocompatibility of polypropylene mesh for incisional hernia repair by using poly-ε-caprolactone nanofibers functionalized with thrombocyte-rich solution. *Int. J. Nanomedicine* **10,** 2635–2646 (2015).

192. Tian, F. *et al.* Quantitative analysis of cell adhesion on aligned micro-and nanofibers. (2007). doi:10.1002/jbm.a.31304

193. Vocetkova, K. *et al.* Nanofibrous polycaprolactone scaffolds with adhered platelets stimulate proliferation of skin cells. *Cell Prolif.* **49,** (2016).

194. Wan, L.-S. & Xu, Z.-K. Polymer surfaces structured with random or aligned electrospun nanofibers to promote the adhesion of blood platelets. *J Biomed Mater Res* **89,** 168–175 (2009).

195. Laurens, N., Koolwijk, P. & de Maat, M. P. Fibrin structure and wound healing. *J. Thromb. Haemost.* **4,** 932–939 (2006).

196. Jakubova, R. *et al.* Immobilization of thrombocytes on PCL nanofibres enhances chondrocyte proliferation in vitro. *Cell Prolif.* **44,** 183–191 (2011).

197. Eppley, B. L., Woodell, J. E. & Higgins, J. Platelet Quantification and Growth Factor Analysis from Platelet-Rich Plasma: Implications for Wound Healing. *Plast. Reconstr. Surg.* 1502–1508 (2004). doi:10.1097/01.PRS.0000138251.07040.51

198. Diaz-Gomez, L. *et al.* Biodegradable electrospun nanofibers coated with platelet-rich plasma for cell adhesion and proliferation. *Mater. Sci. Eng. C. Mater. Biol. Appl.* **40,** 180–8 (2014).

199. Sánchez-Illárduya, M. B. *et al.* Time-dependent release of growth factors from implant surfaces treated with plasma rich in growth factors. *J. Biomed. Mater. Res. - Part A* **101 A,** 1478–1488 (2013).

200. Sahni, A., Altland, O. D. & Francis, C. W. FGF-2 but not FGF-1 binds fibrin and supports prolonged endothelial cell growth. *J. Thromb. Haemost.* **1,** 1304–10 (2003).

201. Grainger, D. J., Wakefield, L., Bethell, H. W., Farndale, R. W. & Metcalfe, J. C. Release and activation of platelet latent TGF-beta in blood clots during dissolution with plasmin. *Nat. Med.* **1,** 932–7 (1995).

202. Dohan, D. M. *et al.* Platelet-rich fibrin (PRF): A second-generation platelet concentrate. Part III: Leucocyte activation: A new feature for platelet concentrates? *Oral Surgery, Oral Med. Oral Pathol. Oral Radiol. Endodontology* **101,** e51–e55 (2006).

203. Campbell, P. G., Durham, S. K., Hayes, J. D., Suwanichkul, A. & Powell, D. R. Insulin-like growth factor-binding protein-3 binds fibrinogen and fibrin. *J. Biol. Chem.* **274,** 30215–21 (1999).

204. Liu, Y., Kalen, A., Risto, O. & Wahlstrom, O. Fibroblast proliferation due to exposure to a platelet concentrate in vitro is pH dependent. *Wound Repair Regen.* **10,** 336–340 (2002).

205. Shrivastava, R. Clinical evidence to demonstrate that simultaneous growth of epithelial and fibroblast cells is essential for deep wound healing. *Diabetes Res. Clin. Pract.* **92,** 92–99 (2011).

206. Alikhan, A. *et al.* Vitiligo: A comprehensive overview. *J. Am. Dermatology* **65,** 473–491 (2011).

207. Lin, S.-J., Jee, S.-H., Hsaio, W.-C., Lee, S.-J. & Young, T.-H. Formation of melanocyte

spheroids on the chitosan-coated surface. *Biomaterials* **26,** 1413–1422 (2005).

208. Ghosh, D., Shenoy, S. & Kuchroo, P. Cultured Melanocytes: From Skin Biopsy to Transplantation. *Cell Transplant.* **17,** 351–360 (2008).

209. Eves, P. C. *et al.* Simplifying the Delivery of Melanocytes and Keratinocytes for the Treatment of Vitiligo Using a Chemically Defined Carrier Dressing. *J. Invest. Dermatol.* **128,** 1554–1564 (2008).

210. Ghosh, D. *et al.* Efficacy and Safety of Autologous Cultured Melanocytes Delivered on Poly (DL-Lactic Acid) Film: A Prospective, Open-Label, Randomized, Multicenter Study. *Dermatologic Surg.* **38,** 1981–1990 (2012).

211. Redondo, P. *et al.* Amniotic membrane as a scaffold for melanocyte transplantation in patients with stable vitiligo. *Dermatol. Res. Pract.* **2011,** (2011).

212. Savkovic, V. *et al.* Polycaprolactone fiber meshes provide a 3D environment suitable for cultivation and differentiation of melanocytes from the outer root sheath of hair follicle. *J. Biomed. Mater. Res. - Part A* **104,** 26–36 (2016).

213. Mansbridge, J. Skin tissue engineering. *J. Biomater. Sci. Polym. Ed.* **19,** 955–968 (2008).

214. Rampichová, M. *et al.* Cell penetration to nanofibrous scaffolds Forcespinning, an alternative approach for fabricating 3D nanofibers. *Cell Adh. Migr.* **8,** 36–41 (2014).

215. Rampichova, M. *et al.* Platelet-functionalized three-dimensional poly-ε-caprolactone fibrous scaffold prepared using centrifugal spinning for delivery of growth factors. *Int. J. Nanomedicine* **12,** 347–361 (2017).

216. Martino, M. M., Briquez, P. S., Ranga, A., Lutolf, M. P. & Hubbell, J. A. Heparin-binding domain of fibrin(ogen) binds growth factors and promotes tissue repair when incorporated within a synthetic matrix. *Proc. Natl. Acad. Sci.* **110,** 4563–4568 (2013).

217. Hirobe, T., Shibata, T., Fujiwara, R. & Sato, K. Platelet-derived growth factor regulates the proliferation and differentiation of human melanocytes in a differentiation-stage-specific manner. *J. Dermatol. Sci.* **83,** 200–209 (2016).

218. Vocetkova, K. *et al.* A comparison of high throughput core-shell 2D electrospinning and 3D centrifugal spinning techniques to produce platelet lyophilisate-loaded fibrous

scaffolds and their effects on skin cells. *RSC Adv.* **7,** (2017).

219. Pham, Q. P., Sharma, U. & Mikos, A. G. Electrospun Poly(ε-caprolactone) Microfiber and Multilayer Nanofiber/Microfiber Scaffolds: Characterization of Scaffolds and Measurement of Cellular Infiltration. *Biomacromolecules* **7,** 2796–2805 (2006).

220. Rampichová, M. *et al.* Elastic three-dimensional poly (ε-caprolactone) nanofibre scaffold enhances migration, proliferation and osteogenic differentiation of mesenchymal stem cells. *Cell Prolif.* **46,** 23–37 (2013).

221. Siegbahn, A., Hammacher, A., Westermark, B. & Heldint, C.-H. Differential Effects of the Various Isoforms of Platelet-derived on Chemotaxis of Fibroblasts, Monocytes, and Granulocytes. *J. Clin. Invest.* **85,** 916–920 (1990).

222. Barnes, C. P., Sell, S. A., Boland, E. D., Simpson, D. G. & Bowlin, G. L. Nanofiber technology: Designing the next generation of tissue engineering scaffolds. *Adv. Drug Deliv. Rev.* **59,** 1413–1433 (2007).

223. Pietramaggiori, G., Kaipainen, A., Czeczuga, J. M., Wagner, C. T. & Orgill, D. P. Freeze-dried platelet-rich plasma shows beneficial healing properties in chronic wounds. *Wound Repair Regen.* **14,** 573–580 (2006).

224. Briggs, T. & Livingston Arinzeh, T. Examining the formulation of emulsion electrospinning for improving the release of bioactive proteins from electrospun fibers. *Inc. J Biomed Mater Res Part A* **102,** 674–684 (2013).

225. Tian, L., Prabhakaran, M. P., Ding, X., Kai, D. & Ramakrishna, S. Emulsion electrospun nanofibers as substrates for cardiomyogenic differentiation of mesenchymal stem cells. *J. Mater. Sci. Mater. Med.* **24,** 2577–2587 (2013).

226. Tian, L., Prabhakaran, M. P., Ding, X., Kai, D. & Ramakrishna, S. Emulsion electrospun vascular endothelial growth factor encapsulated poly(L-lactic acid-co-e-caprolactone) nanofibers for sustained release in cardiac tissue engineering. *J. Mater. Sci.* **47,** 3272–3281 (2012).

227. Maderuelo, C., Zarzuelo, A. & Lanao, J. M. Critical factors in the release of drugs from sustained release hydrophilic matrices. *J. Control. Release* **154,** 2–19 (2011).

228. Sun, H., Mei, L., Song, C., Cui, X. & Wang, P. The in vivo degradation, absorption and excretion of PCL-based implant. *Biomaterials* **27,** 1735–1740 (2006).

229. Numasaki, M. *et al.* Interleukin-17 promotes angiogenesis and tumor growth. *Blood* **101,** 2620–2627 (2003).

230. Kempf, M. *et al.* A denatured collagen microfiber scaffold seeded with human fibroblasts and keratinocytes for skin grafting. *Biomaterials* **32,** 4782–4792 (2011).

231. Noh, H. K. *et al.* Electrospinning of chitin nanofibers: Degradation behavior and cellular response to normal human keratinocytes and fibroblasts. *Biomaterials* **27,** 3934–3944 (2006).

232. Min, B.-M. *et al.* Electrospinning of silk fibroin nanofibers and its effect on the adhesion and spreading of normal human keratinocytes and fibroblasts in vitro. *Biomaterials* **25,** 1289–1297 (2004).

233. Kim, G., Ahn, S., Yoon, H., Kim, Y. & Chun, W. A cryogenic direct-plotting system for fabrication of 3D collagen scaffolds for tissue engineering. *J. Mater. Chem.* **19,** 8817–8823 (2009).

11 PUBLICATIONS RELATED TO THE THESIS

- Sovkova V, Vocetkova K, Rampichova M, Mickova A, Buzgo M, Lukasova V, Dankova J, Filova E, Necas A, Amler E. Platelet lysate as a serum replacement for skin cell culture on biomimetic PCL nanofibers. Platelets 29, (2018). IF = 2.356.
- Vocetkova K, Buzgo M, Sovkova V, Bezdekova D, Kneppo P, Amler E. Nanofibrous polycaprolactone scaffolds with adhered platelets stimulate proliferation of skin cells. Cell Prolif. 49, (2016). IF = 4.936.
- Vocetkova K, Buzgo M, Sovkova V, Rampichova M, Staffa A, Filova E, Lukasova V, Doupnik M, Fiori F, Amler E. A comparison of high throughput core-shell 2D electrospinning and 3D centrifugal spinning techniques to produce platelet lyophilisate-loaded fibrous scaffolds and their effects on skin cells. RSC Adv. 7, (2017). IF = 2.936.

12 OTHER PUBLICATIONS OF THE AUTHOR

- Rampichova M, Chvojka J, Jencova V, Kubikova T, Tonar Z, Erben J, Buzgo M, Dankova J, Litvinec A, Vocetkova K, Plencner M, Prosecka E, Sovkova V, Lukasova V, Kralickova M, Lukas D, Amler E. The combination of nanofibrous and microfibrous materials for enhancement of cell infiltration and in vivo bone tissue formation. Biomed. Mat. 13, (2018). IF = 2.897.
- Lukasova V, Buzgo M, Vocetkova K, Kubikova T, Tonar Z, Doupnik M, Blahnova V, Litvinec A, Sovkova V, Voltrova B, Staffa A, Svora P, Kralickova M, Amler E, Filova E, Rustichelli F, Rampichova M. Osteoinductive 3D scaffolds prepared by blend centrifugal spinning for long-term delivery of osteogenic supplements. RSC Advances. 8, 21889-21904, 2018. IF = 2.936.
- Buzgo M, Filova E, Mickova Staffa A, Rampichova M, Doupnik M, Vocetkova K, Lukasova V, Kolcun R, Lukas D, Necas A, Amler E. Needleless emulsion electrospinning for the regulated delivery of susceptible proteins. J. Tissue Eng. Regen. Med. 12, (2018). IF = 4.089.
- East B, Plencner M, Kralovic M, Rampichova M, Sovkova V, Vocetkova K, Otahal M, Tonar Z, Kolinko Y, Amler E, Hoch J. A polypropylene mesh with poly-ε-caprolactone nanofibers in hernia repair: large animal experiment. In. J. Nanomed. 13, (2018). IF = 4.86.
- Buzgo M, Rampichova M, Vocetkova K, Sovkova V, Lukasova V, Doupnik M, Mickova A, Rustichelli F, Amler E. Emulsion centrifugal spinning for production of 3D drug releasing nanofibres with core/shell structure. RSC Adv. 7, (2017). IF = 2.936.

- Rampichova M, Buzgo M, Mickova A, Vocetkova K, Sovkova V, Lukasova V, Filova E, Rustichelli F, Amler E. Platelet-functionalized three-dimensional poly-ε-caprolactone fibrous scaffold prepared using centrifugal spinning for delivery of growth factors. Int. J. Nanomed. 12, (2017). IF = 4.86.

13 ACKNOWLEDGEMENTS

Firstly, I would like to express my gratitude to my supervisor for everything he had done for me during my Master's and PhD studies, then to all my colleagues/friends, who not only made all the work fun, but without their advice and support, this thesis could not be finished, and above all to my family who has supported my through all the endless years of study.

This research was supported by the Czech Science Foundation (Grants Nos. 15-15697S, and 16-14758S), the Internal Grant Agency of the Ministry of Health of the Czech Republic (Grant No. 15-33094A, 16-28637A, 16-29680A, and 17-32285A), the Grant Agency of Charles University (Grants Nos. 270513, 1246314, 1228214, 545313, 512216, and 44218), the Ministry of Education, Youth and Sports of the Czech Republic within the National Sustainability Programme (Grants No. LO 1605, LO1508, and LO1309) and Operational Programme – Prague Competitiveness (Grants No. CZ.2.16/3.1.00/21528 and CZ.2.16/3.1.00/24006), the Ministry of Interior of the Czech Republic (Grant No. VI20152018010), the Ministry of Industry and Trade of the Czech Republic (Grants No. FV30086) and the University Centre for Energy Efficient Buildings (UCEEB) support IPv6.